MAGNETOM Flash

Special USA Edition · 02/2020

siemens.com/magnetom-world

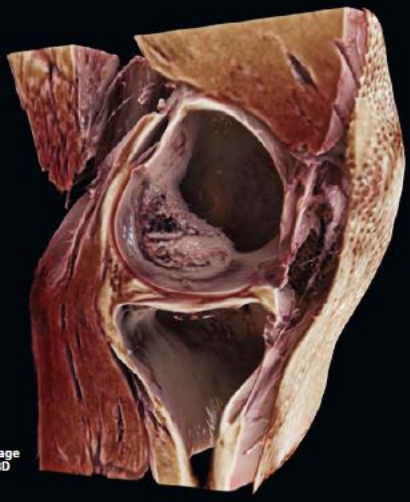

Cover image
GOKnee3D

SIEMENS Healthineers

MAGNETOM Flash Special USA Edition · 02/2020
Content

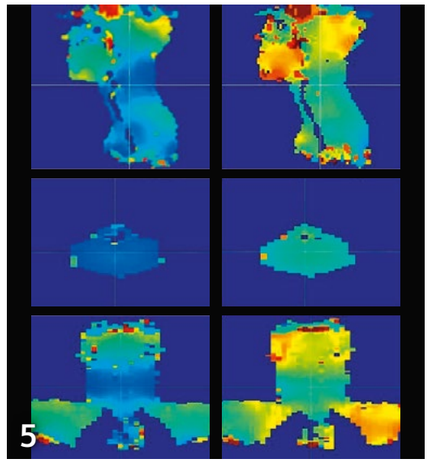

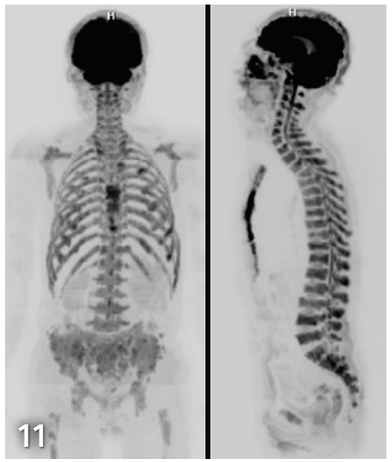

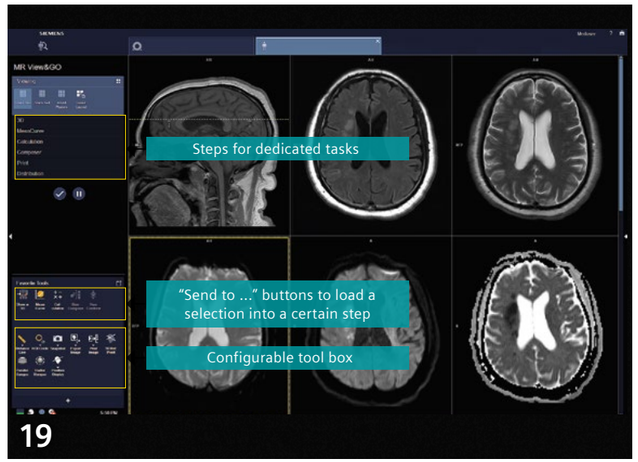

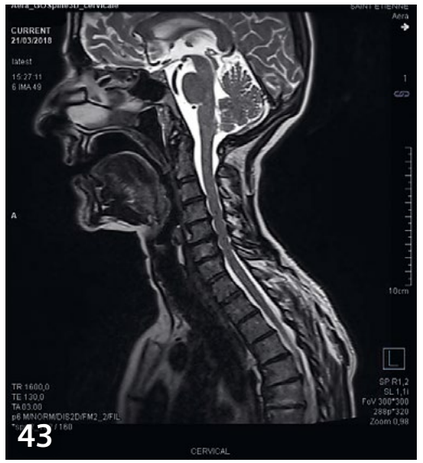

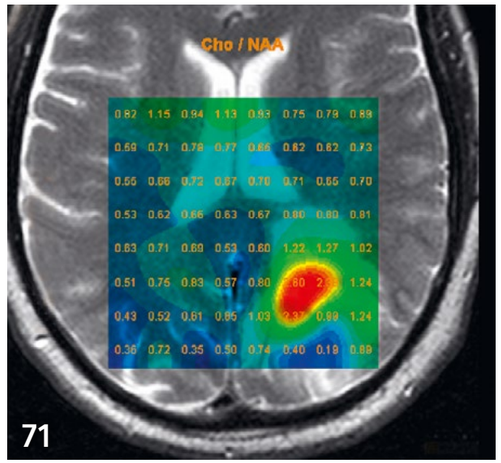

Learn from the experience of other MAGNETOM users

The MAGNETOM World is the community of Siemens Healthcare MR users worldwide, providing you with relevant clinical information. Here you will find application tips and protocols to optimize your daily work. Lectures and presentations from experts in the field will allow you to be exposed to new ideas and alternative clinical approaches.

Put the advantages of the MAGNETOM World to work for you!

usa.siemens.com/vida-flash

Reprinted from BioMatrix and syngo MR XA11 special issue

BioMatrix Tuners: CoilShim

Miriam R. Keil, Ph.D.; Jörg Rothard; Carmel Hayes, Ph.D.

Siemens Healthineers, Erlangen, Germany

A cervical spine or neck MRI can provide valuable diagnostic information for a wide range of different conditions. In particular, MRI's soft tissue contrast helps to detect and monitor a variety of pathologies, misalignments or injuries. It can be useful in evaluating symptoms such as pain, foreign body sensations, numbness, tingling or weakness in the arms, shoulder or neck area and can assist in detecting certain chronic diseases of the nervous system. It is also used in tumor diagnosis and in the assessment of bleeding, swelling, infections, or inflammatory conditions in the vertebrae or surrounding tissues.

In many patients, MR image quality in the neck or cervical spine region might be degraded by B_0 field distortions. These typically arise from tissue interfaces with different susceptibilities in this region, for example in the vicinity of the lung, between vertebrae, fluid-filled cavities, as well as from the body contour itself in the shoulders and neck area (Fig. 1). The low field homogeneity poses a challenge to MR imaging in this region and is often the source of image quality issues. Examples include insufficient fat saturation, spatial variations in the signal strength along the vertebrae, as well as regions showing complete signal loss.

With MAGNETOM Vida a new technology platform, BioMatrix, is introduced, which combines the ability to adapt to the individual patient's biovariability and the established Tim integrated matrix coil technology. This, in particular, allows to substantially improve image quality in the neck area by utilizing CoilShim. CoilShim is one of the new BioMatrix technologies which allows for correction of patient-induced B_0 field inhomogeneities using dedicated shimming channels integrated into the Head/Neck coil.

Two new Head/Neck coils support CoilShim: the BioMatrix Head/Neck 20 TCS (Tiltable, CoilShim) and the BioMatrix 64 CS (CoilShim). A first step in the compensation of patient-induced B_0 field inhomogeneities is the identification of the origin of these variations. Experiments indicate that there are two major sources of B_0 field inhomogeneities in head and neck MRI. These are the patients' shoulders on the one hand and the B_0 field distortion due to the neck on the other hand. The inhomogeneity pattern originates from the geometric shape of the human body in the head and neck area and the resulting difference in susceptibilities. Figure 1 shows a typical B_0 field inhomogeneity 'map' of the head and neck region. The map was generated from a principal component analysis performed on datasets from 19 volunteer scans. The analysis showed that only the first main component contains significant information. This suggests that the inhomogeneity pattern is likely to be the same for different body shapes and sizes and that only the magnitude of the inhomogeneity varies. To correct for B_0 field inhomogeneities in the shoulder and neck region, each of the two head and neck coils is equipped with two CoilShim channels (Fig. 2). The CoilShim channels are located in the posterior part of the Head/Neck coils, allowing the CoilShim technology to be used even when

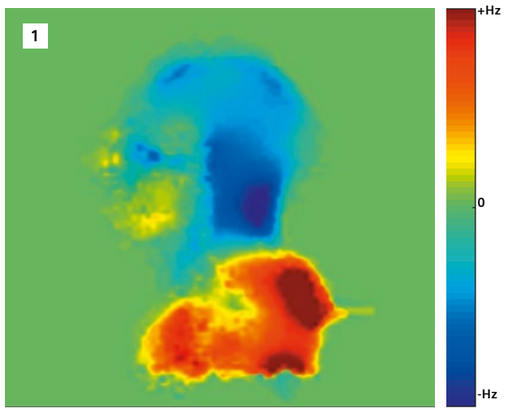

1 Typical B_0 field distortion pattern as seen in the sagittal orientation.

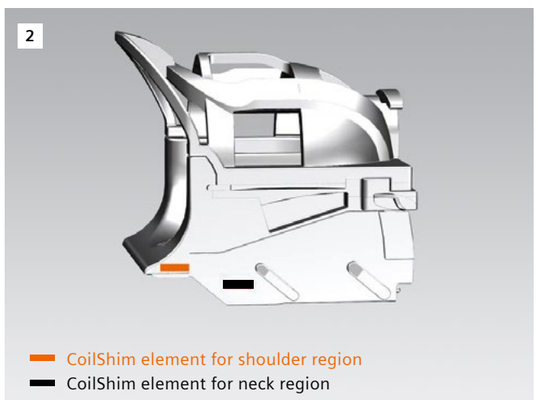

2 BioMatrix Head/Neck 20 TCS coil design and the location of the CoilShim elements in the BioMatrix Head/Neck 20 TCS coil.

the anterior part of the Head/Neck coils are detached. The magnitude of the B_0 field generated by each CoilShim channel can be adjusted independently with very fine resolution. This allows for best possible B_0 homogenization for each individual patient.

In order to ensure both adequate image quality and patient safety with the new Head/Neck coils with integrated CoilShim, special measures have been taken. These measures ensure decoupling of the CoilShim elements during the transmit phase and decoupling from the gradient system during the transmit and receive phase of the MR acquisition.

Applications

The usage of CoilShim requires no dedicated patient preparation: the patient can be positioned within the Biomatrix Head/Neck coil[1] as with any other head coil. When using the 20-channel TCS coil, the tilt angle may be adapted to the patients' needs, thereby providing increased patient comfort. Tilting the coil does not interfere with the CoilShim functionality but CoilShim may improve image quality degradations resulting from tilting.

CoilShim can be used with all clinical head and neck sequences and protocols, provided that the BioMatrix Head/Neck coil is plugged and active. "CoilShim" is turned on in the user interface by switching the respective parameter, which can be found on the tabcard "System", sub tab "Adjustments" from "Off" to "Auto". The actual enabling of CoilShim technology itself is therefore controlled auto-matically, depending on the slice geometry and the protocol parameters.

Results

The physical effect of the CoilShim feature on the B_0 field is illustrated in Figure 3, acquired in a healthy volunteer. The images compare B_0 field maps obtained using clinical state-of-the-art standard shimming with those which result from the usage of CoilShim technology.

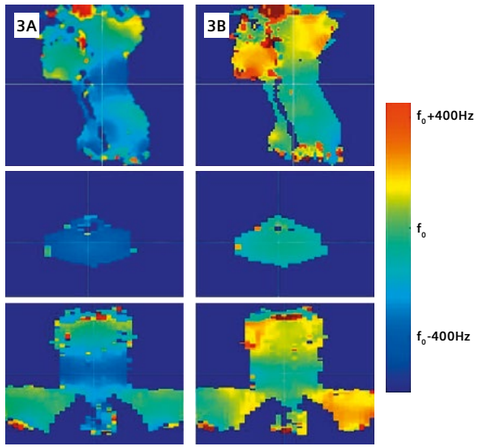

3 B_0 field map in the all three main orientations without **(3A)** and with CoilShim **(3B)**. The frequency shift relative to f_0 is shown in Hz.

The images show relative resonance frequency shifts in three orthogonal slice orientations. Once again, the two dominant sources of field inhomogeneity in the shoulder and in the neck area can be observed. In this example the frequency shift in the shoulder region is about 400 Hz and the frequency shift in the neck area is about -200 Hz. Given that the frequency shift between fat and water is 430 Hz at 3T, non-uniform fat saturation can be expected in such cases.

To further illustrate the impact of CoilShim on the quality of the shimmed region of interest, Figure 4 shows the frequency distribution of all voxels within the adjustment volume both with and without CoilShim. The spectrum of the frequencies within the adjustment volume is significantly narrowed on applying CoilShim.

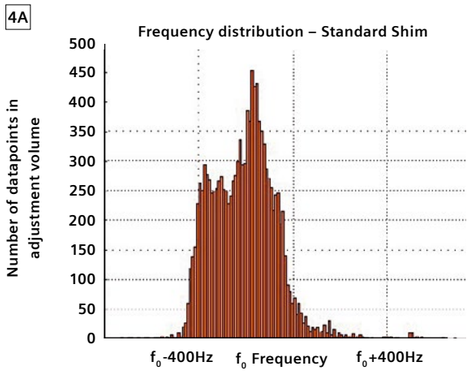

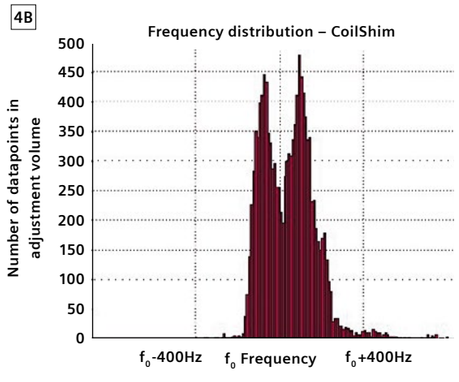

4 Histogram of frequency shift distribution relative to f_0 in Hz without **(4A)** and with CoilShim **(4B)**.

The improved field homogeneity is beneficial for all MR imaging studies in the head and neck. Applications which require a highly homogenous field, for example fat saturated or SPAIR images, or EPI-based imaging, benefit in particular from local shimming. Figures 5 and 6 show typical image examples obtained in several volunteers of different physical constitution. Figure 5 shows T1-weighted, fat saturated TSE images of the c-spine, Figure 6 illustrates the benefits of CoilShim in T2-weighted TSE images obtained with SPAIR preparation pulses. An axial T2-weighted BLADE image with SPAIR preparation pulses is shown in Figure 7. All examples show that more homogeneous fat saturation

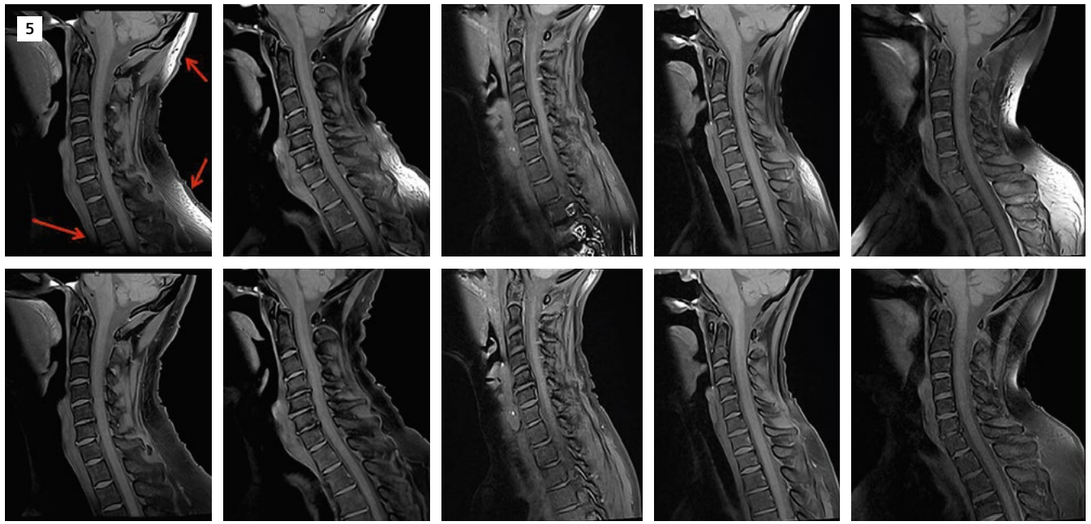

5 T1-weighted TSE images with fat saturation in five different volunteers. Using CoilShim (lower row) improved the fat saturation not only within the vertebrae but also in the posterior areas. The contrast between vertebrae and disk is also improved.

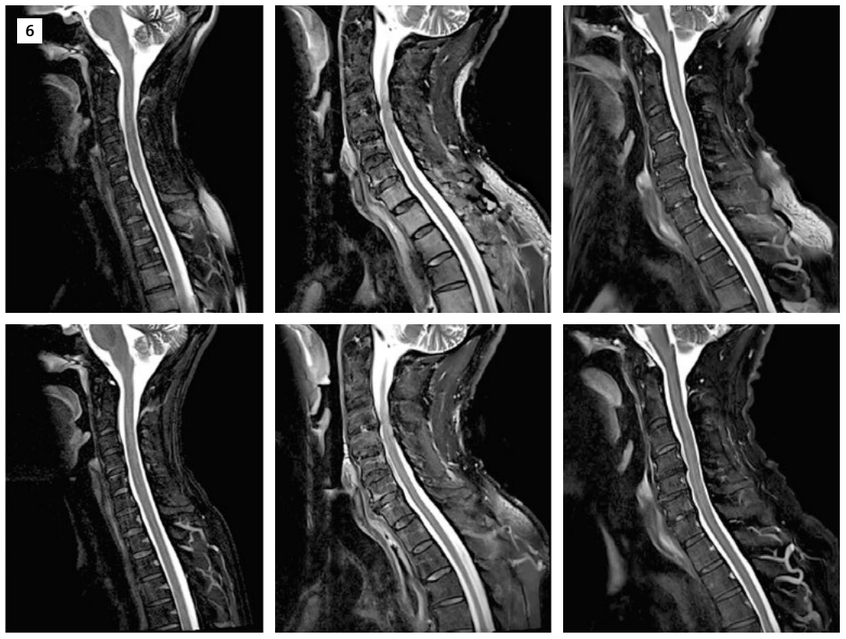

6 T2-weighted TSE images with SPAIR fat saturation in three different volunteers. Note the intensity gradient within the vertebrae without CoilShim (upper row). The image with active CoilShim on the right shows better homogeneity within the vertebrae and less contribution of unsaturated fatty tissue.

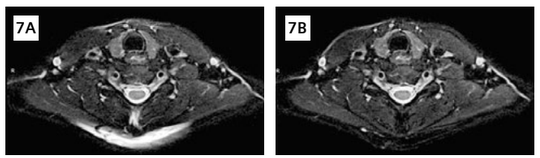

7 T2-weighted BLADE images with SPAIR fat saturation. The same imaging protocol was used with **(7A)** and without **(7B)** CoilShim. The fat saturation is more homogeneous when CoilShim is active.

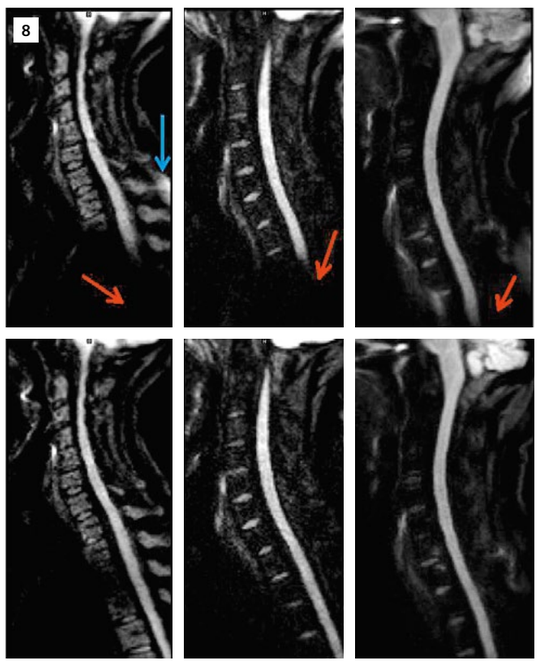

7 RESOLVE images of the c-spine with b=600 mm/s² in three volunteers. Note the lack of signal (red arrow) in the spinal canal when measured without CoilShim (upper row). Fat saturation is also more consistent (blue arrow).

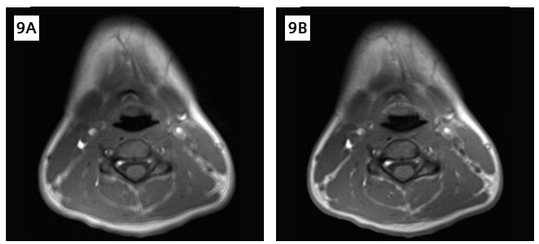

9 Radial sequences like the StarVIBE also benefit from higher field homogeneity. **(9A)** was measured without CoilShim, **(9B)** with active CoilShim. Note the increased image sharpness with CoilShim.

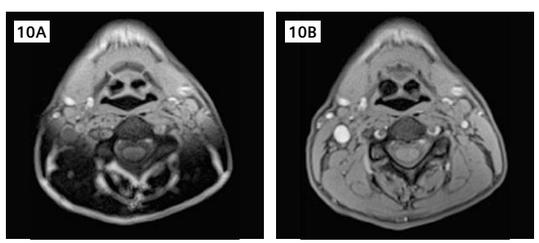

10 T1-weighted StarVibe images acquired in the neck. CoilShim **(10B)**, can correct the field distortions which caused a shift in the frequency spectrum, inducing water saturation and corrupting image quality.

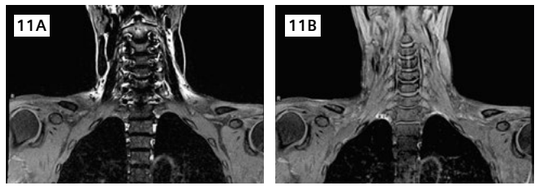

11 In rare cases, the field inhomogeneities at the border between neck and thorax are so severe, that the frequency is shifted. In these extreme examples, CoilShim (11B) also helps to mitigate the effects.

can be achieved with CoilShim. This in turn facilitates better lesion differentiation, in particular in the lower vertebrae.

Figure 8 shows RESOLVE diffusion-weighted images with a b-value of 600 mm/s² with and without CoilShim. Until now the display of the entire spinal canal was challenging, with CoilShim it becomes feasible to follow the spinal canal over the whole field-of-view.

Imaging methods which employ radial trajectories, for example the StarVIBE sequence, or methods such as TrueFISP, which demand a high field uniformity, also benefit from CoilShim technology and produce sharper or more homogeneous images. Figure 9 compares StarVIBE images obtained with and without CoilShim. Less homogeneous B_0 fields broaden the frequency spectra, leading to a shift in the readout direction. Since radial sequences sample *k*-space not in one, but in various directions, any off-resonance dephasing shift effect is propagated into a different direction, leading to blurred images. Larger variations in B_0 homogeneity can cause frequency shifts, which in turn lead to a degradation in image contrast, as shown in Figure 10 for a StarVIBE, and in Figure 11 for a TSE acquisition. Such issues can be avoided when using CoilShim.

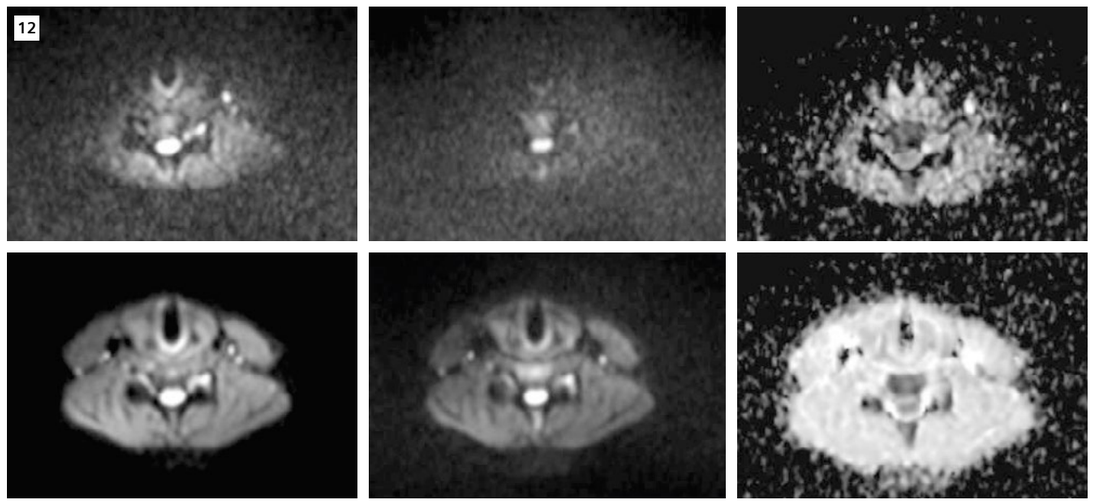

12 Combining CoilShim with SliceAdjust leads to significant image quality improvements in diffusion-weighted imaging. Less distortions and better spatial fidelity, significantly higher SNR for all b-values provides a new level of diagnostic reliability. The same slice is compared without CoilShim and SliceAdjust (upper row) and with active CoilShim and SliceAdjust (lower row). From left to right: b=50 s/mm², b=800 s/mm², ADC.

In combination with SliceAdjust, CoilShim technology allows for robust diffusion-weighted imaging (DWI) in the neck area. In the past, DWI imaging of the c-spine or neck soft tissue was challenged by distortions, low signal intensity and artefacts. On enabling the BioMatrix Tuners, the image quality can be improved significantly. Figure 12 illustrates the advantages of CoilShim and SliceAdjust when activated in a DWI image of the neck.

Practical tips

CoilShim is designed to optimize, in particular, the field homogeneity in the cervical spine. Therefore, it works best when imaging the cervical spine, especially in sagittal slice orientations. However, the whole neck area benefits when using CoilShim, although there are some physical limitations. First of all, as the CoilShim elements are located for safety reasons in the lower part of the Head/Neck coil, the scope of the feature is regionally restricted. For this reason, a drop in B_0 field homogeneity in the vicinity of the anterior part of the neck or the chin area may be observed. This effect may be manifested, as shown in Figure 13 for example, by inhomogeneous fat saturation in the chin area due to the regional limitations of the CoilShim field. The same applies to the shoulders, since the CoilShim elements cannot cover the entire shoulder region. This is shown in Figure 14. Another occasionally-observed effect is a frequency change in the t-spine next to the lung, seen usually in coronal images. As CoilShim optimizes the c-spine and cannot reach the vertebrae of the t-spine, the B_0 field

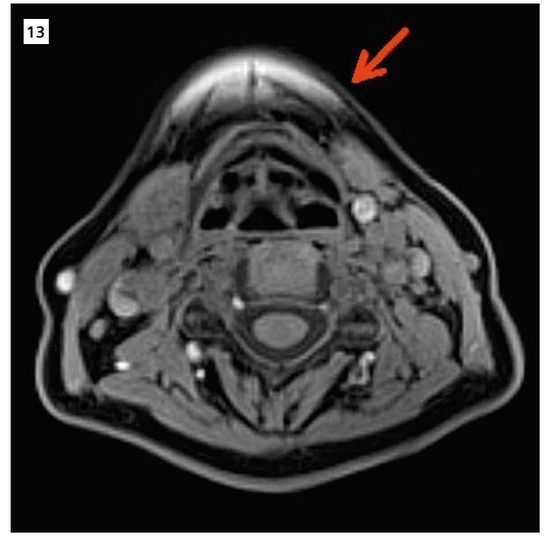

13 Anterior regions like the chin cannot be reached by CoilShim, which is located in the posterior neck coil region. Typically, in such cases, small regions with insufficient fat saturation are observed.

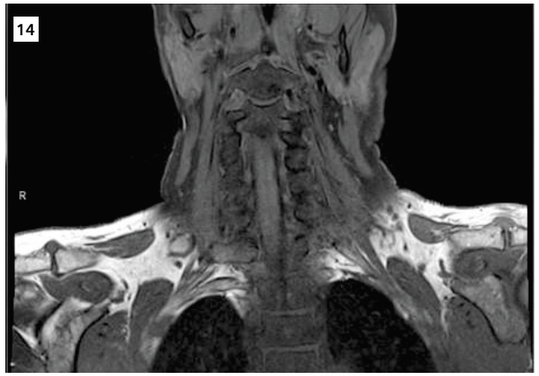

14 The local effectiveness of the CoilShim elements can lead to less efficient fat saturation in the lateral shoulder area.

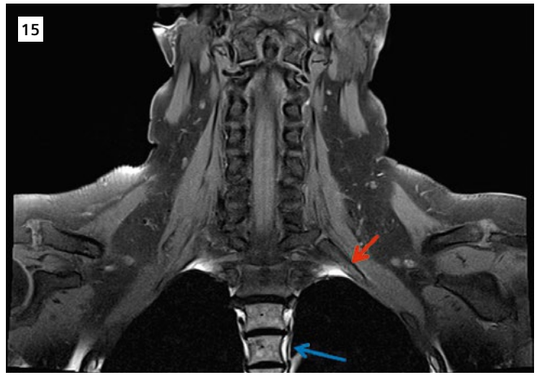

15 Typical lung-tip artefact (red arrow) and water saturation (blue arrow) in the t-spine. Note the homogeneous fat saturation in the neck/ shoulder area.

is dominated by the lung, which might lead to lower field homogeneity with degradations in image quality in the t-spine as shown in Figure 15. The same image also shows the so called lung-tip artefact, which originates from local field distortions, leading to a less efficient fat saturation in a small area around the lung apex.

Summary

CoilShim addresses field disturbances within the head and neck region by local, patient-adapted shim currents. This helps to homogenize the static magnetic field in this region. Thereby the image quality can be improved. Typical benefits include more homogeneous fat saturation, less blurring in radial sequences and more signal with diffusion weighted imaging. Since CoilShim is based on new hardware and transmit pathways, it is currently only available with the BioMatrix Head/Neck coils. Nonetheless, this new technology might also be useful to improve B_0 homogeneity in other body regions in the future.

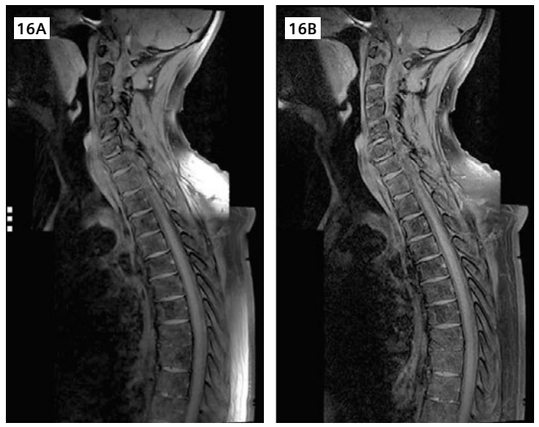

16 Composing for whole-spine representations also benefits from CoilShim **(16B).**

Contact

Miriam Keil
Siemens Healthcare GmbH
HC DI MR R&D SYS APPL

Post Box 91050
91050 Erlangen
Germany
Phone: +49 (9131) 84-4671
miriam.keil@siemens-healthineers.com


Miriam R. Keil


Jörg Rothard


Carmel Hayes

Slice Specific Shimming Improves the Image Quality of Whole-Body Diffusion-Weighted Examinations at 3T

Zhang Haibo[1]; Xue Huadan[2]; Alto Stemmer[3]; Liu Hui[4]; Stephan Kannengiesser[3]; Berthold Kiefer[3]; Jin Zhengyu[2]

[1] Department of Radiology, China-Japan Friendship Hospital, Beijing, China
[2] Department of Radiology, Peking Union Medical College Hospital, Peking Union Medical College and Chinese Academy of Medical Sciences, Beijing, China
[3] MR Application-Predevelopment, Siemens Healthcare, Erlangen, Germany
[4] MR Collaboration, Siemens Healthcare, Shanghai, China

Current whole-body diffusion-weighted imaging

Whole-body diffusion-weighted imaging (WBDWI) is considered a powerful clinical tool to aid the radiologist in the detection, characterization, and treatment-response monitoring of tumors [1, 2]. It has been increasingly used in the evaluation of multiple myeloma, lymphoma, and skeletal metastases [3–8]. Being a measure of the microscopic water motion, WBDWI provides a quantitative way of evaluating the tissue cellularity using the apparent diffusion coefficient (ADC). For example, whole-body magnetic resonance imaging including WBDWI is sensitive to multiple myeloma, especially in the case of diffuse bone marrow infiltration [9]. The combination of WBDWI with Fluorodeoxyglucose Positron Emission Tomography (FDG-PET) may provide a multi-parametric assessment of tumors due to complementary imaging principles, where diffusion-weighted imaging (DWI) can support the radiologist to evaluate the tumor cellularity and the FDG-PET assesses the tumor metabolism [10].

At present it is challenging to meet the clinical demands for image quality with WBDWI at 3 Tesla. The signal-to-noise ratio (SNR) is increased at 3T, but it is still a challenge to perform WBDWI due to the drawback of single-shot echo planar imaging (EPI) acquisition and the stronger susceptibility effects, which lead to stronger geometric distortions and poor fat-suppression performance in specific body regions such as the neck. The distortions Δd in EPI are proportional to the physical field-of-view (FOV) in the phase-encoding direction (FOV_{PE}), the echo spacing Δt_{PE}, and the local off-resonance ΔB_0 ($\Delta d \sim FOV_{PE} \times \Delta t_{PE} \times \Delta B_0$).

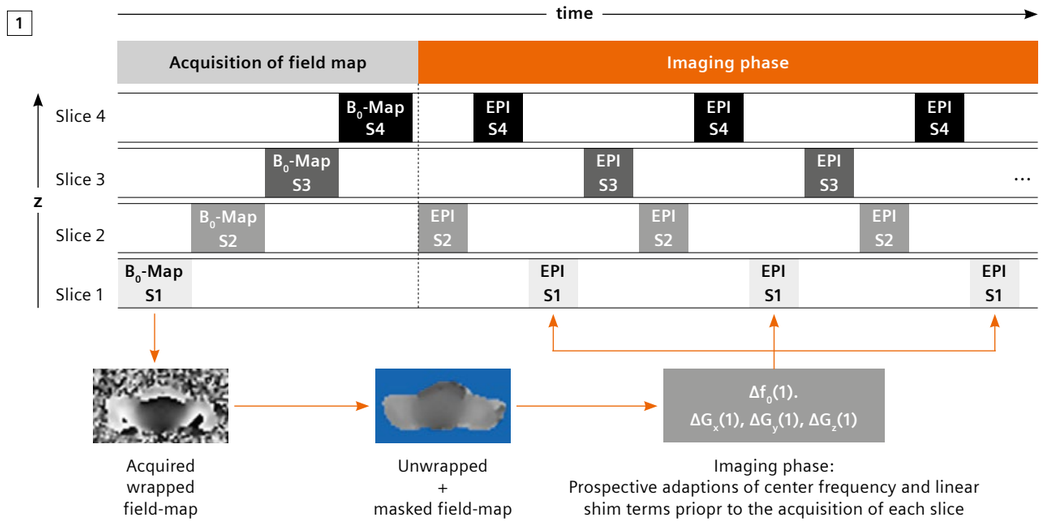

1 Schematics of the prototype of a slice specific adjustment sequence.

Recent technical developments in DWI acquisition such as readout segmented EPI [11, 12], other multi-shot [13] and zoomed techniques [14, 15] have shown improvements with less geometric distortion and higher image quality from the perspective of reducing Δt_{PE} or FOV_{PE}. However, the above techniques are not clinically feasible for whole-body imaging because of longer acquisition time, FOV restrictions, or sensitivity to motion.

Slice specific adjustment

Several past studies have shown the feasibility of reduced susceptibility artifact by dynamically updating optimized shim settings for each individual slice in a multi-slice acquisition [16]. Another study using slice-dependent adjustment has also shown improved image quality in 3T breast DWI [17]. However, its advantage to WBDWI is still unknown. The approach described here is to use slice specific adjustments[1] for WBDWI, where a 2D multi-echo gradient echo (GRE) sequence preceding the WBDWI EPI scan is used to acquire a B_0-map for each imaging slice. From the B_0-map an optimal center frequency and linear shim terms are determined for each imaging slice. Center frequency and gradient offsets are then updated before the acquisition of each EPI imaging slice in real time. In a recent study, its performance was evaluated, comparing slice specific adjustment to a conventional pre-scan based shimming technique (3D Shim) [18].

For the 3D Shim protocol, one set of shim terms up to 2nd order is used for the entire slice stack of each patient table position, and the acquisition of the field map is included in the automatic scanner adjustment, which takes approximately 33 seconds per station (35 slices per station). Additionally, a single center frequency is determined in a separate frequency adjustment. Center frequency and shim currents are set once prior to the EPI scan.

For the slice specific adjustment protocol, the patient-specific 3D Shim procedure in the automatic scanner adjustment is disabled. The acquisition of the field map is integrated into the single-shot DWI EPI sequence. This prototype sequence first acquires 2D multi-gradient-echo images for each imaging slice with its FOV and orientation adapted from the respective imaging slice. The echo-time difference of the first and last echo is chosen such that fat and water are in-phase. Then a phase difference image is calculated from these two echoes. The remaining processing of the field map data is done in 3D and comprised phase unwrapping, background masking and a calibration to avoid global 2π offsets after unwrapping. For the dynamic shimming, a 2D plane is fitted to each field map slice to determine the center frequency and gradient offsets (1st order shim terms). Center frequency and gradient offsets are then updated before the acquisition of each EPI imaging slice in real time (Fig. 1). The time for the acquisition of the field map is approximately 540 ms per slice, or 19 s for a 35 slices station. Processing time of the field map is negligible.

Clinical evaluation

The evaluation of the slice specific adjustment technique for WBDWI in comparison to the conventional 3D Shim was performed at Peking Union Medical College Hospital. The slice specific adjustment and the 3D Shim WBDWI acquisitions with the exact same scan parameters were performed sequentially, and the impact of different shimming techniques on the image quality and detectability of conspicuous lesions were quantitatively analyzed and evaluated. Body-region-dependent signal-to-noise ratio (SNR), body-region-dependent shimming parameters, image quality, and the number of suspicious lesions were compared in 2 volunteers and 29 patients with suspected plasma-disorder. The results were as follows:

1. SNR
Two volunteers' position-dependent SNR ratio of slice specific adjustment over 3D Shim showed a significant SNR improvement with slice specific adjustment in the neck region, and a comparable SNR in other body regions. For the neck region, none of the 29 patients showed obvious signal loss with slice specific adjustment, while 25 patients showed partial to complete signal loss with 3D Shim scanning (Fig. 2).

2. Position-dependent slice specific adjustment parameters
The position-dependent slice specific adjustment parameters, center frequency shift, and linear frequency shift in phase-encoding direction, deviated significantly from the corresponding values of the 3D Shim settings only in the neck region, while they were comparable in the other body regions.

3. Image quality
Spatial displacement of DWI images was quantified by comparison with reformatted T2 SPACE images. This displacement was evaluated from cervical to coccyx vertebrae, excluding the neck region with signal loss (Figs. 2, 3). The mean absolute spatial displacement of the spine was 3.89 mm for slice specific adjustment and 7.21 mm for 3D Shim, respectively. The slice specific adjustment technique showed a significantly better illustration of the body shape than 3D Shim WBDWI.

4. Lesion detection assessment
Visual inspection of slice specific adjustment and 3D Shim DWI images side by side showed that the same lesions could be observed with both techniques in the thorax, abdomen and pelvis regions, while 24 of 72 lesions visible in slice specific adjustment DWI images of the neck region were not visible in 3D Shim DWI images; all lesions observed in 3D Shim DWI were also visible in slice specific adjustment DWI images.

Discussion

Signal loss is very common in the neck region of conventional 3D Shim WBDWI because there the B_0 varies rapidly along the head-foot direction caused by the sudden change of the body shape. Especially when a body station covers the neck and part of the shoulder region, the 3D Shim adjustment may be insufficient since one single setting of resonance frequency and shim terms is not able to homogenize the B_0 field in the whole volume. In this study, the neck region showed a larger variation of center frequency shift and linear frequency shift in the phase-encoding direction than other body regions, and at the same time the lowest image quality of 3D Shim images, which supports this hypothesis. By applying a slice-based individual center frequency and gradient offset setting, the slice specific adjustment technique produced improved SNR and reliable image quality in the neck region and therefore outperforms 3D Shim. In other body regions such as thorax, abdomen and pelvis, there were no significant differences between slice specific adjustment and 3D Shim WBDWI for lesions and muscle.

WBDWI provides a global assessment of whole-body tumor burden by visually assessing the signal intensity distribution on maximum intensity projections (MIPs) from high-b-value images. But practically the whole-body images are acquired with multiple patient table positions, and are then composed to show the whole-body view (Fig. 3). Therefore, the signal homogeneity across different body parts is quite important, and lesions spanning images from adjacent patient table positions might be missed or misidentified as a result of large signal differences between these images. The image quality evaluation showed that the slice specific adjustment technique produced a smoother signal transition between adjacent patient table positions than the 3D Shim technique.

It is possible to further reduce the remaining distortions significantly with a recent extension of the slice specific adjustment prototype sequence as described in [19]. The modification combines the prospective slice-specific center-frequency adjustment and 1st order shimming with retrospective distortion correction based on the field-map method [20]. The field-map method uses a measured field-map to undo the distortion on a pixel-wise scale during post-processing. In the combined method, the field-map needed for the distortion correction is not re-measured after center frequency adjustment and shimming but calculated from the field-map measured at the beginning and the known frequency and shim settings. It therefore does not prolong the acquisition time. It is a matter of further evaluation to enroll new patients to test the slice specific adjustment method together with retrospective distortion correction.

Short TI Inversion Recovery (STIR) fat suppression, which was used here, leads to lower SNR compared with chemical-shift-based fat suppression methods since water signal which is also inverted by the inversion pulse is not fully recovered at excitation time. Chemical shift based fat suppression techniques, however, are very sensitive to B_0 inhomogeneity [21, 22], so that the image quality can be degraded by fat ghosting or water suppression. As slice specific adjustment helps to significantly reduce the B_0 inhomogeneity, chemical shift based fat suppression techniques might provide an efficient fat suppression from head to toe. Chemical shift based fat suppression techniques

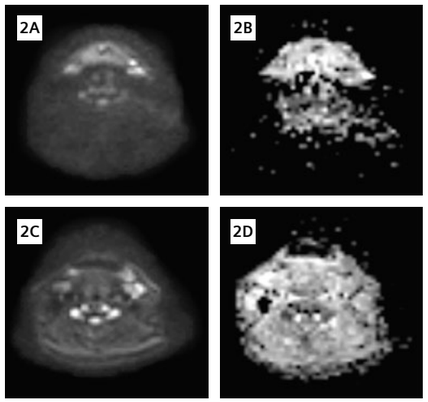

2 Transversal view of the selected single slice of the neck of the same patient: **(2A)** 3D Shim DWI (b = 800 s/mm²), **(2B)** ADC map of 3D Shim DWI (b = 800 s/mm²), **(2C)** slice specific adjustment DWI (b = 800 s/mm²) and **(2D)** ADC map of slice specific adjustment DWI (b = 800 s/mm²). **2A, B** showed massive signal loss in the neck region of 3D Shim DWI, however slice specific adjustment technique improved the image quality of the neck region obviously.

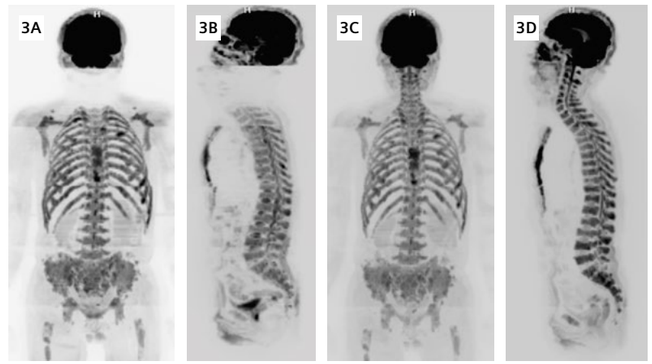

3 Maximum intensity projections (MIPs) with inverted grayscale from high-b-value WBDWI images. **(3A, B)** 3D Shim WBDWI images. The image quality of WBDWI was remarkably improved on 3T MRI. However, in the neck region a strong image quality deterioration can be observed. **(3C, D)** Slice specific adjustment WBDWI images. Compared with 3D Shim WBDWI, slice specific adjustment WBDWI showed artifact-free images.

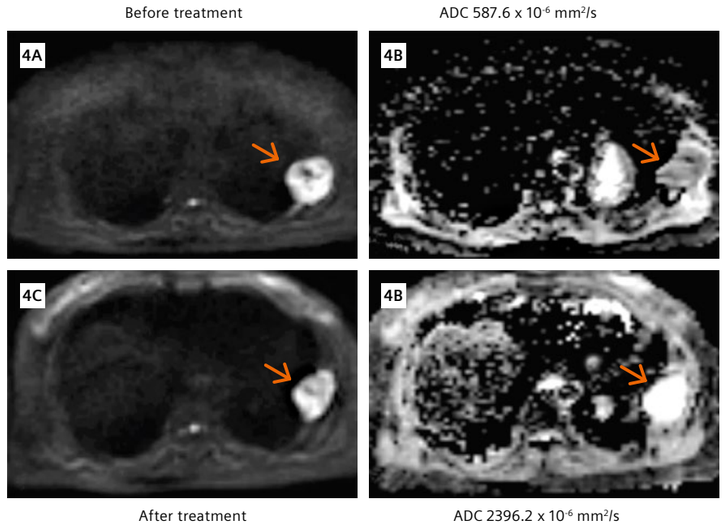

4

57-year-old female patient with multiple myeloma on the left chest wall (arrows). **(4A, B)** show a lesion with high signal on DWI (b = 800 s/mm²) image and low ADC value (587.6 × 10^{-6} mm²/s) before treatment. **(4C, D)** show that the lesion still existed five months later after treatment, but ADC value was much higher than before. The change in ADC corresponds with the clinical results.

like Spectral Adiabatic Inversion Recovery (SPAIR) are not compatible with slice specific adjustment as they exploit non-selective RF-pulses. Instead, slice selective water excitation could be used with slice specific adjustment. The inherently higher SNR of water excitation may allow reducing the number of averages and hence the total acquisition time, and it merits evaluation in a clinical setting.

Conclusion

The slice specific adjustment technique is an effective method to reduce the negative impact of susceptibility effects on whole-body diffusion-weighted imaging at 3T, as supported by the apparent improvement in image quality, as well as improved SNR in the neck region. Compared with the 3D Shim technique, slice specific adjustment showed improved support for the clinician to detect suspicious lesions in the neck region. The slice specific adjustment technique has entered the clinical arena, improving WBDWI. Slice specific adjustment and its future refinements may further improved radiologist ability to improve accuracy of lesion assessment and monitoring treatment response (Fig. 4).

References

[1]*Padhani AR, Liu G, Koh DM, et al. Diffusion-weighted magnetic resonance imaging as a cancer biomarker: consensus and recommendations. Neoplasia 2009;11(2):102–125.*

[2]*Padhani AR, Koh DM, Collins DJ. Whole-body diffusion-weighted MR imaging in cancer: current status and research directions. Radiology 2011;261(3):700–718.*

[3]*Attariwala R, Picker W. Whole body MRI: improved lesion detection and characterization with diffusion weighted techniques. J MagnReson Imaging 2013;38(2):253–268.*

[4]*Petralia G, Padhani A, Summers P, et al. Whole-body diffusion-weighted imaging: is it all we need for detecting metastases in melanoma patients? EurRadiol. 2013;23(12):3466–3476.*

[5]*Brioli A, Morgan GJ, Durie B, Zamagni E. The utility of newer imaging techniques as predictors of clinical outcomes in multiple myeloma. Expert RevHematol 2014;7(1):13–16.*

[6]*Mayerhoefer ME, Karanikas G, Kletter K, et al. Evaluation of diffusion-weighted MRI for pretherapeutic assessment and staging of lymphoma: results of a prospective study in 140 patients. Clin Cancer Res 2014;20(11):2984–2993.*

[7]*Littooij AS, Kwee TC, Barber I, et al. Whole-body MRI for initial staging of paediatric lymphoma: prospective comparison to an FDG-PET/CT-based reference standard. EurRadiol 2014;24(5):1153–1165.*

[8]*Klenk C, Gawande R, Uslu L, et al. Ionising radiation-free whole-body MRI versus (18)F-fluorodeoxyglucose PET/CT scans for children and young adults with cancer: a prospective, non-randomised, single-centre study. Lancet Oncol 2014;15(3):275–285.*

[9]*Zamagni E, Nanni C, Patriarca F, et al. A prospective comparison of 18F-fluorodeoxyglucose positron emission tomography-computed tomography, magnetic resonance imaging and whole-body planar radiographs in the assessment of bone disease in newly diagnosed multiple myeloma. Haematologica.2007; 92(1):50-55.*

[10]*Schmidt H, Brendle C, Schraml C, et al. Correlation of simultaneously acquired diffusion-weighted imaging and 2-deoxy-[18F] fluoro-2-D-glucose positron emission tomography of pulmonary lesions in a dedicated whole-body magnetic resonance/positron emission tomography system. Invest Radiol. 2013;48(5):247-55.*

[11]*Bogner W, Pinker-Domenig K, Bickel H, et al. Readout-segmented echo-planar imaging improves the diagnostic performance of diffusion-weighted MR breast examinations at 3.0 T. Radiology 2012;263(1):64–76.*

[12]*Porter DA, Heidemann RM. High resolution diffusion-weighted imaging using readout-segmented echo-planar imaging, parallel imaging and a two-dimensional navigator-based reacquisition. Magn Reson Med. 2009;62(2):468–475.*

[13]*Chen NK, Guidon A, Chang HC, et al. A robust multi-shot scan strategy for high-resolution diffusion weighted MRI enabled by multiplexed sensitivity-encoding (MUSE). Neuroimage 2013;72:41–7.*

[14]*Riffel P, Michaely HJ, Morelli JN, et al. Zoomed EPI-DWI of the head and neck with two-dimensional, spatially-selective radiofrequency excitation pulses, EurRadiol 2014; 24(10):2507–12.*

[15]*Thierfelder KM, Scherr MK, Notohamiprodjo M, et al. Diffusion-weighted MRI of the prostate: advantages of Zoomed EPI with parallel-transmit-accelerated 2D-selective excitation imaging. EurRadiol 2014; 24(12):3233–41.*

[16]*Morrell G, Spielman D. Dynamic shimming for multi-slice magnetic resonance imaging. MagnResonMed 1997;38(3):477–83.*

[17]*Lee SK, Tan ET, Govenkar A, et al. Dynamic slice-dependent shim and center frequency update in 3 T breast diffusion weighted imaging. MagnReson Med 2014;71(5):1813–1818.*

[18]*Zhang H, Xue H, Stemmer A, et al. Integrated Shimming Improves Lesion Detection in Whole-Body Diffusion-Weighted Examinations of Patients With Plasma Disorder at 3 T. Investigative Radiology, 2015 [Epub ahead of print]*

[19]*Stemmer A and Kiefer B. Combination of integrated slice-specific dynamic shimming and pixel-wise unwarping of residual EPI distortions. Proc. Intl. Soc. Mag. Reson. Med. 2015; 23:3729.*

[20]*Jezzard P and Balaban RS. Correction for geometric distortion in echo planar images from B_0 field variations. Magnetic Resonance in Medicine 1995; 34:65–73.*

[21]*Takahara T, Imai Y, Yamashita T, et al. Diffusion weighted whole body imaging with background body signal suppression (DWIBS): technical improvement using free breathing, STIR and high resolution 3D display. Radiat Med. 2004;22:275–282.*

[22]*Thomas C. Kwee, Taro Takahara, Reiji Ochiai, et al. Diffusion-weighted whole-body imaging with background body signal suppression (DWIBS): features and potential applications in oncology". EurRadiol. 2008; 18:1937–1952*

[23]*Messiou C, Giles S, Collins D J, et al. Assessing response of myeloma bone disease with diffusion-weighted MRI [J]. The British journal of radiology, 2012, 85(1020): e1198–203.*

[24]*Giles S L, Messiou C, Collins D J, et al. Whole-body diffusion-weighted MR imaging for assessment of treatment response in myeloma [J]. Radiology, 2014, 271(3): 785–94.*

Contact

Professor Xue Huadan, M.D.
Department of Radiology

Peking Union Medical College Hospital,
Peking Union Medical College and Chinese Academy of Medical Sciences

Shuaifuyuan 1#, Wangfujing Street,
Dongcheng District
Beijing, China, 100730
bjdanna95@hotmail.com

Zhang Haibo, M.D.
Department of Radiology

Chinese-Japan Friendship Hospital

Yinghuayuan East Street #2
Chaoyang District
Beijing, China, 100029
zhb_hello@163.com

Reprinted from BioMatrix and syngo MR XA11 special issue

Whole-Body Dot Engine: First Clinical Experience with Automated Chest, Abdomen and Pelvis Examinations

Cäcilia S. Reiner[1]; Bernd Kuehn[2]; Daniel Nanz[1]; Tim Finkenstädt[1]; Berthold Kiefer[2]; Gustav Andreisek[1]

[1] Institute of Diagnostic and Interventional Radiology, University Hospital Zurich, University of Zurich, Switzerland
[2] Oncology Application Predevelopment, Siemens Healthcare GmbH, Erlangen, Germany

Introduction

Time and cost efficiency are among the major challenges in clinical magnetic resonance imaging (MRI), mainly driven by the funding cuts in most health care systems [1]. At the same time, there is an increasing overall demand for a higher quality of MRI exams with regard to comparability, i.e. important for primary and/or follow-up studies in oncologic patients. To address these challenges, several vendors and researchers are developing automated scanner workflows for clinical MRI systems. The hypothesis is that these workflows allow a standardized and time-efficient use and provide a robust image quality at only little user interaction. The Whole-Body Dot Engine was developed to meet these needs for multi-station MRI exams of chest, abdomen, pelvis, and even the whole body. Potential indications of multi-station body MRI exams are oncologic staging or follow-up, rheumatic disease and evaluation of myopathies.

MRI technique

The Whole-Body Dot Engine automatically detects landmarks like lung apex, lung recesses, diaphragm, liver apex, iliac bone on a fast low-resolution whole-body scout, which is acquired during moving table. Based on this scout the body regions selected for scanning, namely chest, abdomen and/or pelvis are automatically segmented (Fig. 1). With the information of the segmentation the sequence parameters (field-of-view [FOV] and number of slices) are automatically adjusted in order to ensure proper coverage of the body regions of interest. Additionally, the Whole-Body Dot Engine uses an anticipated patient's breath-hold capacity to automatically adjust the imaging protocols in body regions where breath-hold is required to generate optimal image quality. The user can configure which parameters shall be adjusted for each protocol individually. In our protocol, base resolution was used for this purpose in 3D sequences, and number of concatenations was used in 2D sequences. We set the breath-hold capacity to 20 seconds. The protocol included a coronal and transverse T2-weighted single-shot turbo-spin-echo sequence (HASTE) acquired in breath-hold technique, transverse single-shot diffusion-weighted echo-planar imaging with slice-specific shim optimization (EPI-DWI, iShim [2]) in free-breathing, and a transverse T1-weighted pre- and post-contrast 3D spoiled gradient-echo 2-point Dixon (VIBE) sequence acquired in breath-hold technique pre- and post-contrast (delay: chest 35 s, abdomen 70 s, pelvis 90 s after injection of 0.1 mmol/kg bodyweight gadoterate meglumine, Dotarem, Guerbet) (Table). Imaging after contrast-injection was timed by using automated bolus detection. The cranio-caudal coverage per block was adjusted to 400 mm.

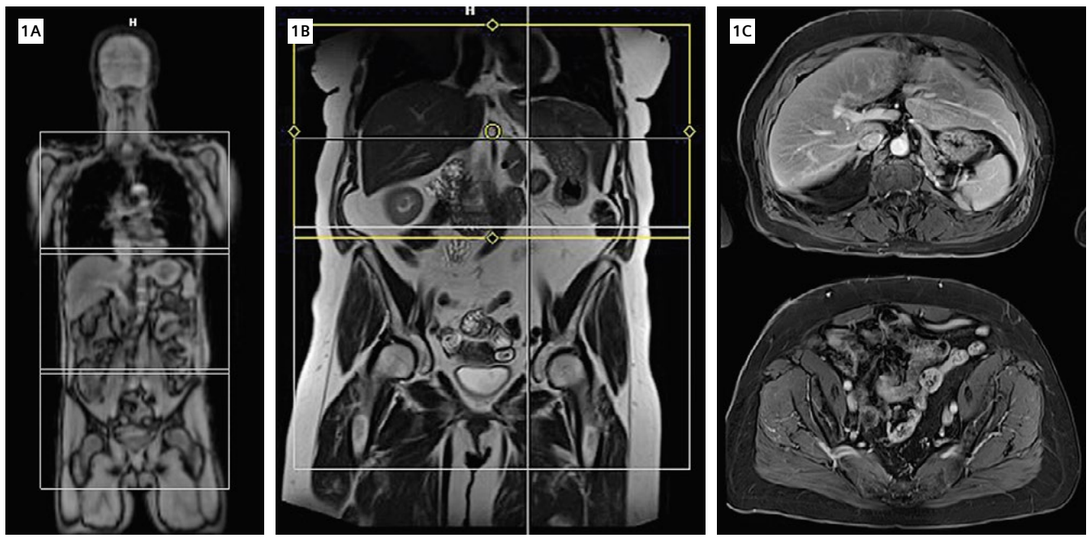

1 **(1A)** Fast low resolution whole-body scout with automatically segmented abdomen and pelvis for multi-station scanning. **(1B)** Coronal T2 single-shot turbo-spin-echo images with automatically segmented abdomen and pelvis split into two blocks for the transverse T1-weighted sequence **(1C)** with an acquisition time of 15 s for each lying within the preset 20-second breath-hold capacity. The cranio-caudal coverage per block is set to 400 mm with a fixed overlap of 2 cm between blocks and is adjusted to patient size and breath-hold capacity.

	T2w HASTE	T2w HASTE	iShim[1] EPI DWI	T1w VIBE Dixon without and with contrast	T1w VIBE Dixon with contrast
Scan plane	coronal	transverse	transverse	transverse	coronal
Repetition time / Echo time (ms)	1230/92	1000/60	6100/56	4.27/1.28	3.93/1.23
Flip angle (°)	160	160	90	12	12
Slice thickness (mm)	6	5	6	3	1,5
Spacing (mm)	1	1	1	0	0
Acquisition matrix	256 x 256	256 x 109	128 x 84	320 x 180	192 x 162
Acceleration, factor	GRAPPA, 3	GRAPPA, 3	GRAPPA, 2	CAIPIRINHA, 2	CAIPIRINHA, 6
Number of excitations	1	1	6 and 15	1	1
b-values (s/mm²)	na	na	50, 800	na	na

T1 MRI protocol.

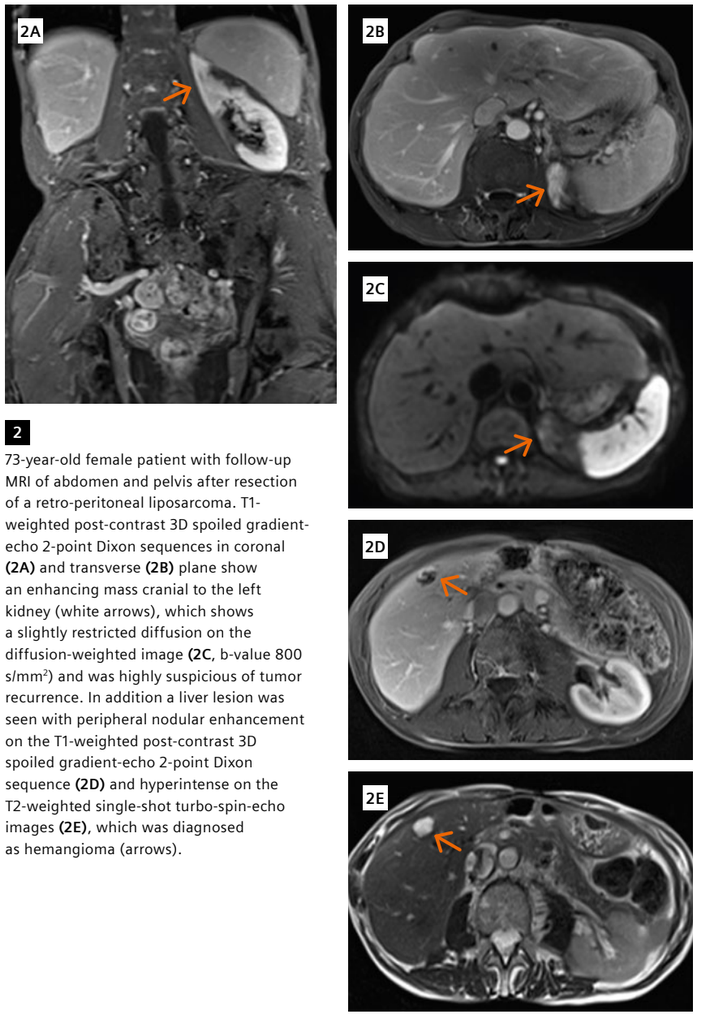

2
73-year-old female patient with follow-up MRI of abdomen and pelvis after resection of a retro-peritoneal liposarcoma. T1-weighted post-contrast 3D spoiled gradient-echo 2-point Dixon sequences in coronal **(2A)** and transverse **(2B)** plane show an enhancing mass cranial to the left kidney (white arrows), which shows a slightly restricted diffusion on the diffusion-weighted image **(2C**, b-value 800 s/mm²) and was highly suspicious of tumor recurrence. In addition a liver lesion was seen with peripheral nodular enhancement on the T1-weighted post-contrast 3D spoiled gradient-echo 2-point Dixon sequence **(2D)** and hyperintense on the T2-weighted single-shot turbo-spin-echo images **(2E)**, which was diagnosed as hemangioma (arrows).

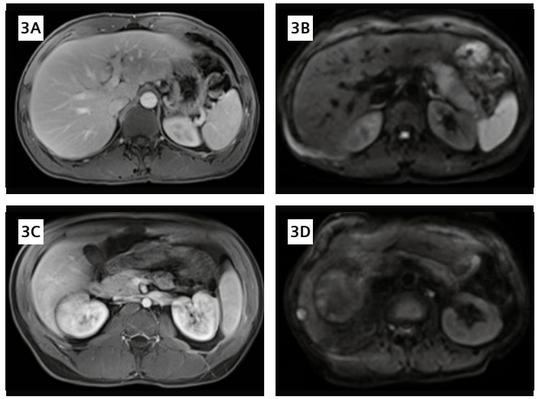

3 T1-weighted post-contrast 3D spoiled gradient-echo 2-point Dixon sequences with excellent image quality **(3A)** and with mild respiratory motion artifacts **(3B)**. Single-shot diffusion-weighted echo-planar imaging sequence with slice-specific shim optimization with excellent image quality **(3C)** and with mild motion artifacts **(3D)**.

We chose a rather short scan protocol without dynamic acquisitions in a focus region (e.g. liver), because we wanted a fast and straightforward protocol for general oncologic imaging comparable to computed tomography. We used this scan protocol for oncologic follow-up imaging of abdomen and pelvis or chest, abdomen, and pelvis.

Patients

20 patients (9 females, 11 males; mean age 52 years, range 21–79 years) were examined on a 3T MRI scanner (MAGNETOM Skyra, Siemens Healthcare) using the Whole-Body Dot Engine. Multi-station exams were performed on 11 patients for oncologic follow-up, in 2 for primary staging, and in 7 for tumor screening. The clinical diagnosis of these patients was: genitourinary malignancy (n=8), sarcoma (n=3), gastrointestinal malignancy (n=1), poly-posis syndromes (n=2), and chronic abdominal pain (n=6). In 18 patients abdomen and pelvis were scanned and in 2 patients chest, abdomen and pelvis. An image example is given in Figure 2. To validate whether our straightforward protocol results in an acceptable duration of this multi-station MRI, patients scored their satisfaction with exam duration on a visual analogue scale from 0 (not acceptable, too long) to 10 (ideal exam duration).

Image quality

The scans were evaluated for overall image quality (IQ) (5 = excellent, 4 = good, 3 = moderate, 2 = poor, 1 = non-diagnostic) and artifacts (5 = no artifacts, 4 = mild artifacts, 3 = moderate artifacts, 2 = severe artifacts, 1 = non-diagnostic) on a 5-point scale by a board-certified abdominal radiologist with 8 years of experience. The image acquisition time was noted, as well as whether the coverage of the targeted body region was complete.

In all but one patient (19 of 20, 95%), the selected body regions were covered completely by the automated algorithm. An exception was the DWI, which showed markedly reduced signal in the sub-diaphragmatic part of the right liver in four patients (4 of 20, 20%), which impaired diagnostic ability of DWI in these liver parts.

The mean score for overall IQ was 4.7 ± 0.47 standard deviation (SD) and for artifacts overall was 4.4 ± 0.5 SD. Mild to moderate respiratory motion artifacts were seen in three patients (3 of 20, 15%) on T1-weighted post-contrast images with a mean IQ score of 4.8 ± 0.52 (Fig. 3). Mild motion artifacts were observed in four patients (5 of 20, 25%) on DWI with a mean IQ score of 4.75 ± 0.44. The mean examination time was 27.4 ± 6.5 min for chest, abdomen and pelvis and 21.0 ± 6.9 min for abdomen and pelvis. The mean score of patient satisfaction regarding exam duration was 6.45 ± 2.19 (median, 6) and did not correlate with scan duration.

Conclusion

MR scanning with the automated Whole-Body Dot Engine results in good to excellent image quality within a reasonable total examination time with only small patient-dependent variations. An almost 'single-button protocol' for standardized fast, reproducible, and automated workflow of chest, abdomen, and pelvis could open up new possibilities in the diagnostic process. However, further comparison studies with traditional manual scan modes need to be performed to support our preliminary experience.

Contact

Cäcilia Reiner, M.D.

Institute of Diagnostic and Interventional Radiology
University Hospital Zurich

Raemistrasse 100
8091 Zurich, Switzerland
caecilia.reiner@usz.ch

References

[1] *Andreisek G. Point-of-Care MR Imaging and how we can learn from other imaging modalities. Thoughts on a potential new strategy. MAGNETOM Flash (63) 3/2015:4-7. www.siemens.com/magnetom-world*

[2] *Stemmer A, Kiefer B. Combination of integrated slice-specific dynamic shimming and pixel-wise unwarping of residual EPI distortions. Proc Intl Soc Mag Reson Med. 2015;23:3729.*

syngo MR XA Software Line – Your New Work Environment for More Comfortable Scanning and Intuitive Image Processing

Alexander Aulesjord; Gregor Thörmer, Ph.D.
Siemens Healthineers, Erlangen, Germany

To counter falling reimbursement and increasing cost pressure many imaging facilities seek ways to both increase productivity and patient throughput. One example of these efforts can be seen directly in the continuously increasing number of patients scheduled for MRI per hour over the course of the last years.

Higher patient throughput not only increases the technologists' workload but also their expectations towards the tools available to them. The user interface (UI) to the MR scanner is arguably the most important tool that technologists have at their disposal. Most interactions with the MR scanner over the course of the examination will happen via the UI. As such, the UI can have substantial influence over how productive an MR scanner is operated. Great care should be taken such that when designing a new UI, it will be easy to navigate, task cards for scanning and processing should not overlap, and the workflow should follow the natural course of the MR examination.

It is also crucial to carefully preserve the overall functionality and the known appearance of any new software, be it in MR technology or consumer electronics, in order to make the transition to a new UI for experienced users easy.

Our new 3T MRI system, MAGNETOM Vida, introduces a completely redesigned MR UI running on a new hardware platform. Evolving from the successful *syngo* MR E11 platform, the new *syngo* MR XA software platform is a user-centric control center for patient registration, scanning, post-processing, and result distribution.

Optional dual monitor setup

Studies have shown that even standard office applications substantially benefit from a dual monitor setup, resulting in 45% easier task tracking, 32% higher performance, and 24% more comfortable use than single monitor setups [1].

To ease the work of the MR technologist in a similar manner, *syngo* MR XA software platform offers a dual monitor scanning workplace with two large 24-inch monitors with a reorganized user interface.

For a more natural scanning and viewing process, different tasks have been clearly separated: The left screen is reserved for patient registration, scanning, and protocol management, while the right screen, especially with the new MR View&GO application which encompasses reconstructions, post-processing, image quality check, and distribution of results to the PACS and other DICOM nodes (Fig. 1). This dual monitor setup, with separated scan and viewing monitors, makes for a more natural working environment in which the technologist has a complete overview of the examination and results. Constant context switches and distractions are reduced, enabling stronger focus on the patient and true multitasking for increased quality and productivity.

syngo MR XA platform builds on the established *syngo* MR E11 platform, inheriting many known features and UI elements, which makes orientation for users of the existing platform easy.

1

1 *syngo* MR XA software line offers optional dual monitor setup with two 24-inch screens. Clear task separation with image acquisition on the left-hand side and processing with MR View&GO on the right-hand side.

As shown in Figure 2, central UI elements and features on the left screen have been preserved but newly arranged on the larger monitor. Furthermore, the new layout now provides fixed positions for UI elements like the physio display and the inline display. Other useful components like the Dot Cockpit for protocol management have not been changed in their appearance. They do, however, offer the ability to be opened on the right monitor while scanning, therefore not interfering with other processes.

"The new interface is clearly structured. It is easy to get used to it."[1]

Andreas Lingg, MTRA
Tübingen University Hospital, Tübingen, Germany

[1]*The statements by Siemens' customers presented here are based on results that were achieved in the customer 's unique setting. Since there is no 'typical' hospital and many variables exist (e.g., hospital size, case mix, level of IT adoption), there can be no guarantee that other customers will achieve the same results.*

MR View&GO

MR View&GO is a dedicated MR viewer that allows viewing, routine post-processing, filming and result distribution in one comprehensive workflow with consecutive steps (Fig. 3A). As soon as a patient has been registered a corresponding MR View&GO automatically opens for the respective patient. Every scan that has been acquired and reconstructed automatically appears on the right screen in MR View&GO.

Pre-processing with Recon&GO

Powerful image pre-processing capabilities, e.g. automatic InlineSubtraction of dynamic series, InlineMPR calculation of 3D datasets or InlineComposing of multi-station exams, which are all standard, run automatically in the background. This helps to reduce the workload for the MR technologist.

2A

***syngo* MR E11**

2B

***syngo* MR XA**

2

The new workplace on the *syngo* MR XA platform evolves from *syngo* MR E11. Planning segments (orange), queue (yellow), scan parameters (purple) have kept their appearance but were newly arranged. The new layout provides fixed positions for hovering UI elements such as the physio display and the inline display (blue).

3A

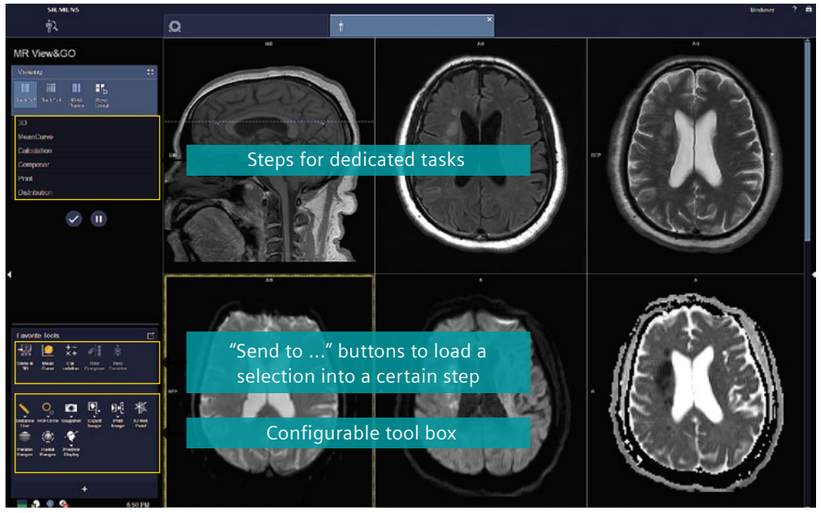

3A

MR View&GO is a dedicated viewer for MR studies, offering consecutive steps for image viewing, processing and distribution. The user can configure an individual tool box of frequently used features such as image markers, distance measurements or ROI analysis in the lower left corner. Further analysis tools can be found in so-called "corner menus" in the edges of individual image segments.

MAGNETOM Flash Special USA Edition · 02/2020

Step-by-step from quality control to distribution

Following the natural workflow, MR View&GO guides you from basic viewing and quality control towards result distribution to the PACS and other DICOM nodes (Fig. 3B). Intermediate post-processing steps which might be indicated depending on the case can be easily launched by selecting an image series and transferring it to the respective step with one mouse click.

This, for example, enables the reformatting of images in 3D as Multiplanar Reconstructions (MPR), Maximum Intensity Projection (MIP), or with a Volume Rendering Technique (VRT). Furthermore, arithmetic image analysis or the interactive extrapolation of very high b-values (up to 5000 s/mm^2) can be easily performed while the scan is running. The resulting images, for example multiplanar reconstructions of a 3D dataset, can be easily inserted to the planning segments to precisely plan subsequent scans.

To evaluate dynamically acquired contrast-enhanced image series, MR View&GO also offers a dedicated MeanCurve analysis step as a standard feature. This, for example, helps in the evaluation of a test-bolus scan, prostate DCE series (Fig. 4) or contrast-enhanced breast MRI.

In addition to InlineComposing, MR View&GO provides manual composing for complex cases to support, e.g., whole-spine, whole-body, or angiography exams.

Advanced image processing

For more advanced image processing requirements, e.g. to perform neuro perfusion and mismatch analysis (Fig. 5), dedicated applications are optionally available. These applications cover the entire radiological spectrum from neurology (MR Neurology, Neuro3D Tractography and fMRI), cardio-vascular evaluations (Cardiac Perfusion, Cardiac Flow, 4D Ventricular Function, Vascular Analysis), to oncology (Breast, Prostate, OncoCare, 3D Lesion Segmentation)[1]. Many of these only require minimal user interaction: for example, flow quantification is fully automated after a vessel has been selected for analysis. This allows preparing MR datasets ready-to-read, saving one of the most precious resources: the radiologists' time. Depending on the institutional setup and needs, it is also possible to operate a satellite console with a shared database for basic (MR View&GO) and advanced processing purposes (Fig. 6). This configuration has the particular advantage that licenses for advanced applications are shared between the acquisition workplace and the satellite console.[2]

3B

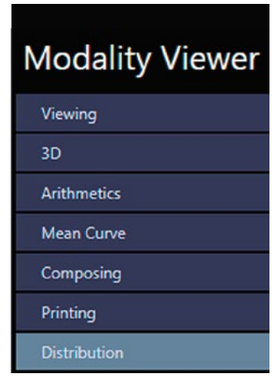

3B

MR View&GO offers consecutive steps to guide you from basic quality control through potential further processing steps towards result distribution. To launch a specific step, e.g. the 3D card, you only have to select a series of images and press the "Show in 3D" button on the left-hand side (see Figure 3A).

[1]*This reflects only a selection of advanced applications, further options are available.*
[2]*Only one user can process data at a time with one license.*

4

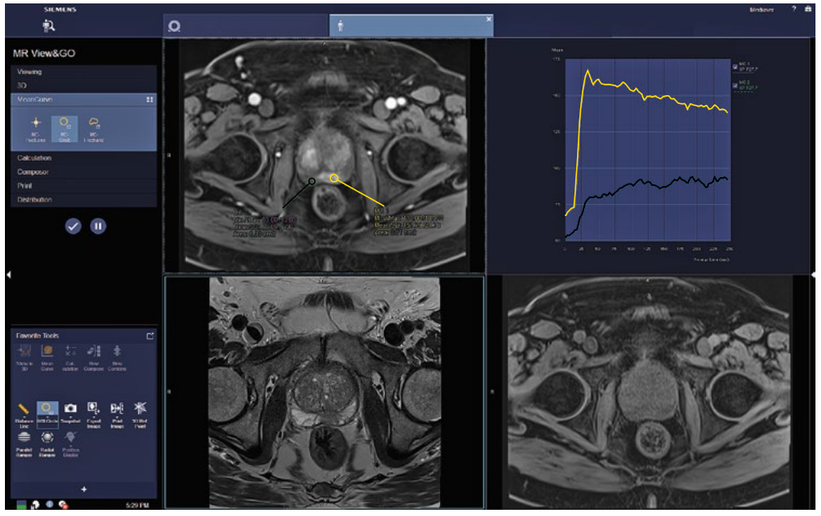

4

The standard MeanCurve analysis step for evaluation of the dynamic behavior of contrast enhancement in tissues. As shown in this example of a patient with prostate cancer, ROIs have been placed in the peripheral zone, illustrating fast wash-in and distinct wash-out for the yellow selection while the purple ROI is showing moderate enhancement and a plateau.

5

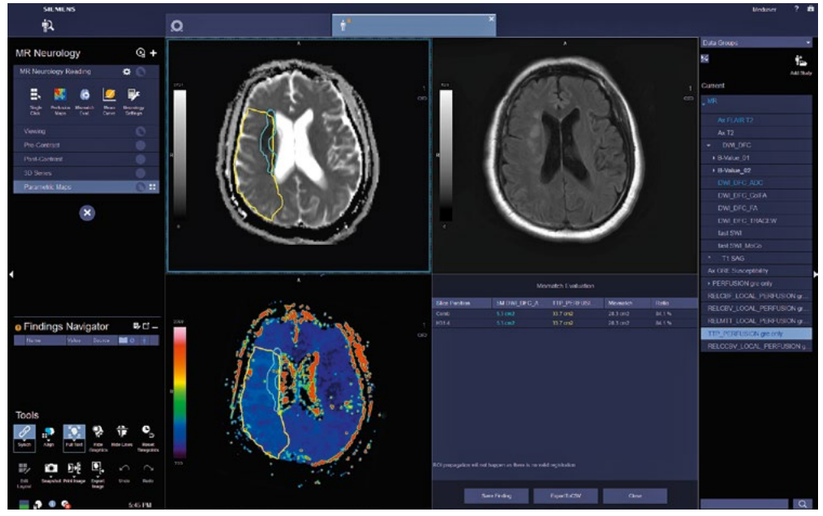

Acquistion Workplace *syngo*.MRXA10

Post-processing Console *syngo*.MRXA10

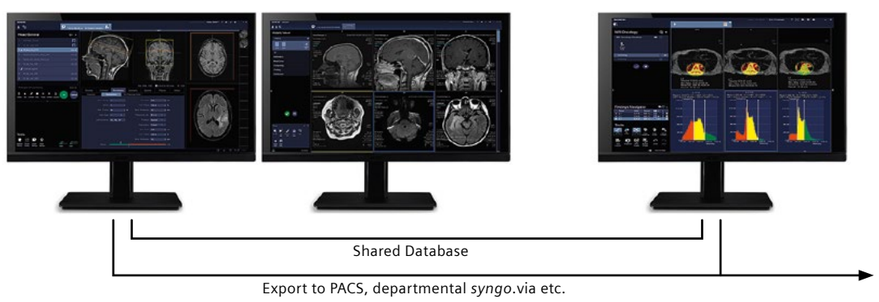

6 Deployment overview and departmental integration of the MR acquisition workplace and the optional post-processing console.

Finally, the appearance and usability of all applications has been harmonized with our departmental post-processing platform *syngo*.via, helping to improve workflow efficiency.

Summary

The new user interface on the *syngo* MR XA platform is designed to improve the technologist's user experience with clearly separated tasks following the natural flow of their work. This not only helps to make routine exams more comfortable to perform and focus more on the patient than on the machine, but also supports in cases where rapid results are decisive. For example in imaging of acute stroke the combination of highly optimized exams using GOBrain, which only needs 5 minutes acquisition time, together with subsequent mismatch analysis (Fig. 5) right at the scanner can save precious time and may help to gain therapy-relevant information faster.

Reference

[1]*Anderson, JA; et al. CIC Report 200311.*

Contact

Gregor Thörmer, Ph.D.

Global Segment Manager
MR Imaging in Oncology

Siemens Healthcare GmbH
HC DI MR CRM AW
Phone: +49 (9131) 84-7726
gregor.thoermer@siemens-healthineers.com

Clinical Acceleration: From the Console

James Hancock
Benson Radiology, North Adelaide, Australia

In Clinical MR the challenge to scan faster, in higher resolution and with consistent reproducibility always has been and always will be the challenge that drives technological development within the modality. Traditional thinking in MR dictates that speed comes at the cost of compromised image quality and is achieved with a decrease in spatial resolution or at risk of increased artifacts often at the expense of signal-to-noise ratio (SNR).

The implementation of technology such as Compressed Sensing (CS), CAIPIRINHA and Simultaneous Multi-Slice (SMS) is changing our thinking on just what is possible and providing maximum flexibility in imaging. Imaging is now being better tailored to the patient and their capabilities rather than the patient having to bend to the requirements of the imaging. This is a fundamental principle of Siemens BioMatrix technology.

With a big focus on body imaging applications Benson Radiology installed a 3T MAGNETOM Vida system into a private imaging department in the central business district of Adelaide, South Australia in July 2017. Without access to government-based medical rebates the quality, speed and reproducibility of examinations performed on the MAGNETOM Vida system are key to a successful business outcome. The MAGNETOM Vida offers technology like Compressed Sensing (CS), CAIPIRINHA and Simultaneous Multi-Slice (SMS) providing maximum flexibility in imaging.

CAIPIRINHA

CAIPIRINHA (Controlled Aliasing in Parallel Imaging Results in Higher Acceleration) is a unique *k*-space acquisition scheme for parallel imaging techniques (PAT) that improves the SNR of a sequence by up to 18% compared to conventional acceleration of the same sequence with SENSE or GRAPPA. With a particular focus on body imaging, Benson Radiology is leveraging the combination of very high coil density with CAIPIRINHA VIBE to fit an imaging solution to the capabilities of the patient. In a competent breath-holder this allows traditional breath-hold examinations to be acquired at higher spatial resolutions than ever before. Here we use the SNR gain from the parallel imaging technique combined with high coil density to improve fine edge sharpness and better delineate the conspicuity of pathology in the abdomen.

In the subset of patients where the ability to hold ones breath is compromised acceleration factors can be increased, thereby driving down scan time to achieve robust reproducible outcomes without the traditional sacrifice in spatial resolution or the risk of imaging artifacts traditionally associated with high PAT factors. This is achievable at both 1.5T and 3T field strengths.

1 **T1 VIBE CAIPIRINHA post contrast**

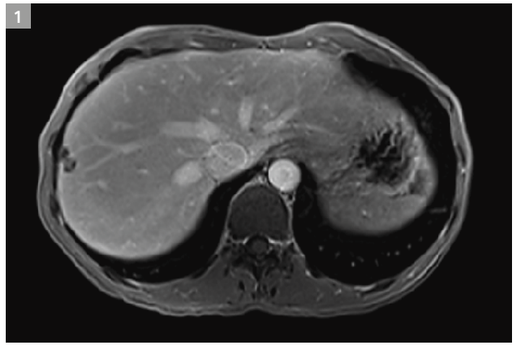

1.3 x 1.3 x 2 mm, 88 slices, complete liver coverage. Achieved using CAIPIRINHA total acceleration factor of 5. High resolution clearly defines liver lesion with features suggestive of hemangioma in this delayed dataset acquired 5 minutes following administration of gadolinium contrast. Scan time of 16 seconds.

2 **T1 VIBE CAIPIRINHA post contrast at 1.5T**

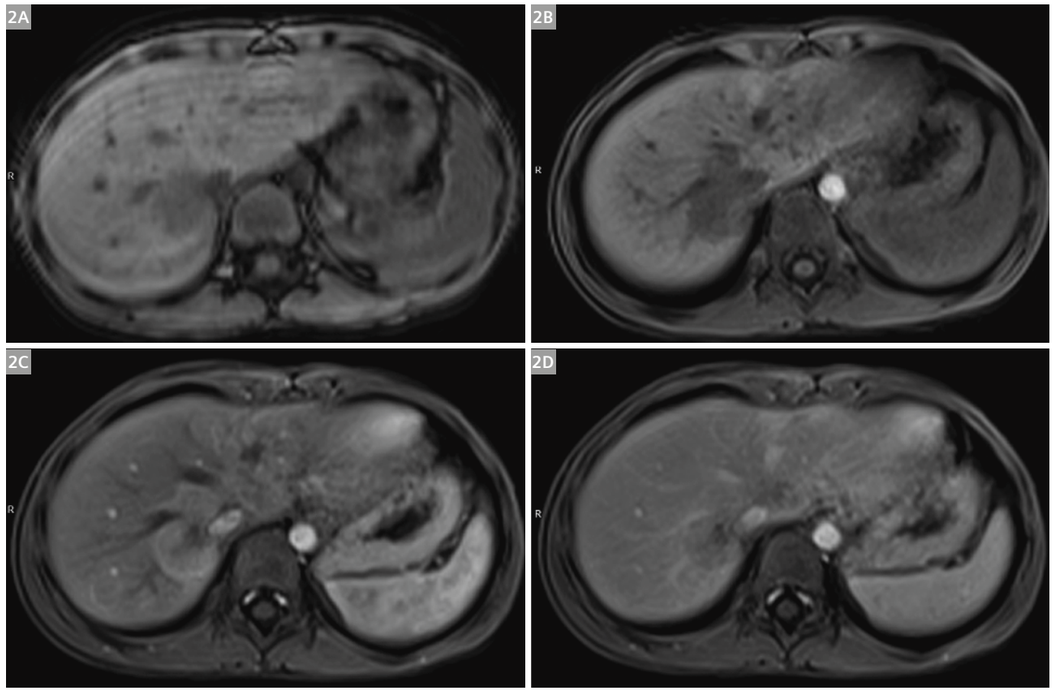

(2A) Traditional 2D T1 FLASH in-phase acquisition time of 11 seconds adversely affected by poor breath-hold in a 7-year-old male with a liver lesion. Repeat imaging using CAIPIRINHA (1.25 x 1.2 x 3 mm) with an acceleration factor of 4 reduced the breath-hold time to 7 seconds and allowed artifact free images to be obtained pre **(2B)**, and post contrast **(2C)** arterial and **(2D)** venous.

Simultaneous Multi-Slice (SMS)

With a focus on body imaging, diffusion-weighted imaging (DWI) is always going to be a key aspect of the imaging service offered at Benson Radiology. DWI offers well-known benefits in abdominal and pelvic imaging.

Conventional EPI-DWI techniques can be acquired in multiple ways, including a free-breathing (FB) approach with the use of navigators or with multiple breath-hold techniques. Breath-hold techniques are constrained by the breath-hold capacity of the patient as well as the reproducibility of these breath-holds. This further constrains the usefulness of the technique as b-values become limited, as does the spatial resolution that can be achieved. If using a free breathing technique the acquisition time itself is the tradeoff. Here navigating the approach can become inefficient depending on the patients respiratory cycle. Multiaverage free breathing, while the current gold standard at our institution, is still a lengthy approach. This is despite making use of parallel imaging techniques like GRAPPA for acquisition acceleration. The conventional EPI-DWI approach is inefficient as every imaging slice has to be excited individually, then the diffusion encoding gradients applied, and finally the image information acquired with EPI encoding. This process needs to be repeated multiple times, once for each imaging slice, until the entire volume of interest is covered.

The inefficiencies mentioned above can be overcome with Simultaneous Multi-Slice acquisition combined with a free breathing approach, which we have implemented at our institution. Instead of successive excitation of slices, slices are exited simultaneously with a multiband pulse and blipped-CAIPIRINHA SMS-EPI ensures preservation of high SNR and low artifact levels. Since multiple slices are excited simultaneously, the overall TR for a desired spatial coverage or number of slices is reduced, leading to a scan time reduction by the same factor. The big advantage of SMS over other acceleration techniques is that it does not suffer from the typical square-root of acceleration factor SNR penalty due to data under-sampling.

The inclusion of SMS or simultaneous multi-slice acquisitions has been very well received on our MAGNETOM Vida system given the amount of body imaging that the system is performing. For liver imaging we traditionally used a free breathing approach, combining a PAT factor of 3 and a very high number of averages to allow for signal rich b800 imaging across a broad spectrum of patient sizes. Our scan times with 3 b-values within the sequence were around 5:27. Switching to a SMS 2 PAT 2 approach we can achieve very comparable results in just 2:58 seconds (see Fig. 3).

We now routinely use a PAT factor of 2 and an SMS factor of 2 for our abdominal diffusion imaging. As described above, we have used some of the speed improvements for image quality. We have traded off some of the acceleration for better SNR in the higher b800 images via a higher number of averages 7–10 whereby the spatial resolution has improved with an increase in the relative image matrix. Further we have gone from 36 slices acquired at 5 mm to 40 slices at 5 mm ensuring slightly more coverage within the standard protocol, meaning fewer adjustments at the console for technologists based on patient and liver size.

3 **SMS DWI in the liver**

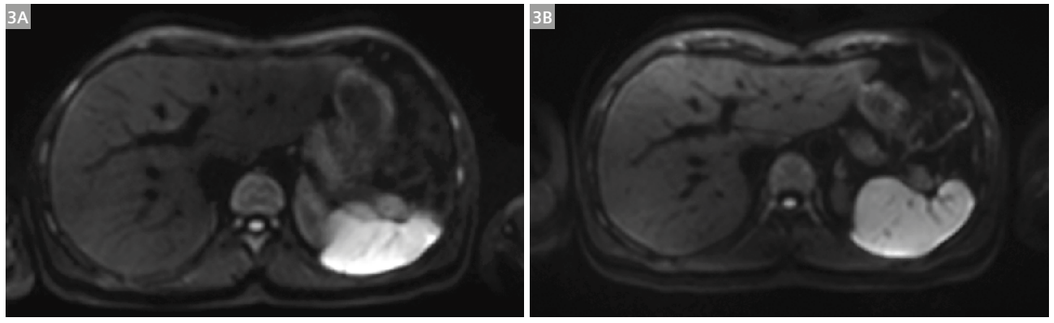

(3A) PAT 3 b800 DWI and **(3B)** SMS 2 PAT 2 b800 DWI of the liver in the same patient at similar slice locations comparing image quality. **(3A)** was acquired on a 3T MAGNETOM Skyra system with a scan duration of 5:27, TR 6300 ms. **(3B)** was acquired on a 3T MAGNETOM Vida system with a scan duration of 2:58, TR 3000 ms.

4 **SMS DWI of a pelvic mass**

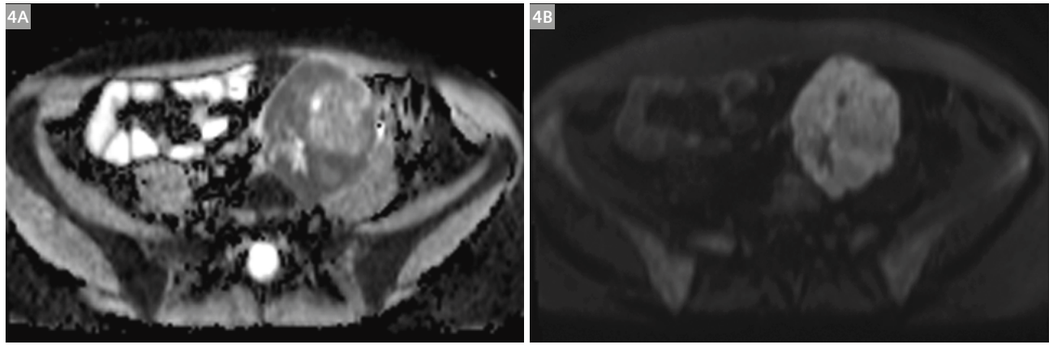

(4A) ADC map and **(4B)** SMS 2 PAT 2 b1000 DWI in the pelvis of a patient with a likely paraganglioma/pheochromocytoma. SMS DWI acquired with 3 b-values, b1000 with 12 averages. Scan time 3:18.

MAGNETOM Flash Special USA Edition · 02/2020

Reprinted from MAGNETOM Flash (70) 01/2018

In prostate imaging we see a very broad spectrum of patient sizes. Traditionally, maintaining resolution and SNR from the center of larger patients has been challenging, especially at higher b-values. SMS combined with the Body 30 coil allows us to take the associated decrease in scan time and translate this to SNR in our higher b-values. This approach has allowed a 3 b-value DWI sequence to be acquired in 4:26 combining SMS 2 PAT 2 with the b1000 making use of 23 averages. Comparatively the traditional PAT 2, 3 b-value DWI approach was a 5:28 acquisition. Clinically this results in reproducible image quality in a wider variety of patients in a shorter scan time than the non SMS technique.

Compressed Sensing (CS)

With a focus on body imaging, cardiac and liver MRI are two of the most challenging examinations for producing consistent reproducible image quality in a given time period. Traditionally it has been difficult to overcome the challenges associated with patient limitations such as breath-holds and ECG gated acquisitions without sacrifice in other areas.

Both cardiac and liver MR are making use of compressed sensing (CS) techniques to overcome these challenges. Benson Radiology has embraced the use of CS accelerated cine imaging in cardiac MR for all indications. This has enabled real-time cine MRI for short axis (SA) and other stack imaging to be completed with a spatial and temporal resolution that compares to segmented acquisitions. The traditional segmented approach to a 10–12 slice SA stack for the left ventricle can take as long as 6 minutes. Using CS, we are acquiring the stack in 25 seconds. If the patient is able to hold their breath this sequence can be split into 2 acquisitions or if the patient is respiratory challenged they can breathe quietly away for the duration of the acquisition. The benefits of this approach are three fold:

- Acquisition of high-resolution cardiac cine images – independent of patient's breathing capability and in the presence of arrhythmia.
- Capture across the whole cardiac cycle for precise quantification.
- Increase the number of patients eligible for cardiac MRI at our facility.

Prior to compressed sensing, when encountering arrhythmias, the technologist would tend to take three approaches to overcome the issue and all of these techniques have drawbacks.

Prospectively gating offers an approach whereby the heart rhythm is studied and the technologist tries to pick an acquisition window which compensates for the arrhythmia by shortening the RR period. Although this can be effective, the downside is you sacrifice acquisition of the entire cardiac cycle, meaning your quantification will suffer.

5 **SMS DWI prostate**

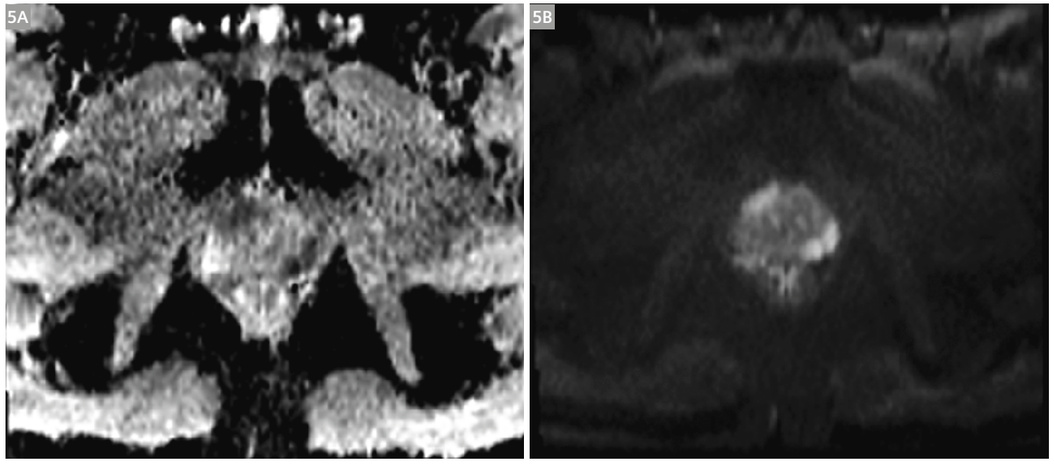

(5A) ADC map and **(5B)** b1000 for apical prostate cancer. Left posterolateral PZ and right anterolateral PZ both graded as PI-RADS 5. Images acquired using SMS 2 PAT 2. Increased number of averages (23) used in acquiring the b1000 produces noise free images and high clarity in the corresponding ADC map. Scan duration 4:26.

MAGNETOM Flash Special USA Edition · 02/2020

6 **CS in the presence of cardiac arrhythmia**

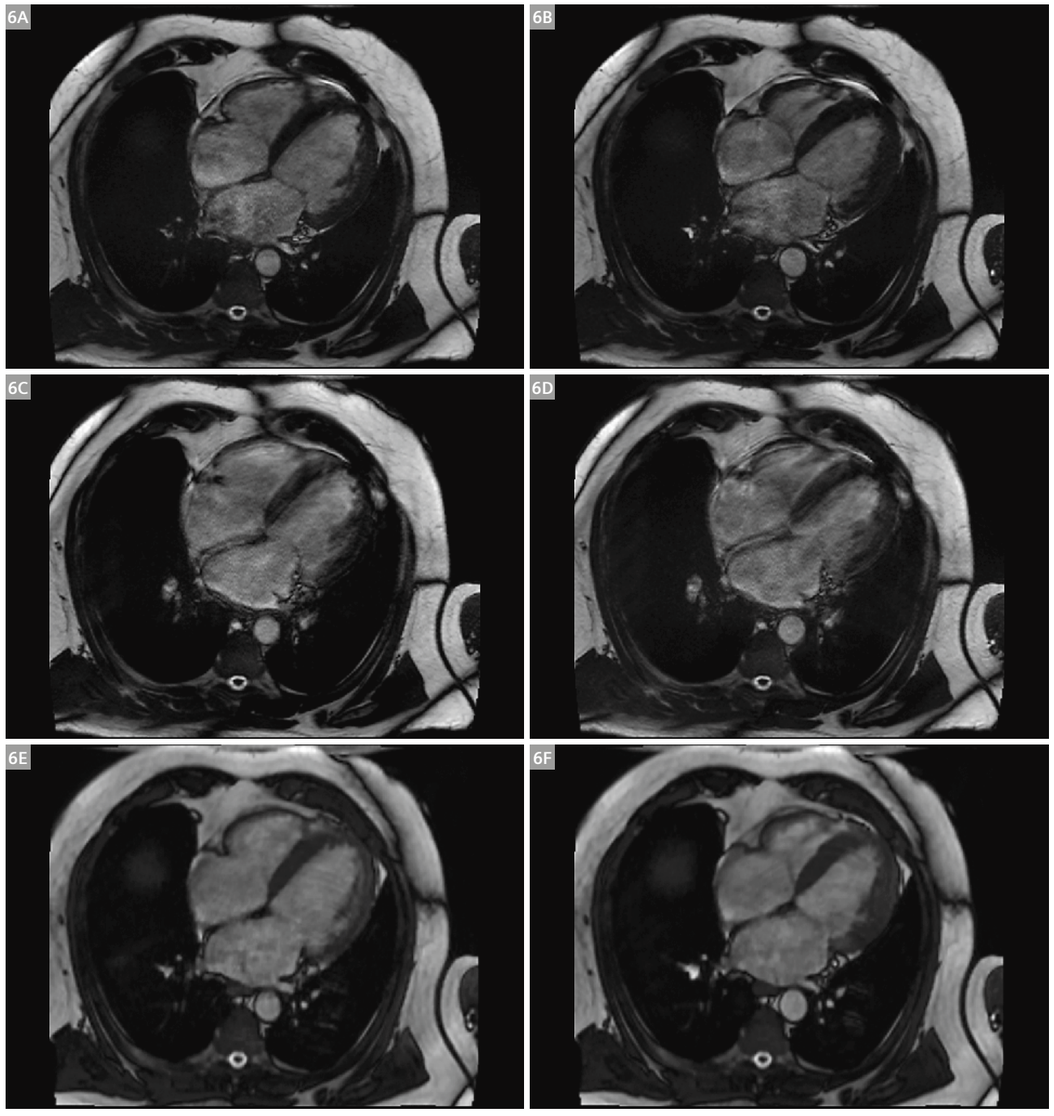

ED and ES 4-chamber trufi cine using multiple approaches in the same patient with chronic cardiac arrhythmia **(6A, B)** prospective approach demonstrates acceptable image quality however with underestimation of true ES. Acquisition time 11.32 seconds.
(6C, D) Arrhythmia rejection technique demonstrates unacceptable image quality due to chronic arrhythmia lengthening breath-hold times to an unobtainable level for the patient. Acquisition time 35.41 seconds. (**6E, F)** Compressed Sensing technique demonstrates optimal image quality and samples entire cardiac cycle allowing better quantification of ES versus either of the previous techniques. Acquisition time sub 2 seconds.

7 **CS GRASP VIBE liver**

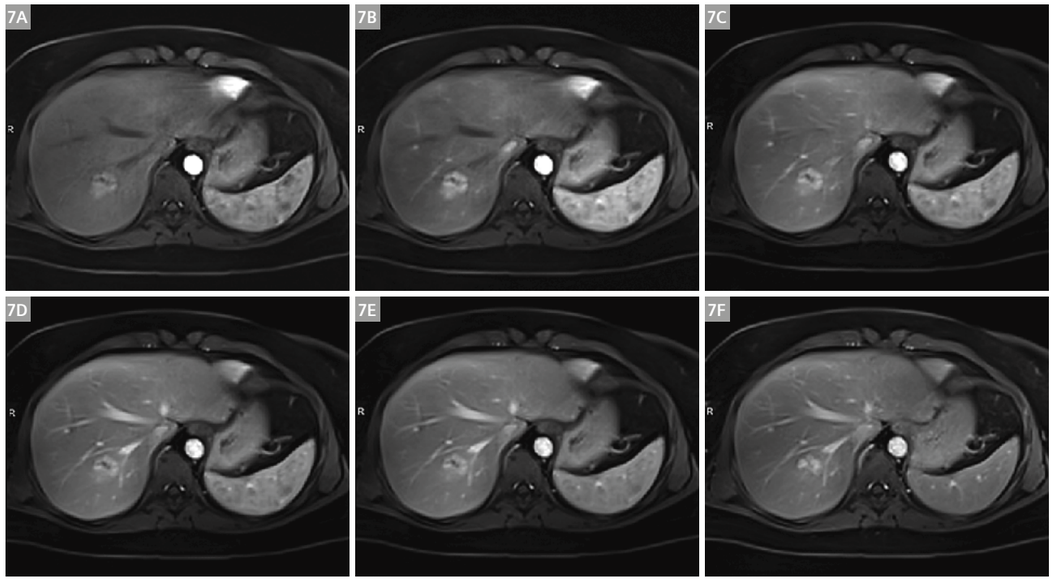

Compressed Sensing T1 Fatsat GRASP VIBE. 6 of 21 phases shown here. Technique is acquired in free breathing with a contrast timing independent acquisition running over approximately 5 minutes. **(7A–C)** are very early, mid and late arterial phases. **(7D, E)** are venous phases and **(7F)** being a delayed phase at nearly 5 minutes post contrast. Arterial enhancement, with contrast retention, central scar and minimal background T1/T2 change favours diagnosis of FNH.

Another available tool is the arrhythmia rejection tool, whereby we set an acceptance window and the scanner rejects any RR periods which do not fall within this window. The downside of this is that if the patient has a chronic arrhythmia then the scan time can increase beyond the ability of the patient to hold their breath.

Prior to CS this leaves the technologist with nowhere to go other than to use real time imaging with poor spatial and temporal resolution. CS has changed this. Using compressed sensing the heart can be imaged with both high spatial and temporal resolution in a robust reproducible fashion independent of the patient's breath-hold ability and in the presence of considerable arrhythmia.

In the liver or any abdominal/pelvic indication that requires a dynamic contrast injection, the quality of the final images is reliant on both a skilled technologist who can trigger the acquisition for an accurate arterial phase or phase(s) and a compliant patient who can follow breathing instructions at the right time and also maintain a breath-hold for the duration of the acquisition. In the liver in particular temporal resolution in lesion characterization is becoming important for diagnosis.

Compressed Sensing GRASP-VIBE offers a technique for patients with limited breath-hold capability or who are unable to follow breathing commands. The technique takes the pressure off technologists as the critical timing-dependant arterial phase of an acquisition is removed. The acquisition is a simple push-button exam.

The acquisition is performed in one continuous run, using a golden-angle stack-of-stars radial scheme that gives robustness towards motion and the flexibility to choose the temporal resolution. The sequence itself guides the user on the correct time point for contrast administration. Reconstruction is performed using a Compressed Sensing GPU accelerated algorithm.

This new approach gives us a reliable post contrast technique on any patient. It is changing the way abdominal post contrast imaging is reviewed and making it a more dynamic cine experience at each slice location for the radiologist. Radiologists receive a temporal dataset which can be viewed akin to a cine series allowing contrast arrival, enhancement and wash out to be viewed on a slice by slice basis. The high temporal resolution is particularly useful for HCC detection and small thrombus within vessels. The insensitivity to breathing

MAGNETOM Flash Special USA Edition · 02/2020

8 **CS GRASP VIBE pelvic mass**

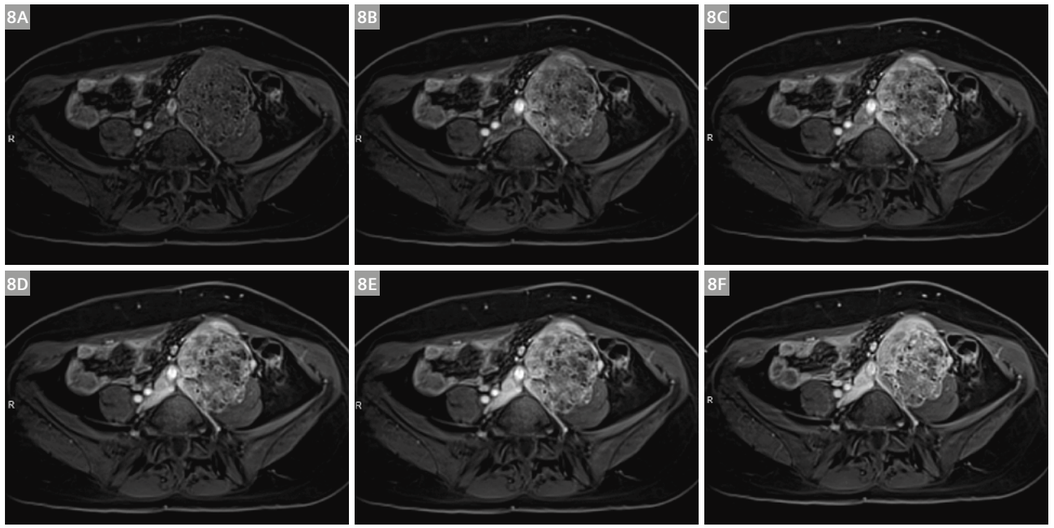

Compressed Sensing T1 Fatsat GRASP VIBE. 6 of 21 phases shown here from the same patient as Figure 4. Patient with a likely paraganglioma/pheochromocytoma. Starting with **(8A)** plain phase **(8B–D)** arterial time points to **(8E, F)** venous and delayed.

motion is particularly useful when combined with Primovist contrast where a subset of patients find holding their breath for a traditional arterial phase an issue. The dedicated arterial, venous and transitional phase datasets can be individually reconstructed and displayed as separate series for review in the traditional manner also.

Worldwide MRI is continuing to operate in an environment where the volume of exams is ever increasing with pressure on technologists and radiologists to maintain both image quality and diagnostic confidence. This continues against a background of decreasing reimbursements from government while patients expect high quality exams in an ever decreasing amount of time. Siemens Healthineers continue to innovate to provide solutions to these problems with yet more applications in SMS and CS coming soon to a magnet near you.

Contact

James Hancock

Modality Manager – MRI
Benson Radiology

229 Melbourne Street
North Adelaide, South Australia, 5006
Tel.: (08) 8239 0550
Mobile: 0434 279 466
James.Hancock@bensonradiology.com.au

Reprinted from MAGNETOM Flash (70) 01/2018

First Experiences with the World's First MAGNETOM Vida

Mike Notohamiprodjo, M.D.
Associate Chair and Section Chief MRI, Department of Diagnostic and Interventional Radiology, University Hospital Tübingen, Germany

The Department of Clinical and Interventional Radiology at the University Hospital Tübingen had the rare opportunity to host the world's very first installation of the MAGNETOM Vida, the first BioMatrix equipped scanner, incorporating the latest advances in MR technology.

Current demands for biometrical imaging and personalized medicine

One of the current trends in medicine is the acquisition and analysis of so-called 'big data', to improve disease management and patient outcome.

The University Hospital Tübingen has dedicated itself to this approach and founded the "Center for Personalized Medicine", incorporating all activities in this rapidly developing field. One of the central tasks is a universal database for quantitative data, so that imaging data, for example, can be correlated to histopathology, molecular biology, or clinical outcome.

The Department of Radiology is also part of this inter-disciplinary center, giving us the exciting chance to perform 'Radiomics' on a greater scale by evaluating image phenotypes as a potential biomarker, for example, to predict and assess therapy response and outcome. However, the fundamental requirement for quantitative or at least structured data is robust and reproducible image acquisition (Fig. 1). Up-to-date Computed Tomography is the mainstay of Radiomics since it is highly standardized and accomplishable in most patients. Magnetic Resonance imaging, by contrast, provides more detailed data due to its superior soft-tissue contrast and offers complex functional quantitative methods such as DCE-MRI and diffusion-weighted imaging. However its robustness and reproducibility is often limited due to long acquisition times and the sensitiveness to respiratory and gross motion. One of the focuses of our MR research group is to develop and establish methods for clinical routine to overcome these constraints to acquire robust results in every patient. We have a long-standing experience with advanced parallel imaging methods, free-breathing examinations, compressed sensing, and novel multi-channel coils. Thus, we were very excited to be the first to work with the 3T MAGNETOM Vida[1] and BioMatrix[1], bringing all together work-in-progress- and prototype technology, incorporating and uniting technical and sequence advances.

Our MAGNETOM Vida

Our Magnetic Resonance Department is equipped i.a. with the 1.5T MAGNETOM Espree, Avanto^{fit}, and Aera

[1] *510(k) pending. The product is not commercially available. Future availability cannot be guaranteed.*

1

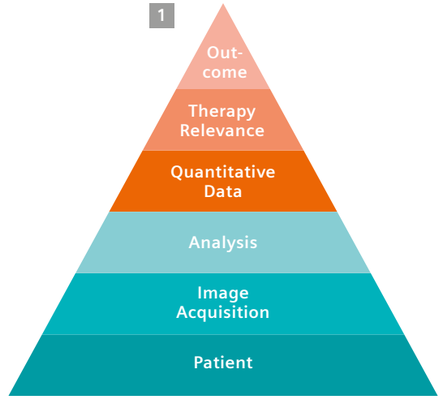

1 The pyramid of imaging in personalized medicine. Personalized medicine starts with the patient. Only if the patient is feeling comfortable can sufficient data be obtained. Image acquisition should be of high quality, robust and reproducible. The images are then read in PACS; functional imaging is analyzed with postprocessing software. Quantitative or at any rate structured data should then be derived from the analysis. Based on this data individualized therapy can be induced. Therapy response and/or outcome should be monitored and in the best-case scenario predicted by the imaging data acquired before. Optimized scanner hardware, such as BioMatrix and MAGNETOM Vida, help to optimize the fundament of this pyramid. Only if the patient is comfortable and image acquisition optimized can further data analysis and processing be performed.

scanners; the 3T MAGNETOM Skyra and Prisma^{fit} scanners, and the MR-PET scanner Biograph mMR. The focus of our daily clinical work is on oncological, musculoskeletal, and neuro-imaging. We have experienced a steady increase in demand particularly in multiparametric prostate MRI and functional brain MRI. We have also noticed a steady increase in multi-region oncologic imaging, corresponding to the rapidly growing number of anticancer therapeutics, such as immune or antibody therapy. The latter examinations in particular are repeatedly performed in prospective studies and require a fast and highly reproducible acquisition to reliably assess therapy response.

During the first months of our early installation we performed the initial mandatory conformity marking (CE-certificate), a so-called 'MPG-(medicine devices act)-study'. This means that we had to examine a particular number of patients on both the new scanner and a routine 3T scanner (in our case MAGNETOM Skyra, Prisma^{fit}, and Biograph mMR) and compare image quality.

In short the MAGNETOM Vida features a 70 cm bore, strong 60/200 XT gradients, and a very homogeneous large field-of-view (55 x 55 x 50 cm) (Fig. 2). We believe that it combines the magnet homogeneity of a MAGNETOM Avanto and the performance of a MAGNETOM Prisma, but features the similar comfort of the wider 70 cm bore MAGNETOM Skyra. Furthermore, it features 128 receive channels enabling state-of-the-art coil technology, such as a 72-channel Spine coil, 30-channel Body coils, a 64-channel or a tiltable 20-channel Head coil. The high number of channels is particularly useful for achieving higher parallel imaging acceleration factors, significantly shortening acquisition time while maintaining adequate signal-to-noise ratio (SNR). From our experience, the combination of the 72-channel Spine coil and the 30-channel Body coil delivers up to 30% increase in SNR, particularly at high PAT-factors.

The new scanner also features a novel fully-motorized dockable table concept with an integrated respiratory sensor as well as an updated software with a user interface combining the well-known *syngo* MR E11-software with *syngo*.via functionality for viewing and postprocessing.

First experiences with the user interface

The new user interface and scanner software is now presented on two large 24-inch screens, one for acquisition and one for postprocessing. Thus, the technical staff can view the images and perform postprocessing, without switching the task cards, always keeping acquisition under supervision (Fig. 3).

While the new software looks quite different at first glance, the *syngo* MR E11-functionality is still maintained and only a few minor changes were obvious. We found that all technical staff could operate the scanner after only a short (<5 minutes) basic training. The *syngo*.via-interface was already familiar to our physicians, but the technical staff were also quickly able to perform basic postprocessing, such as composing and advanced postprocessing, e.g. perfusion assessment with Tissue4D was also quite quickly doable.

One of the central aspects of MAGNETOM Vida is to provide optimal reproducibility of MR studies, so that

2 Professor Notohamiprodjo and Professor Nikolaou in front of their MAGNETOM Vida, the world's first clinical installation.

3 To ease the work of the MR technologist, the new *syngo* MR XA10 software operates on a dual monitor scanning workplace with two large 24-inch monitors.

MAGNETOM Flash Special USA Edition · 02/2020

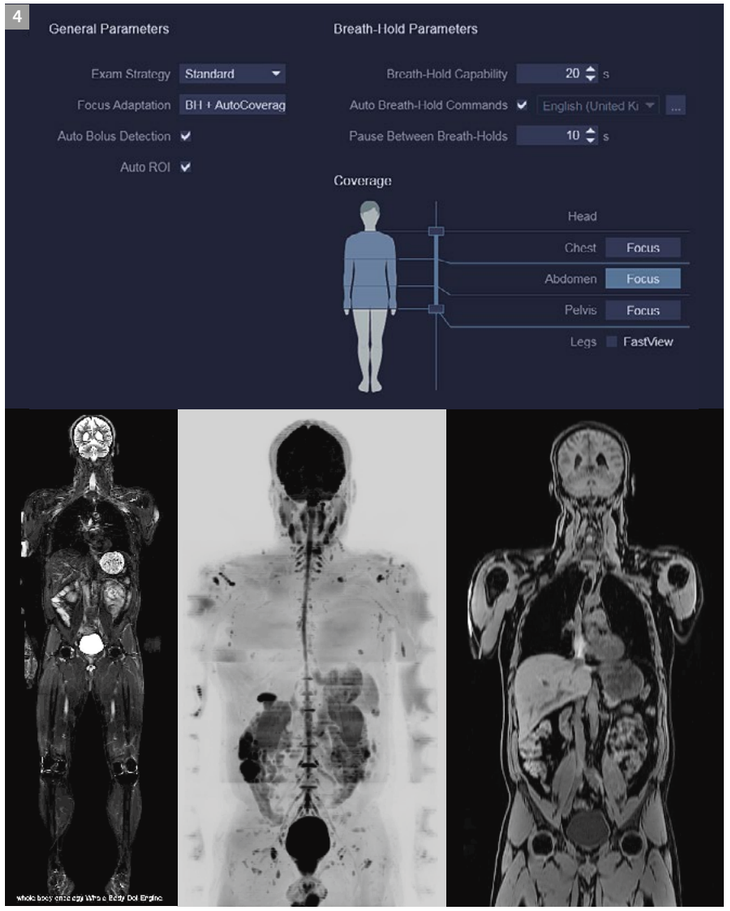

4 Whole-Body Dot Engine.The Whole-Body Dot Engine enables fast and robust multi-region imaging with reproducible results. Images show a whole-body STIR-HASTE and coronal multi-planar reconstructions (MPRs) of a diffusion-weighted and a VIBE sequence.

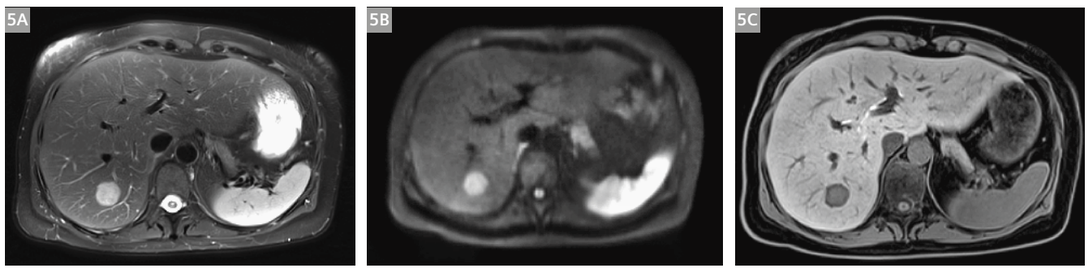

5 38-year-old patient with hepatic adenoma. **(5A)** T2-weighted fast BLADE sequence: A hyperintense 2 cm sized mass in the Coinaud-segment VII. The acquisition with optimized radial spokes makes the sequence robust against respiratory motion and reduces typical star and hook artifacts. Furthermore, phase-encodiung artifacts caused, for example, by pulsation, do not occur due to the radial acquisition. **(5B)** Diffusion-weighted sequence with b-value 800 s/mm² with SliceAdjust: The lesion shows diffusion restriction. The strong 60/200 XT gradients provide high signal even at high b-values. Slice selective shimming with SliceAdjust reduces distortion artifacts.
(5C) Dixon-VIBE sequence with PAT6: The lesion shows some uptake of the hepatocyte specific contrast agent Eovist (Bayer, Berlin, Germany). High acceleration factors are possible with the combination of the 72-channel Spine coil and the 30-channel Body coil. Breath-hold duration is only 8 seconds, still delivering high image quality.

high image and data quality is guaranteed. Several Dot engines enable semi-automated acquisition of e.g. the brain, joints, or the cardiovascular system with a focus on either speed, resolution or, robustness. We were particularly interested in the new Whole-Body Dot Engine, allowing the rapid planning and acquisition of multi-region examinations, giving MRI-acquisition a feeling similar to CT, automatically adjusting the field-of-view, number of stacks, and slices (Fig. 4).

First experiences with the hardware

Our technical staff were very happy with the fully motorized table, making it possible to maneuver even with obese patients with ease. The respiratory sensor enables respiratory triggering even for sequences without navigator. We think that the sensor is particularly useful to monitor if a patient correctly performs the breath-hold maneuvers, so that the duration of sequences can be individually adapted to the patient's respiratory capacity.

The two tablet-like touchscreens at the gantry were also quite popular, giving full control of the room parameters such as ventilation and volume levels. Automated coil position recognition also accelerates the workflow, as positioning of the coil center is not required anymore.

The basic coil design was already known and compatible to Tim4G scanners, however many coils feature more elements such as the 72-channel Spine coil, 30-channel Body coil, or 18-channel Knee coil, while others provide more patient comfort, such as the flexible Shoulder coil or the tiltable 20-channel Head/Neck coil, allowing for more comfort in the case of cervical kyphosis.

First clinical experiences

Of course, of greatest interest to us was image quality. The multi-channel coils, particularly the combination of the above mentioned 72-channel Spine coil and a 30-channel Body coil, allow for application of high PAT-factors, such as R = 6 for CAIPIRINHA-imaging (Fig. 5).

We noticed a high diagnostic image quality even for very fast examinations such as a 5 minutes brain (T2, FLAIR, T1, Diffusion) (Fig. 6) or a 6 minutes knee examination (PD fs in 3 planes and T1). Simultaneous Multi-Slice acceleration is also available for diffusion-weighted imaging enabling acquisition of a complete body region in only 2 minutes, so that diffusion-weighted imaging of the chest-abdomen-pelvis can be performed in under 7 minutes. The whole-body-protocol can be further accelerated with a free-breathing or multi-breath-hold STIR-HASTE-sequence,

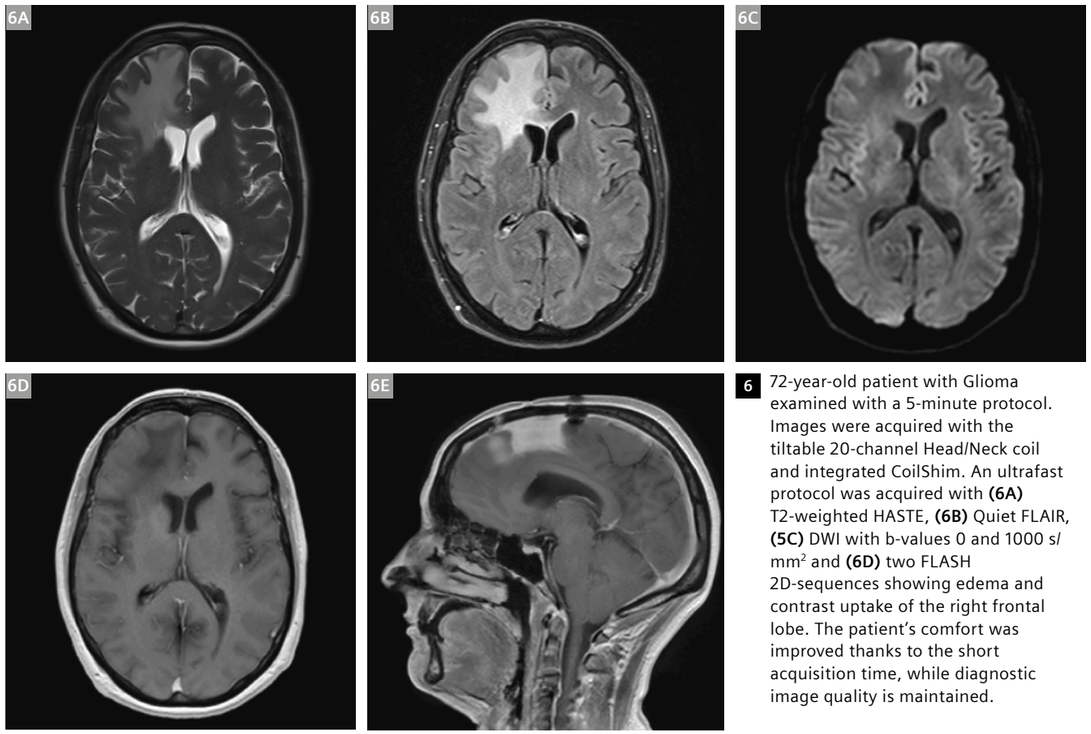

6 72-year-old patient with Glioma examined with a 5-minute protocol. Images were acquired with the tiltable 20-channel Head/Neck coil and integrated CoilShim. An ultrafast protocol was acquired with **(6A)** T2-weighted HASTE, **(6B)** Quiet FLAIR, **(5C)** DWI with b-values 0 and 1000 s/mm² and **(6D)** two FLASH 2D-sequences showing edema and contrast uptake of the right frontal lobe. The patient's comfort was improved thanks to the short acquisition time, while diagnostic image quality is maintained.

MAGNETOM Flash Special USA Edition · 02/2020

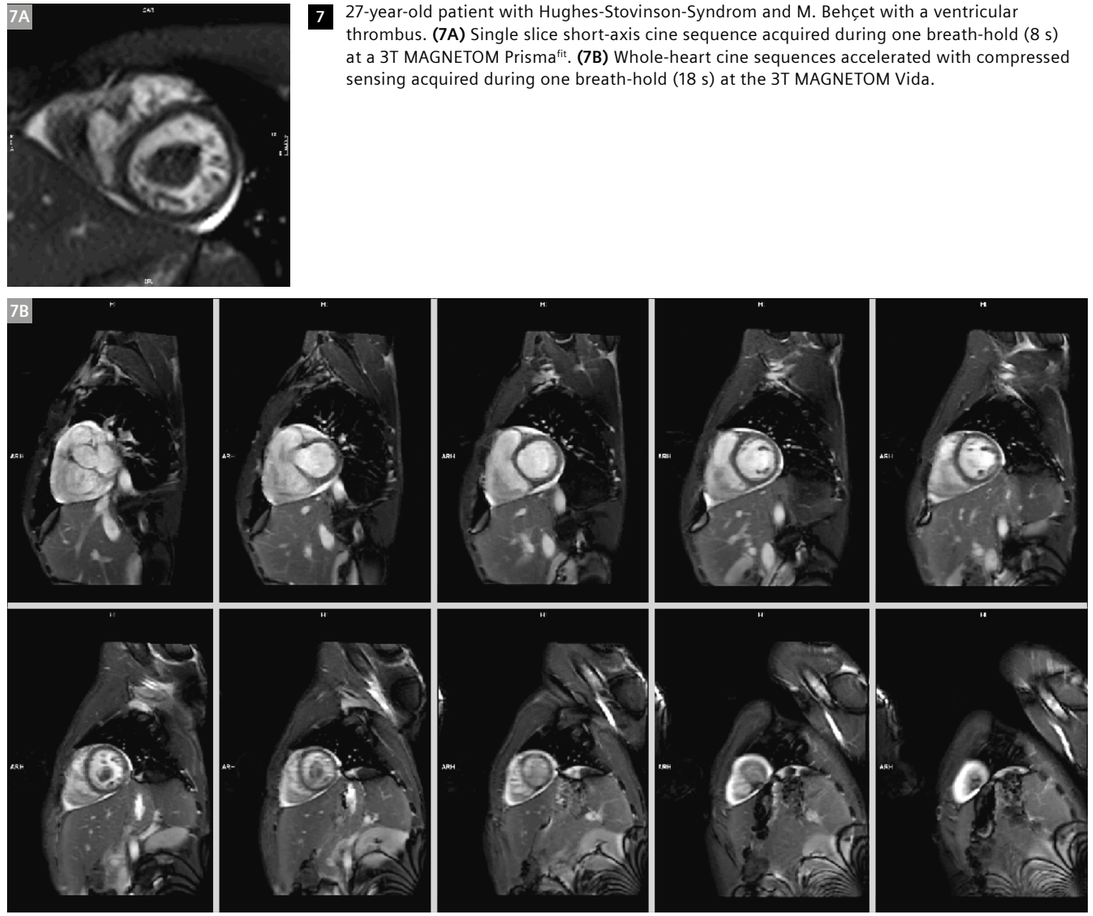

7 27-year-old patient with Hughes-Stovinson-Syndrom and M. Behçet with a ventricular thrombus. **(7A)** Single slice short-axis cine sequence acquired during one breath-hold (8 s) at a 3T MAGNETOM Prisma^{fit}. **(7B)** Whole-heart cine sequences accelerated with compressed sensing acquired during one breath-hold (18 s) at the 3T MAGNETOM Vida.

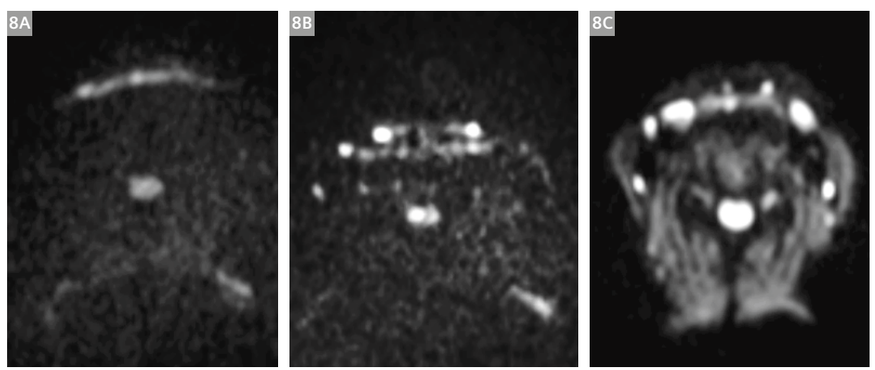

8 57-year-old patient with parotid cancer. Diffusion-weighted images (b-value 800 s/mm²) acquired with the tiltable 20-channel Head/Neck coil. **(8A)** The standard shim shows heavy distortions and almost no anatomical structures. **(8B)** SliceAdjust decreases distortions, however image quality is still impaired. **(8C)** The combination of SliceAdjust and an integrated CoilShim provide good image quality without distortion even of the lower neck, allowing optimal delineation of the cervical lymph nodes.

which can also be acquired much faster but with similar image quality than a conventional TSE-STIR (Fig. 4). We currently aim at a 30-minute time slot for a complete whole-body-protocol, allowing for a potential dramatic increase of patient comfort and throughput.

We were also very excited to test the first commercially available version of radial GRASP[1] (Golden Angle Radial Sparse Parallel MRI), enabling continuous free-breathing radial T1-acquisition with a temporal resolution of <2 seconds. The resulting images are of diagnostic quality, similar to breath-hold sequences, while the image reconstruction time (seconds per phase) was considerably faster than the first prototypes, due to the two integrated GPUs.

Other applications profiting from compressed sensing include, for example, cardiovascular examinations. We were able to obtain a complete short axis scan of the whole heart during only a single breath-hold, using Compressed Sensing Cardiac Cine. The diagnostic image quality is similar to that of classic single-slice acquisition requiring multiple breath-holds, so that examinations are significantly shortened, improving patient comfort and workflow (Fig. 7).

The strong gradients and homogenous magnetic field also allow for examination of obese patients, advanced diffusion applications, such as high b-value imaging and high-resolution 3D-imaging. Furthermore slice selective and dedicated coil-shims allow to decrease distortion artifacts e.g. of diffusion-weighted imaging, particularly at problematic body areas, such as the neck (Fig. 8).

Altogether we experienced an image quality, very similar to that of a MAGNETOM Prisma, which however comes with a 60 cm bore. The multi-channel coils may allow further acceleration, making it possible to shorten examination time, so that robust imaging data can be derived from every patient.

Where do we see the MAGNETOM Vida

As the MAGNETOM Vida brings together many advanced hardware and software solutions, we plan to use the scanner for clinical applications related to biometrical disease assessment. In the framework of our 'Center for Personalized Medicine' we will perform multiparametric assessment of primary tumors such as ENT-tumors, sarcoma, glioma, or prostate cancer to gain further insight into tumor biology and predict outcome and therapy response. Highly standardized multi-region examinations to objectify therapy effects will also be performed at this scanner. We also seek to quantify these effects and study tissue and tumor microcirculation and structure with GRASP and advanced diffusion-weighted imaging. The rapid and free-breathing imaging possibilities allow us to quickly examine children[2] or patients with limited general condition or respiratory status and to obtain adequate image quality in the shortest possible acquisition time.

In summary, the MAGNETOM Vida will enable us to acquire robust and reproducible imaging data in almost all patients, forming the groundwork for biometric MR-imaging, personalized medicine and individually tailored therapies.

[2] MR scanning has not been established as safe for imaging fetuses and infants less than two years of age. The responsible physician must evaluate the benefits of the MR examination compared to those of other imaging procedures.

Contact

Professor Mike Notohamiprodjo, M.D.

Diagnostic and Interventional Radiology
University Hospital Tübingen

Hoppe-Seyler-Str. 3
72076 Tübingen
Germany
Phone: +49 (0)7071 29-86676
mike.notohamiprodjo@uni-tuebingen.de

Reprinted from MAGNETOM Flash (68) 02/2017

3D Localization for Cardiac Views: Saving Time While Increasing Accuracy

Julian Gan
Head of Product & Clinical Imaging, Siemens Healthineers, Singapore

2D single-slice scans in a variety of anatomical planes are the mainstay of cardiac functional and flow imaging. This requires fast and accurate planning. However, localization of cardiac views can be difficult in cases of deviant anatomy.

'Standard' cardiac views for the left ventricle (LV) typically comprise 2-chamber, 3-chamber, 4-chamber, short-axis (SAX) views, or coronal LVOT. Right ventricle (RV) views typically comprise RVOT and RV 2-chamber views.

Other common views are the main pulmonary artery, aortic arch 'candy cane', en face views of the aortic / mitral / tricuspid / pulmonary valve for function, or just distal to the valve leaflets for flow measurements.

More esoteric views might include, e.g., right and left pulmonary artery, coronary sinus, the right and left superior / inferior pulmonary veins, as well as SVC and IVC view of the right atrium etc. In cases of pathology, patient-specific custom views might be required to visualize abnormal flow due to shunts, defects, or stenosis.

Current planning tools

1. Multiple 2D single-shot localizers. A 'pseudo' or close approximation view is obtained, and planning is then iteratively refined using the most recent cine view. However, multiple breath-holds are required for each localizer; inconsistent breath-holding can result in slices becoming incongruent. Also, as planning is prospective, it is always necessary to wait for the latest image, which may be inefficient.

2. 3-point localizer tool. This assumes that the point selected is actually the optimum location – which may not be the case if there is no stack of 2D or 3D images to choose. Furthermore, tortuous anatomy may necessitate some compromise for all structures to be seen, e.g., the optimum plane showing the ascending arch and descending aorta in its entirety (the candy cane view) may not pass through the exact center of the vessel.

3. Specialized software such as the Cardiac Dot Engine. Through training and recognition of landmarks, this will automatically and consistently localize the 2C , 3C, 4C, and SAX views after the acquisition of an 'AA scout'. However, automatic alignment for other specialized views is not yet available. This software is licensed and is not available on older software platforms such as VA, VB, and VC lines.

3D localization technique

An alternative method of localizing cardiac views involves the use of 3D Task Card to generate MPR images, which are then imported back onto the Exam Task Card to copy the center slice location.

1. The only images required are a stack of triggered single-shot images in breath-hold. TrueFISP bright blood or HASTE dark blood anatomical datasets are fine, and are typically routinely acquired anyway.

The recommended orientation is axial, leaving no gap. According to the standard triggered trufisp_singleshot_tra protocol in the Siemens-Heart-Morphology, the only modifications are to:

- set **Distance Factor = 0**, and a slice thickness of **6–8 mm**, which should allow coverage of the heart to the aortic arch in about 25 slices. For pediatric cases, slice thickness should be reduced to 4–5 mm.
- **Geometry = Ascending** is preferred, so that the more critical slices covering the heart are acquired first, in case the patient's breath-hold capability deteriorates midway through the measurement.
- **Cardiac Shim** (optional for 1.5T, mandatory for 3T). The green shim volume box should be positioned over the heart.
- **Capture Cycle** ensures that acquisition is conducted in the diastolic window.
- **Properties** – Auto Open Inline Display is also helpful for monitoring the acquisition and obtaining a real-time overview of the cardiac anatomy.

Reprinted from MAGNETOM Flash (71) 2/2018

2. Load the dataset onto 3D Task Card. The stack of gapless 2D single-shot images is sufficient to visualize most cardiac anatomy in mult planar images with acceptable resolution. The orientation of the MPR lines can be set to obtain the desired views (as described later). Either click the quick 'Save' button (all images are put into an MPR Series), or the 'Save As' button to give the MPR series a unique name (this could be helpful to avoid mix-up, e.g., if doing across section of the right and left pulmonary arteries).

3. Drag and drop the newly created MPR series from the browser, directly into the GSP (it may also be loaded onto the stamp segment for quick access).

Open the Cine scan for planning:

- Right click – **Copy Image Position** on the MPR image to inherit that exact image position.
- If **Lock rotation** is enabled (within the Phase Encode '…' Properties), the scan will automatically be inplane rotated to be parallel to the posterior of the patient. This works well for transverse or sagittal oblique scans. For coronal LVOT scans, a manual rotation may be preferred.

To avoid misalignment:

- The Cine scan must be conducted in the same respiration state as the trufisp_tra series. Expiration is recommended for consistency.
- Do not use REF mode. The Cine scan must either be in **ISO mode**, or FIX for the same table position as the TrueFISP tra series.

An effective way of doing this is to ensure that the table is always centered correctly from the very beginning, and then to keep all protocols saved with FIX = H0.

4. Press the Scan button to apply this sequence. A copy will automatically be appended and opened ready for another immediate Copy Image Position on the next MPR view. In this way, all the Cine scans can be quickly queued up and ready to go. The acquired Cine should match very closely with the predicted MPR image (Figs. 1 and 2). Further corrections and tweaking on the newly acquired Cines are generally not required.

This technique is not exclusive to single-slice scans, of course – a 3D slab or 2D stack (odd-numbered) could also benefit from using the Copy Image Position of an MPR image to quickly inherit the center slice location.

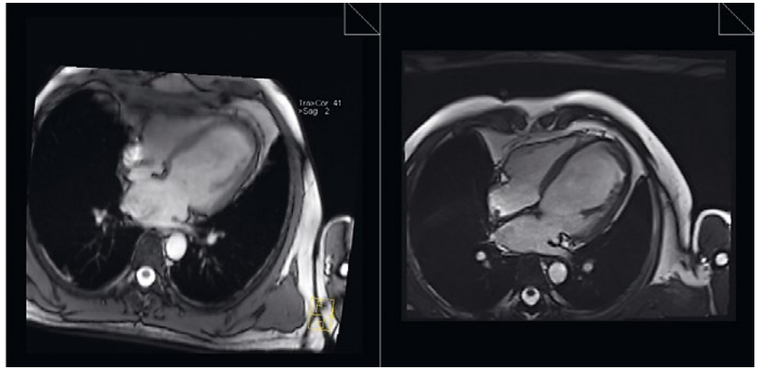

1 MPR image (left) and actual Cine (right) of the 4-chamber view showing an identical anatomic view. The auto inplane rotation feature has optimally aligned the FOV to the patient's back, and previewing the actual image has allowed aggressive setting of the rFOV to shorten breath-hold time.

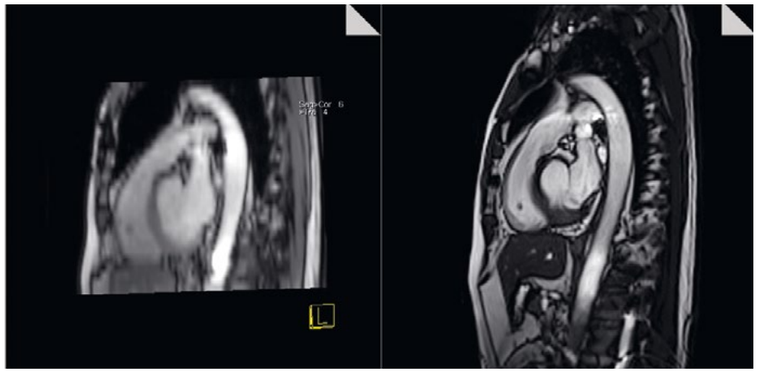

2 MPR image (left) and actual Cine (right) of the RVOT showing an identical anatomic view.

Localizing of the common left lentricular (LV) views: 2C, 3C, 4C, SAX, LVOT

As the planning sequence is nearly identical to the traditional method using 2D localizers, no additional learning effort is required.

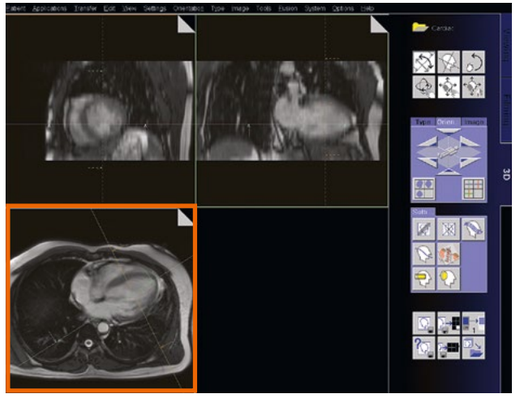

3 Step 1: Start with the true axial in the bottom left, and align the long axis (green) roughly from middle of mitral valve to apex. Align the other axis (red) perpendicularly.

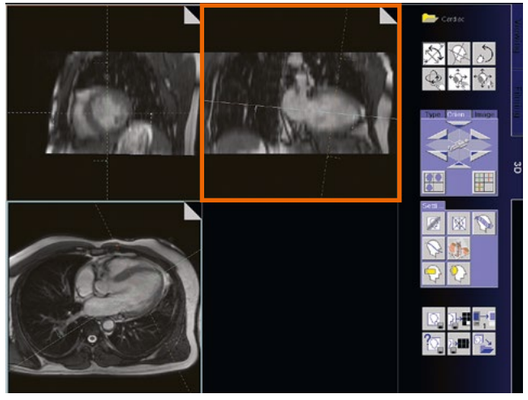

4 Step 2: Moving anti-clockwise to the upper right image (pseudo 2C view): Align the long axis (blue) from mitral valve to apex. Align the other axis (red) perpendicularly.

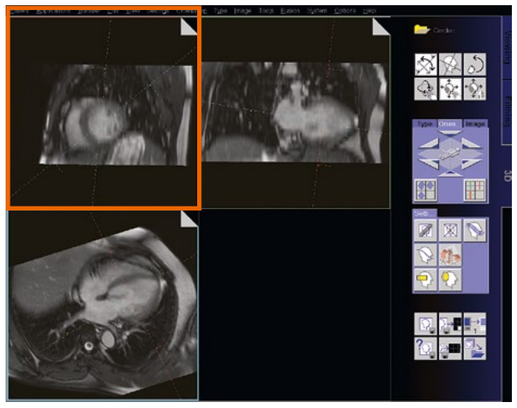

5 Step 3: Moving anti-clockwise to the upper left image (SAX view), align the 2C orientation (green line) parallel to the RV insertion points, and the 4C orientation (blue line) passing through the apex. Iteratively make fine adjustments on all segments to further correct the 2C, 4C, and SAX orientations, until the localization is perfect. Highlight each desired segment and click 'Save' or 'Save As'.

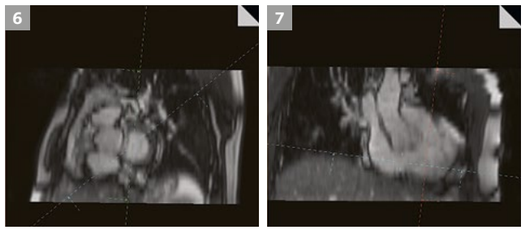

Note that one may obtain more accurate 4C orientation by:
a) scrolling to a more basal SAX slice and checking that the slice does not cut into the outflow tract. Adjusting the angulation allows to dynamically check the resulting 4C view to ensure that the septum is clear (Fig. 6).
b) moving the 2C line (green) over to the RV, thereby obtaining the RV 2 chamber view, and checking that the slice passes through the middle of the tricuspid valve (Fig. 7).

6 Basal short axis slice to check the outflow tract.

7 RV 2-chamber view, to show the tricuspid valve and RV inflow and outflow tracts.

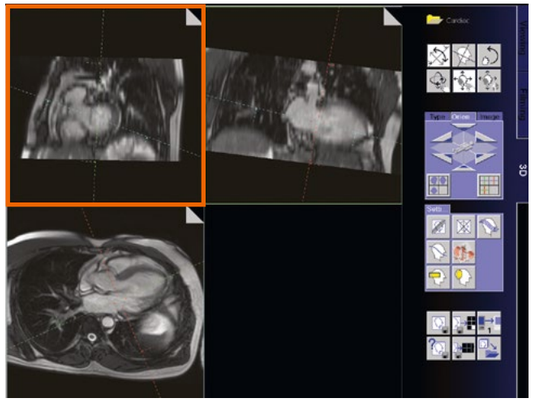

8 Step 4: Scroll the SAX series to a basal SAX slice, and align either the blue or the green long-axis line through the LVOT to obtain the 3-chamber view.

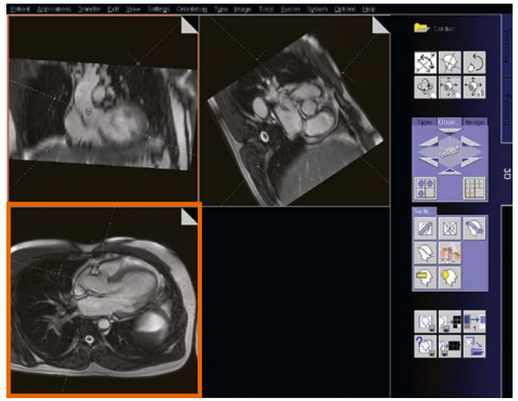

9 Step 5: Aligning a long-axis slice through the LVOT on the 3-chamber view (bottom left) will obtain the coronal LVOT projection (top left). At the same time, the en face aortic valve view can be planned by placing the cross-sectional lines perpendicularly, on both orthogonal views. It can be confirmed on the resultant view that the vessel appears circular (top right). Of course, on a static single-shot, the movement of the valve leaflets cannot be seen; thus a long-axis Cine acquistion is required for accurate prescription of the valve view.

Localizing the RVOT

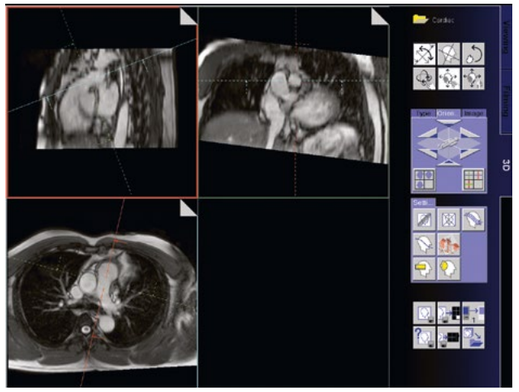

10 Click on the Reset Orientation icon to return to the initial straight MPR views. On the axial MPR (bottom left), locate the main pulmonary artery. Angle the sagittal (red) line along the MPA, and the other line perpendicularly. On the resultant pseudo RVOT (top left), angle the coronal (blue) line along the RVOT, and the other line perpendicularly. The sagittal red line can now be adjusted and rotated to optimize the degree of RV vs. RVOT visualization, and previewed accordingly. The en face pulmonary valve view can also be checked.

Localizing the pulmonary arteries

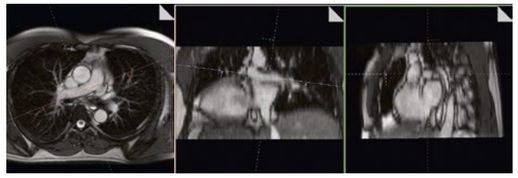

11 Right PA – On the axial MPR, look for the right pulmonary artery branch and angle the long- and short-axis lines accordingly. Do the same on the resulting orthogonal long axis view. The en face RPA view can be directly copied for through-plane flow studies, without further localization scans.

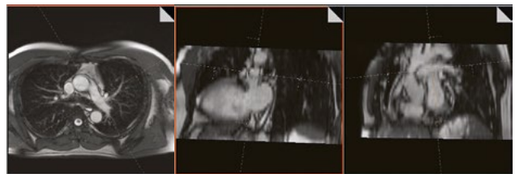

12 Left PA – On the axial MPR, look for the left pulmonary artery branch, and angle the long- and short-axis lines accordingly. Do the same on the resulting orthogonal long axis view. As there is usually only a narrow space between the main LPA and further branches, previewing the circular en face projection allows accurate prescription for through-plane flow studies.

Localizing the coronary **sinus**

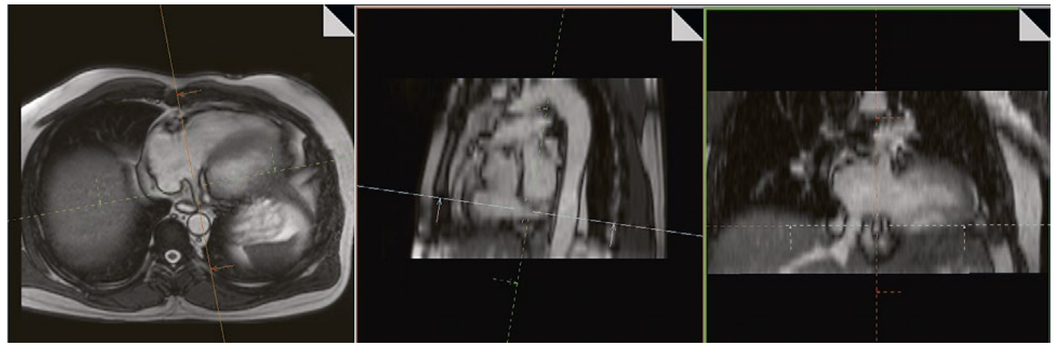

13 Coronary Sinus – Starting from the axial MPR, examine the right atrium for the coronary sinus and angle the long and short-axis lines accordingly. Do the same on the resulting orthogonal long-axis view.

Localizing the SVC and IVC

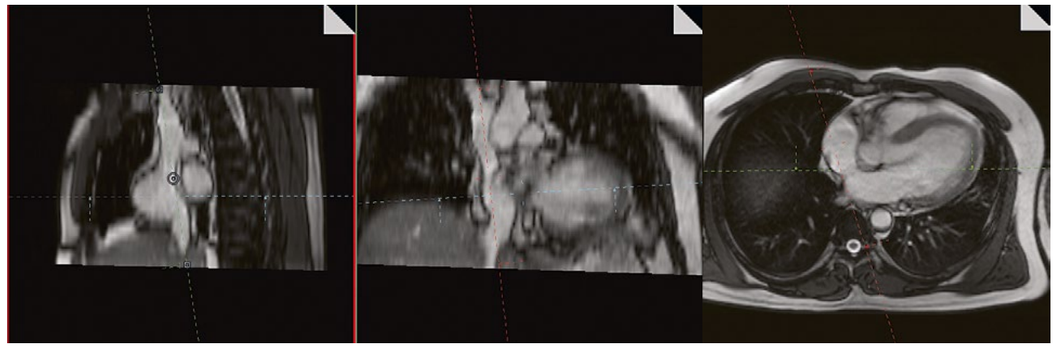

14 SVC and IVC. Starting from the sagial MPR, examine the right atrium for the opening of the IVC and SVC and angle the coronal long-axis line along both. On the resultant coronal MPR, adjust the sagittal MPR line to pass through the IVC and SVC. Check the preview and make fine adjustments accordingly.

Localizing the pulmonary veins

15 Right superior PV. The four pulmonary veins are distinct, yet in close proximity. Careful scrolling of the axial MPR stack can distinguish the individual vessels.

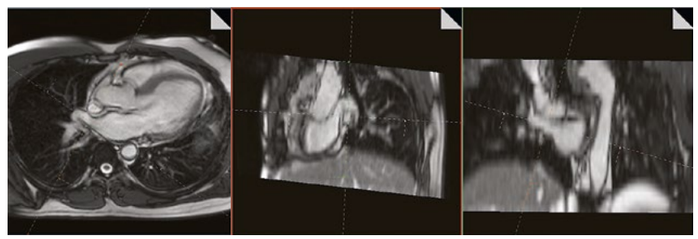

16 Right inferior PV. Usually easy to locate due posterior direction.

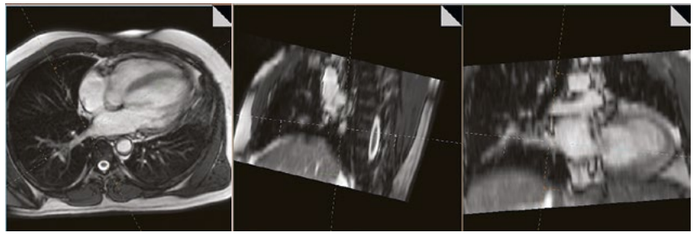

17 Left superior PV. Can be difficult to locate due to the presence of many vessels above and below.

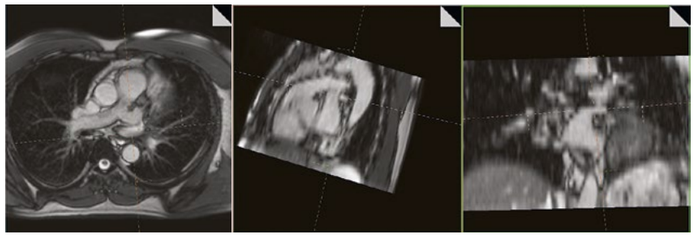

18 Left inferior PV. Usually easy to locate due posterior direction.

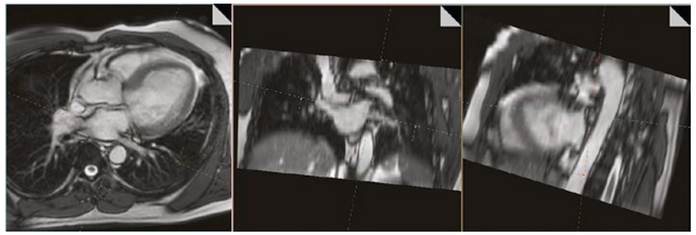

Summary

The 3D Localization technique is an efficient and reliable way to localize cardiac views, especially in unfamiliar anatomical territory e.g. complex cardiomyopathies, post-surgical changes, or animal scans. For new trainees, the ability to visualize anatomy in 3D also promotes a better understanding and appreciation of the required angulations.

The unique advantages are:

- Time saving. It uses the same stack of transverse single-shot TrueFISP or HASTE_db images, which is usually routinely acquired for every examination. No additional 2D localizers are required, thus fewer breath-holds for the patient.
- Higher accuracy from the beginning, due to the benefit of visualizing all other planes. This avoids the initial pseudo or approximation views.
- Reliability and consistency, due to the ability to preview the exact appearance of the projection. This is useful, for example to avoid the aortic outflow tract appearing on the 4C view, or to adjust the appearance of the RVOT and pulmonary valve. It also allows optimization of the rFOV to shorten scan time or avoid aliasing without guesswork or test scans.
- Allows multi-tasking. Since planning is done retrospectively in the 3D Task Card, this can be done while other scans are running. If an MRWP console is available, another person could perform the planning simultaneously (e.g., in complex cases) – saved MPR images will be automatically available on the AWP for the operator.

Contact

Julian Gan
Head of Product & Clinical Imaging
Siemens Healthineers
Singapore
Tel.: +65 8123 4341
Julian.Gan@Siemens-Healthineers.com

CAIPRINHA and SPACE – a Winning Combination

Michel Paret[1]; Pr FG Barral[2]; Christophe Barles[3]; Sylvain Doussin, Ph.D.[4]

[1] GIE IRMAS, Saint-Priest-en-Jarez, France
[2] Department of Neuroradiology, University Hospital Saint-Etienne, France
[3] Siemens Healthineers, Aix-en-Prevence, France
[4] Siemens Healthineers, Erlangen, Germany

Introduction

"MRI is, or is becoming, the medical imaging modality of choice in more and more diverse applications ..." [1].

Magnetic resonance imaging can be described as the success story of medical imaging mainly due to two characteristics: its harmlessness and its ability to manipulate contrast. However, the acquisition technique, which is relatively slow, can be considered a limiting factor, inducing patient discomfort and patient motion. Furthermore, data acquired is mainly 2D.

Acquisition time acceleration has become a major target in these last few years, on the one hand to reduce examination time and, on the other hand, to make MRI accessible to patients suffering from pain and/or non-cooperative patients.

SPACE var T2 with fatsat	SPACE var T1	CAIPIRINHA	Slice thickness (mm)	Voxel size R (mm)	Total TA min:sec Without adjustment
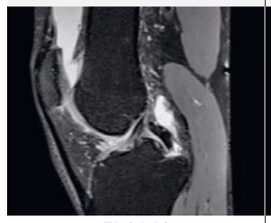 TA 04:46	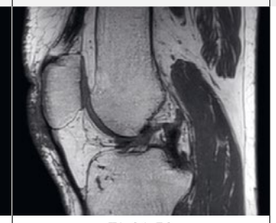 TA 01:50	p4: 2 x 2	0.6	0.5 x 0.5 x 0.6	06:36
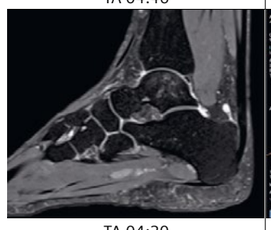 TA 04:20	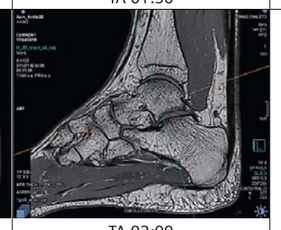 TA 02:09	p4: 2 x 2	0.6	0.5 x 0.5 x 0.6	06:39
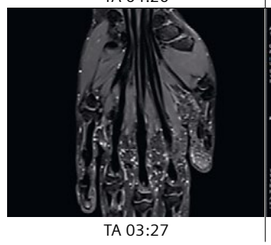 TA 03:27	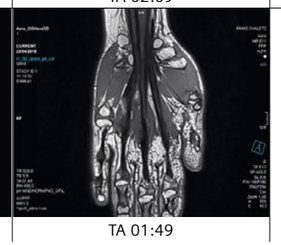 TA 01:49	p4: 2 x 2	0.5	0.5 x 0.5 x 0.6	05:16

Table 1: It is now possible to perform a 3D MSK examination in less than 10 minutes including patient setup (in and out). SPACE with variable (var) flip angle mode for T1 and T2.

Several questions, however, remain:

- How can speed and diagnostic potential be combined? (The GOBrain protocol is the perfect answer to this question [2–4]).
- Is speed related to 2D acquisition? (Jan Fritz et al. propose GOKnee3D for efficient 3D imaging of the knee joint [5]).

GOKnee3D is the explosive combination, mixing SPACE acquisition technique (Sampling Perfection with Application optimized Contrasts using different flip angle Evolution) and the parallel imaging technique CAIPIRINHA (Controlled Aliasing in Parallel Imaging Results in Higher Acceleration) [6, 7]. This protocol gives to radiologists the possibility to explore the knee joint in 3D without acquisition time constraints.

If this combination 3D and parallel imaging technique answers radiologists' expectations for the knee joint, it is justified to consider it for other body regions. We focused on the CAIPIRINHA-SPACE evaluation for various body parts.

Method

Patients were examined with 1.5T MRI MAGNETOM Aera and 3T MAGNETOM Prisma. In our first step, we used the GOKnee3D for other body parts and compared it with conventional 2D acquisitions as regards sensitivity and specificity for the targeted pathologies. We were immediately faced with the tough reality of MRI: tissue characteristics, coils (different g-factors), and protocol parameters (fatsat type, contrast type for SPACE: various proton density or T2 values) are different for each body region and it is necessary to revisit the CAIPRINHA-SPACE parameters to adapt to the anatomical region of interest. Detection of bone edema was a typical example.

To avoid testing the infinite possible combinations, we decided to use a SPACE with various T2 contrast parameters and add, when needed, other protocol parameters (fatsat mode, shim, etc.). This philosophy made it possible to combine our needs in terms of sensibility/specificity and an acceleration factor of 4 (2 x 2 using CAIPIRINHA).

The main optimization strategy was focused on time reduction in 3D acquisition to enable its use in clinical routine without compromise on diagnostic potential.

The second step was to compare conventional SPACE to the new CAIPIRINHA SPACE technique. Main body parts were studied on a 1.5T MRI system. Only the brain could also be studied on 3T, because our 3T system configuration does not include MSK coils. We use this 3T system exclusively for neurology.

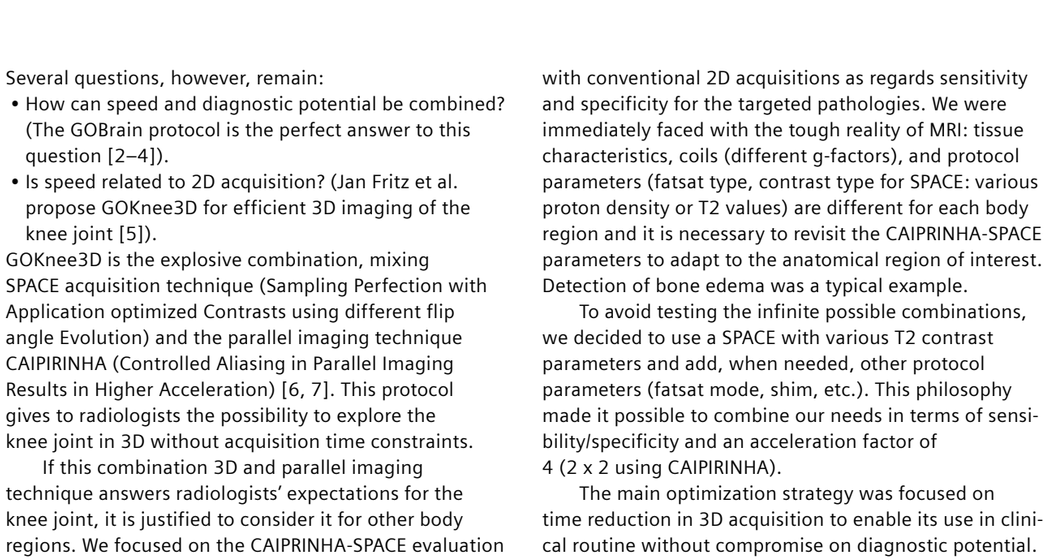

1 MPR reconstruction of 3D SPACE T2 fatsat **(1A)**. Sagittal plane **(1B)** shows meniscus tear better than 2D **(1C)**.

Optimizing MR acquisition and reducing scan times

MSK

Acquisition time reduction is significant. It is now possible to perform a 3D MSK examination in less than 10 minutes including patient setup (in and out) (Table 1). Two fast protocols, 3D T2 fatsat, and T1 are acquired. From a radiologist's perspective, it is no longer necessary to multiply acquisition planes and contrasts; it also avoids a situation in which you have to skip one plane or one contrast.

The multiplanar reconstruction (MPR) potential enables the radiologist to adapt to different patients and pathologies, in a similar approach to MSK in ultrasound (Fig. 1). Complex joint imaging, for example of the ankle or elbow, is facilitated (Figs. 2, 3).

Neurology

CAIPIRINHA SPACE really demonstrated its full potential in this application. It represents, for us, a solution to a major diagnostic challenge. It made it possible to examine in 3D, with a similar examination time compared to the time needed with our two protocols: brain and spine

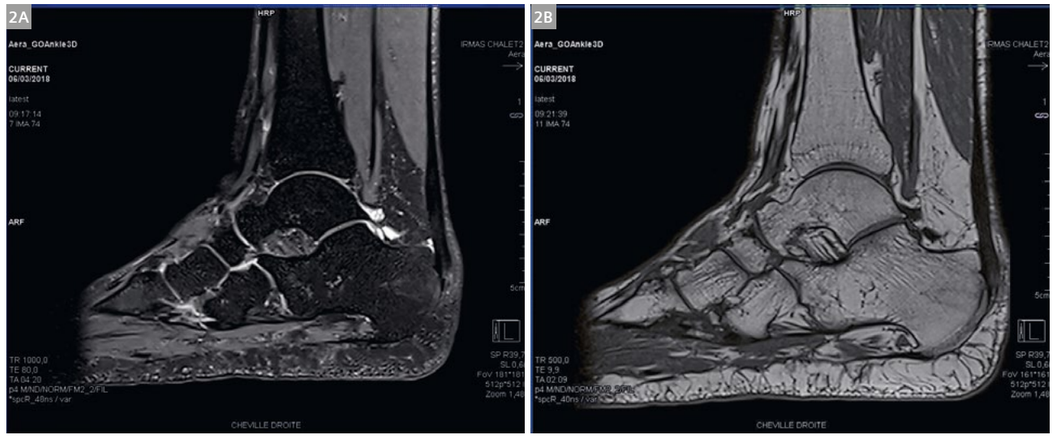

2 3D T2 fatsat and T1 in the ankle. These two acquisitions, with MPR reconstructions of 0.6 mm nicely visualize the Achilles tendon and the bone reactions close to calcaneal insertion.

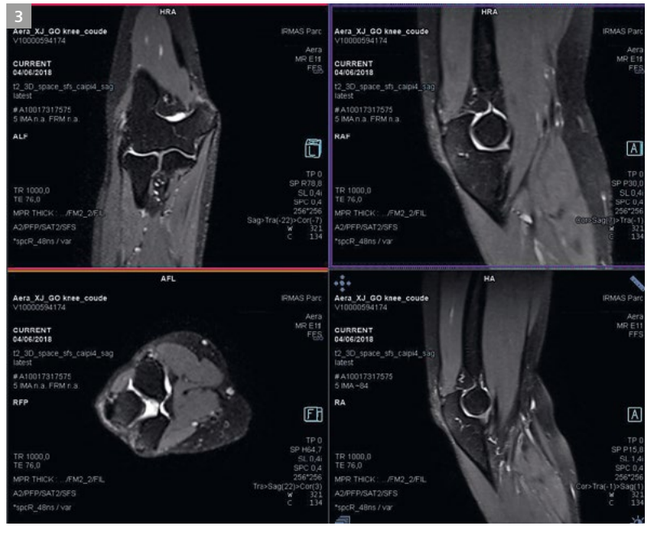

3 3D T2 fatsat of the elbow. Acquired using the 15-channel knee coil. We have used the knee protocol without modification of acquisition parameters. Here the test was focused on the coil.

(Table 2, Fig. 4). 3D imaging for difficult patients becomes possible in MRI and is compatible with examination time constraints. It is the case for non-cooperative patients (e.g., pain symptoms, dementia) or unstable patients (requiring medical assistance: e.g. pediatric anesthesia ...) (Fig. 5).

The AutoAlign localizers started this philosophy of initiating an examination with a 3D protocol. Today, CAIPIRINHA SPACE enables 3D to do more than automating protocols by really imaging the brain. 2D protocols would be used in addition to bring ultra-high resolution and specific contrasts for specific pathologies.

SPACE var T1	SPACE var T2	SPACE FLAIR	Slice thick-ness (mm)	Voxel size R (mm)	Total TA min:sec Without adjustment
MAGNETOM Aera 1.5T					
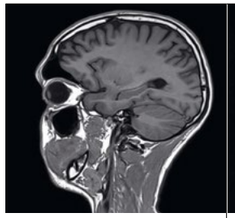	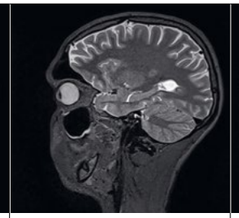	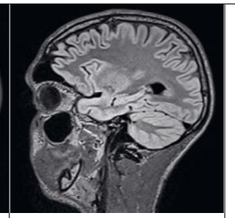	1	0.5 x 0.5 x 1	07:56
TA 02:39	TA 02:50	TA 02:27			
MAGNETOM Prisma 3T			CAIPIRINHA p4: 2 x 2		
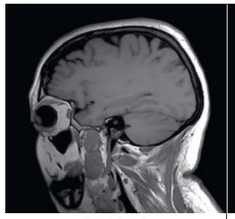	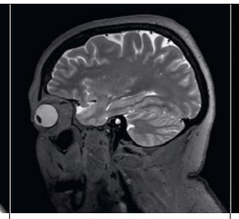	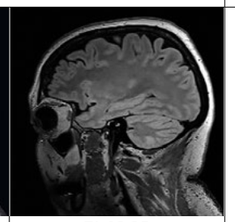	0.9	0.5 x 0.5 x 0.9	07:20
TA 02:43	TA 02:02	TA 02:35			

Table 2: CAIPIRINHA SPACE really demonstrated its full potential in brain imaging. SPACE with variable (var) flip angle mode for T1 and T2.

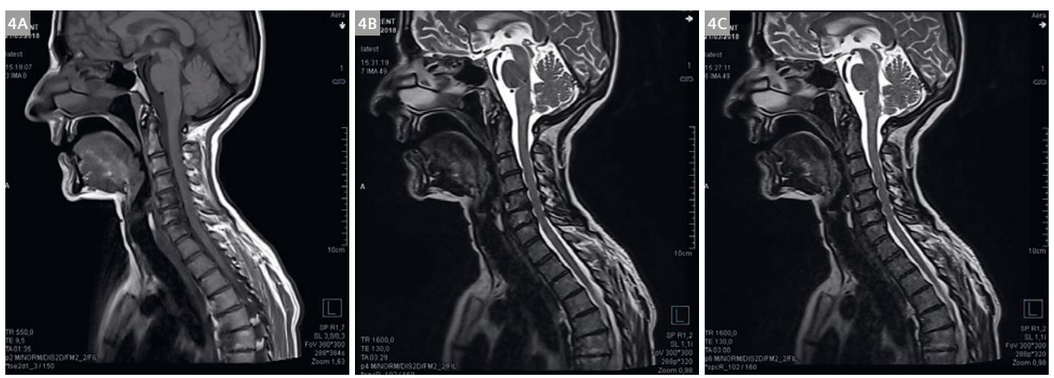

T1 TSE 2D
TA 01:35

T2 SPACE
CAIPIRINHA 4
TA 03:29

T2 SPACE
CAIPIRINHA 6
TA 03:00

4 Time necessary for c-spine exploration in T1 TSE 2D 3 mm and T2 3D 1 mm can be less than 5 minutes. The Head/Neck 20-channel coil used here enables the use of CAIPIRINHA factor 6 (3 x 2) without reconstruction artifacts.

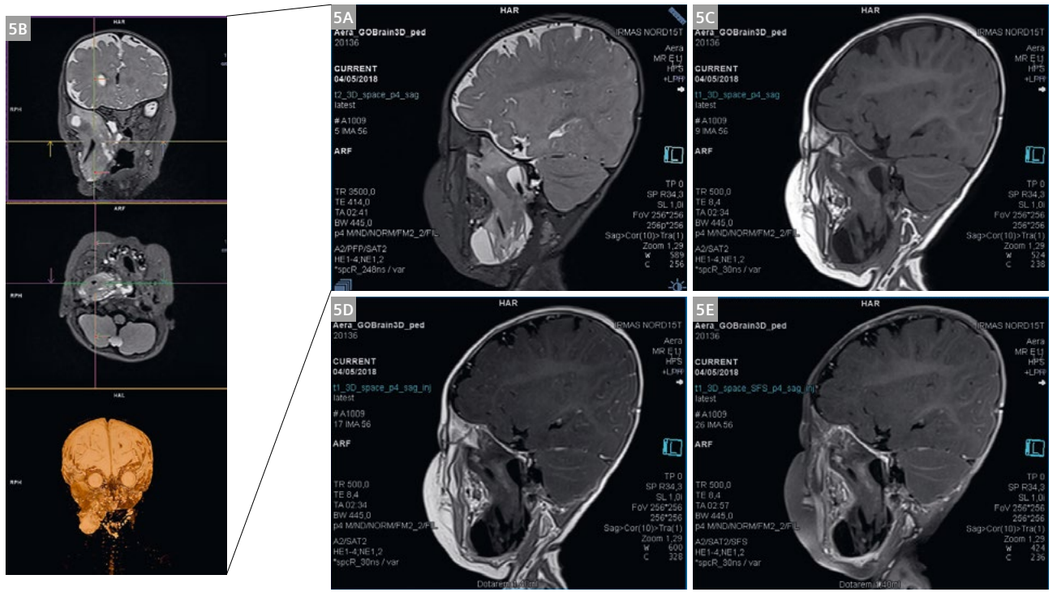

5 Examination of a 10-months-old child[1] under general anesthesia, in the context of ENT pathology follow-up. Target was to provide to radiologist all necessary information to evaluate patient response to therapy, in a very short acquisition time. In 10 minutes it was possible to run four 3D protocols with different contrasts (T2, T1, T1 with contrast enhancement, T1 fatsat with contrast enhancement), with MPR reconstructions (all consistent as done by the system through MPR Planning Dot AddIn). Anesthesia has been shorter, with easier recovery. A win/win examination for both patient and radiologist!

[1] *Siemens Healthineers disclaimer does not represent the opinion of the author. MR scanning has not been established as safe for imaging fetuses and infants less than two years of age. The responsible physician must evaluate the benefits of the MR examination compared to those of other imaging procedures.*

With the spine version of CAIPIRINHA SPACE, one usual argument of 3D spine imaging detractors disappears. Acquisition time and MPR reconstruction quality make it possible to outperform 2D protocols (Table 2).

Distributing CAIPIRINHA SPACE protocols to remote MR scanners

Our institution owns eight MR scanners (including five MAGNETOM Aera 1.5T). As a result, homogeneity within our fleet is a major issue. The more MRIs you have, the harder it is to reach this target. Using our MRIs in a coordinated way as well as being faster and more efficient in the optimization process of CAIPIRINHA-SPACE for multiple body parts made it possible to examine more patients. To improve reactivity and for better ease-of-use, this process was achieved with the help of teamplay Protocols for real-time distribution (Fig. 6). The distribution of the different versions, the exchange between different systems via the web platform of teamplay, in real time, realized a true gain in efficiency. The MR protocol hub option also gives access to the protocol/study files (.exar) published on MAGNETOM World at **www.siemens.com/magnetom-world** > Clinical Corner > Protocols.

Conclusion and outlook

CAIPIRINHA SPACE represents more than an acquisition technique; it really is a new acquisition philosophy where 3D finally takes the place it deserves in our imaging specialty. No body region is excluded (Fig. 7). CAIPIRINHA SPACE is currently accessible on all *syngo* MR E11C AP04 platforms, without an additional software license.

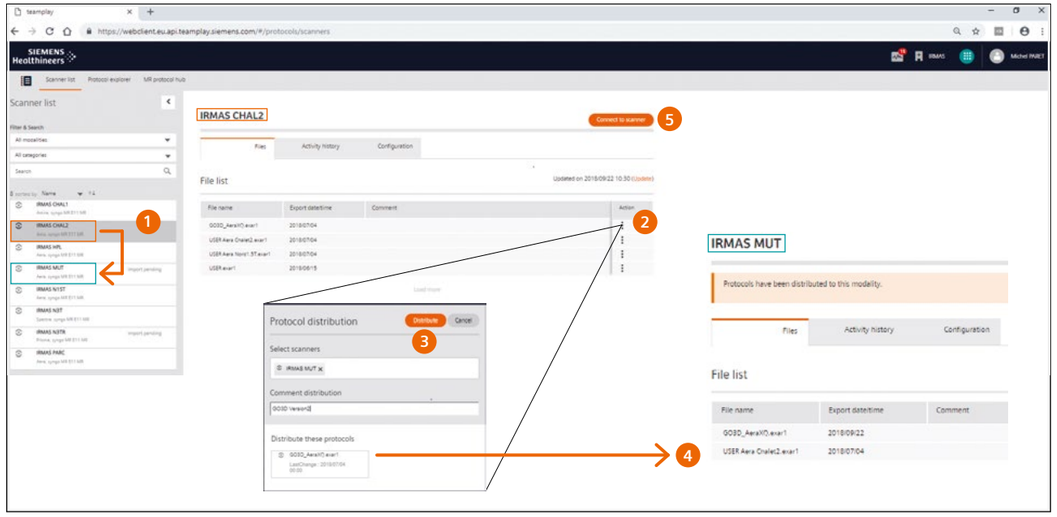

6 CAIPIRINHA SPACE protocol distribution (protocol name GO3D), using .exar file format, from one system to another. First the GO3D protocol is exported from the source system to be accessible in the teamplay Protocols interface. Protocol distribution is done from the teamplay interface, by first selecting the source system protocol, and then the destination system. Once distributed, the .exar file GO3D is accessible on the selected system. Two solutions are possible for the .exar file importation in the client user: either let the remote site import it through shared folder, or initiate a remote control session from the source system.

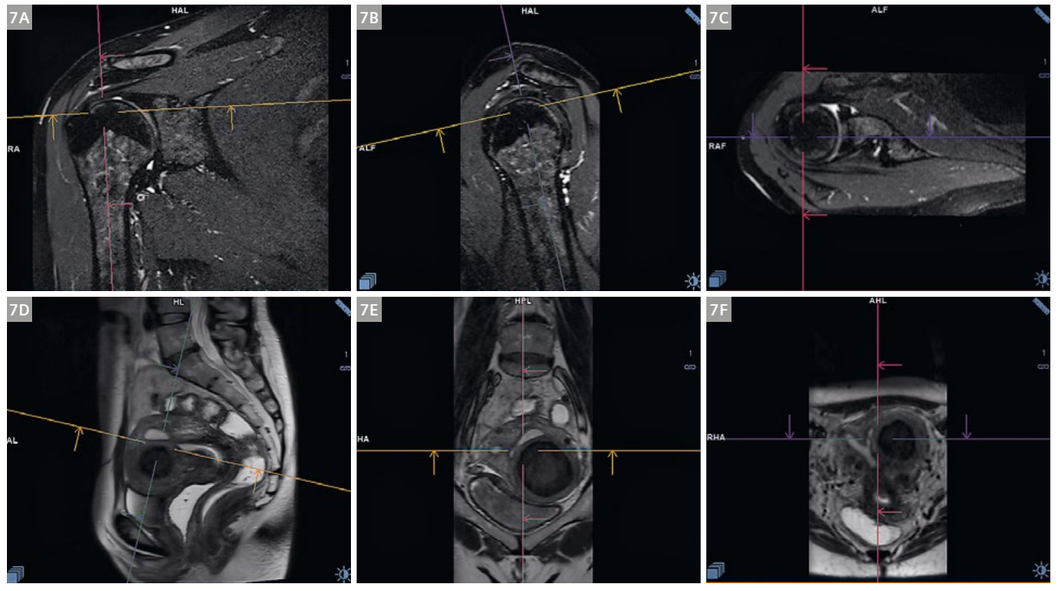

7 The CAIPIRINHA SPACE technique is robust enough to be used on more complex organs, sensitive to motion like shoulder **(7A–C)** or pelvis **(7D–F)**.

Acknowledgements

Our recognition and gratitude goes to all the people participating in the development and optimization of the CAIPIRINHA SPACE technique multi-organs, operators, and radiologists in GIE IRMAS, our institution, marketing team, IT & Digital Care, Customer Service, and application specialists at Siemens Healthineers France, but also to Julien Gervais and Michaela Martin, Siemens Healthineers, with whom we collaborated intensively to digitalize our imaging processes.

Download CAIPIRINHA SPACE protocols for 1.5T MAGNETOM Aera and MAGNETOM Sola at
www.siemens.com/magnetom-world
> Clinical Corner > Protocols

Contact

Michel Paret
MR Technologist
GIE IRMAS
110 avenue Albert Raimond
42270 Saint-Priest-en-Jarez,
France
mparet@irmas.fr

References

1 Meder J, Pruvo J (2011). Magnetic resonance imaging: round-up of current applications and outlook. Controle ASN (Paris), (192), 40-42.
2 Miller E, Smith B. Pediatric GOBrain-5-Minute Protocol MR Imaging at 3 Tesla. MAGNETOM Flash (68)2/2017, 14-18.
3 Prakkamakul S, et al. Ultrafast Brain MRI: Clinical Deployment and Comparison to Conventional Brain MRI at 3T. J Neuroimaging, 2016(5):503-10.
4 Fagundes J, Longo M, Huang S, Rosen B, Witzel T, Heberlein K, Gonzalez R, Schaefer P, Rapalino O. Diagnostic Performance of a 10-Minute Gadolinium-Enhanced Brain MRI Protocol Compared with the Standard Clinical Protocol for Detection of Intracranial Enhancing Lesions, American Journal of Neuroradiology, 38, 9, 1689.
5 Fritz J, et al. Three-dimensional CAIPIRINHA SPACE TSE for 5-minute high-resolution MRI of the knee. Invest Radiol 2016; 51: 609-617.
6 Mugler III J, Optimized Three-Dimensional Fast-Spin-Echo MRI. Journal of MRI 39:745–767 (2014).
7 Breuer F, et al. Controlled aliasing in volumetric parallel imaging (2D CAIPIRINHA). MagnReson Med 2006 55(3),549-556.

Improving Resolution, Productivity, and Diagnosis. SMS TSE and GO Protocols in an Optimized Clinical Workflow.

Johan Dehem, M.D.
VZW Jan Yperman, Ypres, Belgium

SMS TSE for shorter scan times and thinner slices

Simultaneous Multi-Slice (SMS) acquisition is a technique that we know from EPI DWI that delivers consistently good results. SMS enables faster scan times and thinner slices, leading to an increase in resolution, better diagnosis, and more productivity at the scanner.
The value of SMS is known from extensive experience with the MAGNETOM Aera system. Since SMS TSE (turbo spin echo) is an integral part of MAGNETOM Sola, we were eager to start using SMS in TSE imaging.

Using SMS with a factor 2 on MAGNETOM Sola renders twice the amount of slices in the same time.
So, you can either scan faster (halving the number of concatenations in T1 for example), or scan 50% thinner slices, or achieve 200% coverage with the same slice thickness, or combine all of them. Numerous thin slices are especially beneficial in the axial plane; however, where you need many coronal or sagittal slices, SMS is also the best option since it does not consume time or signal.

Using SMS in small joint imaging like wrist, elbow, and ankle, we are able to achieve large coverage with really thin slices. Also it allows us to scan the complete pelvis/both hips with thin slices – as thin as 3 or even 2 mm. This would have required a prohibitive amount of time before SMS TSE. It can also be employed whenever you need the combination of large coverage and thin slices, e.g., to examine the course of a peripheral nerve.

Looking at our initial experiments with SMS TSE, we began by simply ticking the checkbox SMS factor 2 in the acceleration subcard of the resolution card in a coronal T1 TSE sequence and using that SMS factor to bring the number of concatenations from 2 to 1:

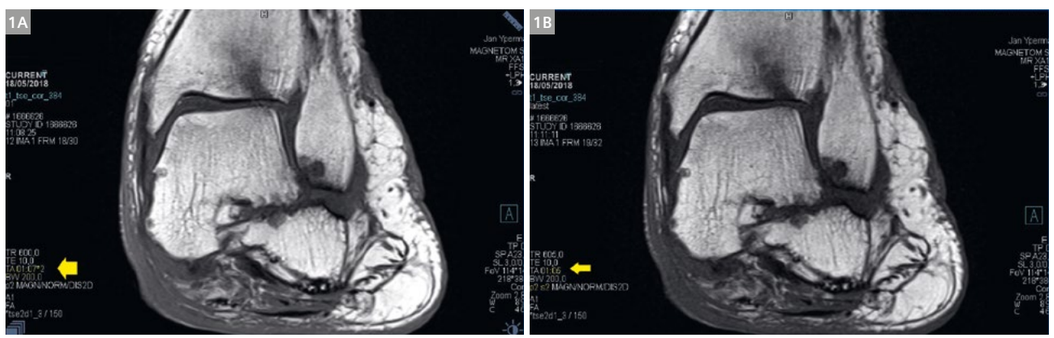

1 Corresponding image of the first attempt at SMS: Simply ticking SMS factor 2 halves the number of concatenations from 2 to 1. This effectively halves the acquisition time from 02:14 min to 01:05 min (yellow arrow) without discernable loss in signal or image quality.

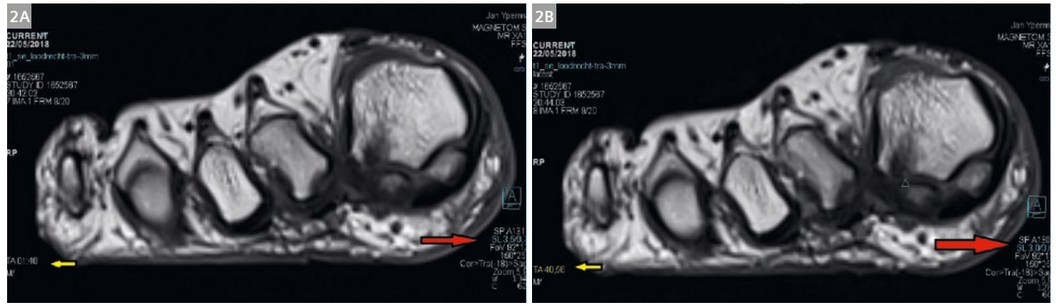

2 Another early experiment using SMS to scan with a thinner slice thickness (red arrow). This actually leads to better depiction of osteochondral lesion (top of yellow triangle) and 60% reduction in acquisition time (yellow arrow). **(2A)** 3.5 mm in 100 seconds, **(2B)** 3 mm slice thickness in 40 seconds.

This early experimenting was quite convincing and SMS TSE was subsequently adopted in most of our 2D TSE MSK sequences early on. The only exception was in regions where there is already enough coverage with thin slices, e.g., coronal slices of distal extremities (fingers, toes ...), where only a small number of slices are needed. Our main goal is to scan quickly (SMS halves the number of concatenations in T1; halves the TR in intermediate-weighted sequences) and/or increase resolution by scanning thinner slices where SMS halves the TR. This eliminates the time penalty one normally gets by increasing the number of slices. One can also use SMS to remaster and optimize sequences from scratch to combine thinner slices, more coverage, and a shorter acquisition time. SMS is yet another degree of freedom to further optimize your imaging.

Some examples from our clinical routine in the following cases:

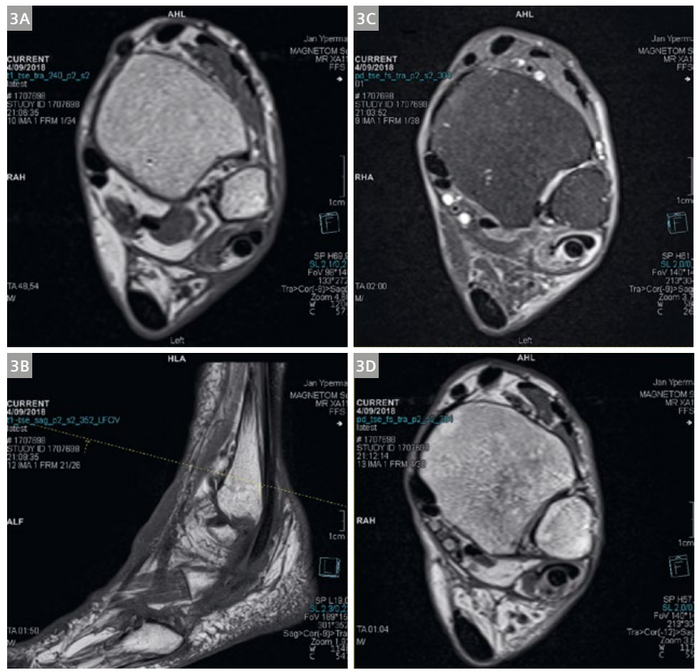

3 Example of SMS in an ankle exam. Sagittal and axial T1, 2 mm slices **(3A, B)** and axial PD and PD fatsat 2 mm images **(3C, D)** in high resolution and short imaging times nicely demonstrating peroneal tendon rupture.

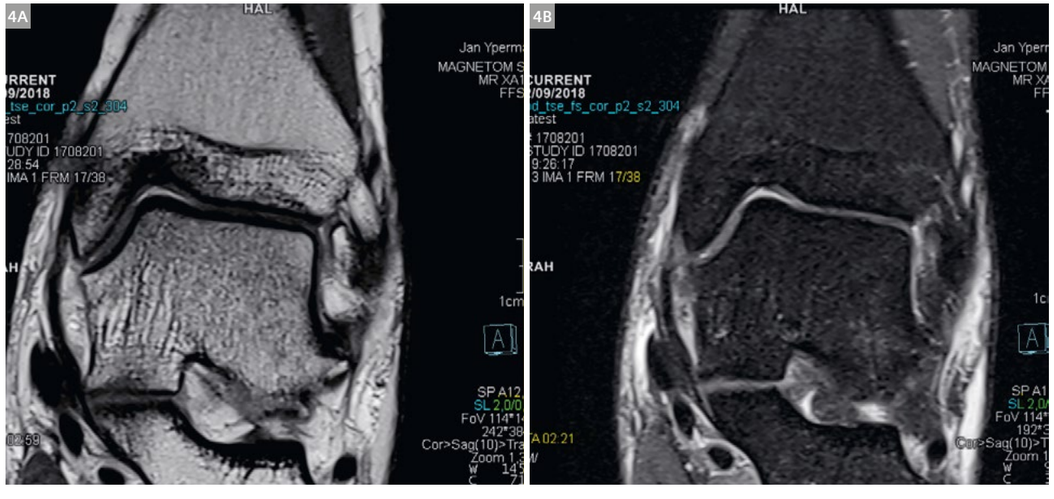

4 Coronal PD and PD fatsat 2 mm slice thickness, 0.5 mm in-plane resolution and 38 slices in 2.21 seconds for the PD fatsat. Great delineation of cartilage in talar dome and distal tibia; at 1.5T.

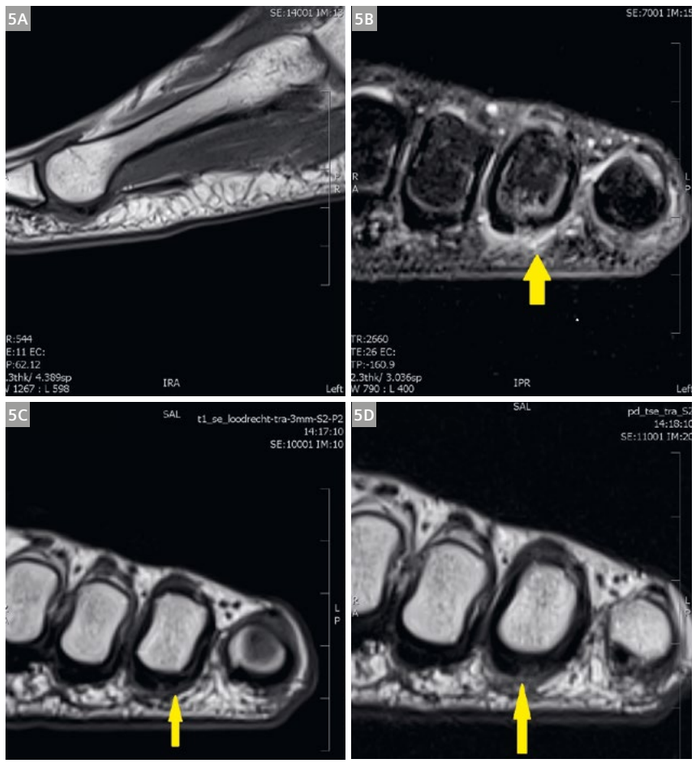

5 Plantar plate tear (yellow arrow) easily depicted on thin slice imaging: Fast and with many thin slices is the new adage in foot imaging!

In hip imaging, standard full coverage of both hips and complete pelvis was formerly done with 5 mm slice thickness, since thinner slices would demand more TR and or concatenations, making it impossible to fit this exam into our 20-minute timeslot. Again, SMS imaging is the solution to scan more and thinner slices in the same or shorter acquisition time, leading to standard use of SMS for standard hip/pelvis imaging (Fig. 6).

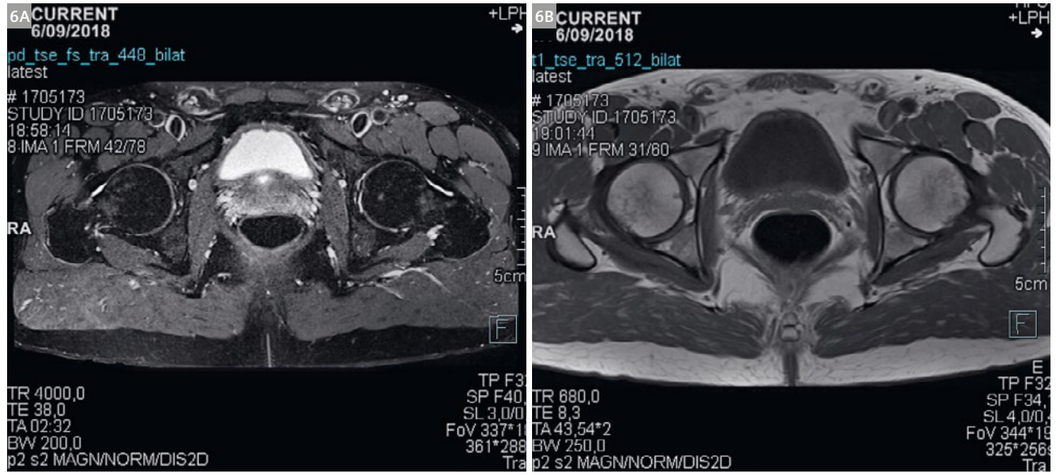

6 Standard imaging of both hips: standard SMS PD fatsat 3 mm thick slices covers complete pelvis with 78 slices two and a half minutes and standard SMS T1 4 mm with 60 slices in one and a half minutes.

The combination of large coverage in the z-axis with thin axial slices can be especially challenging, e. g., scrutinizing the course of small peripheral nerves like the gluteal branches of the nervus cutaneus femoralis dorsalis, which is still considered to be a 3T indication. Thin-slice SMS with this convincing image quality in a reasonable time (4 minutes for 90 slices of 2 mm) improves the reputation of your facility by allowing you to say, "Of course we can because Sola is better than the 3T results we have seen in various studies." It takes some nerve, however MAGNETOM Sola and SMS thin slices allow you to perform these scans with confidence.

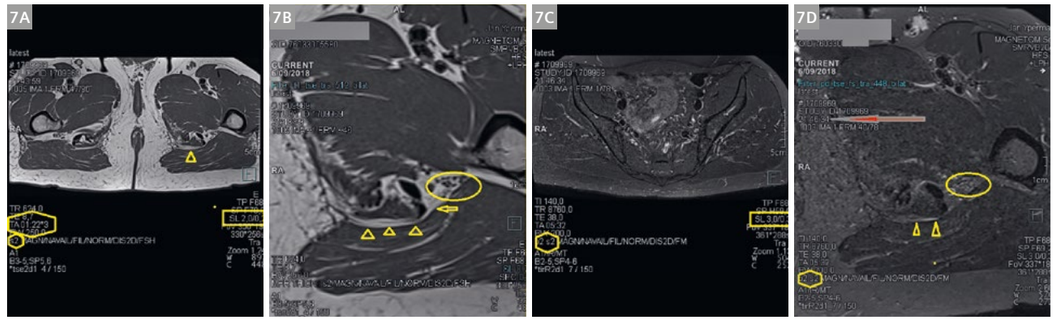

7 SMS T1 TSE **(7A, B)**: 2 mm slices, 90 slices in 4 minutes. SMS PD fatsat 3 mm slices thickness **(7C, D)**. The images 7B and 7D are magnified. The yellow arrows point at the upper gluteal branch of the nervus cutaneus femoralis dorsalis dorsal to the semitendinosis, ventral to the gluteus maximus just caudal to tuber ischiadicum. Red arrow points to time in the evening. Sciatic nerve fascicles in yellow circle.

In the wrist, tendons run a long way. A great many thin slices are required to image them properly. SMS handles this task with ease and accuracy, in short acquisition times.

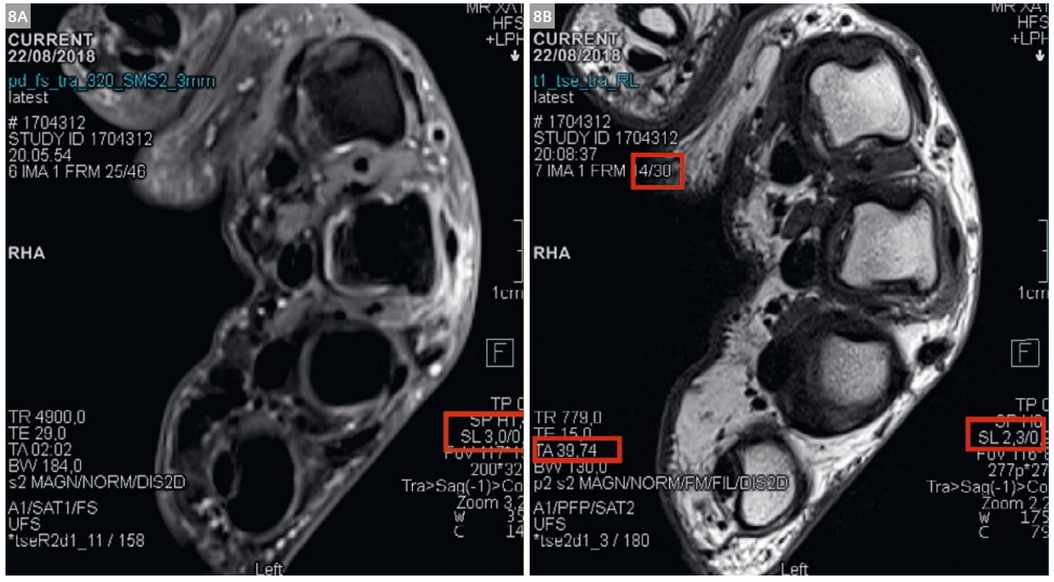

8 Axial PD FS 46 slices 3 mm thick in 2 minutes, axial T1 TSE 30 slices 2.3 mm thick in 40 seconds. Ultra Flex Small 18-channel coil, imaged off center. SMS factor 2.

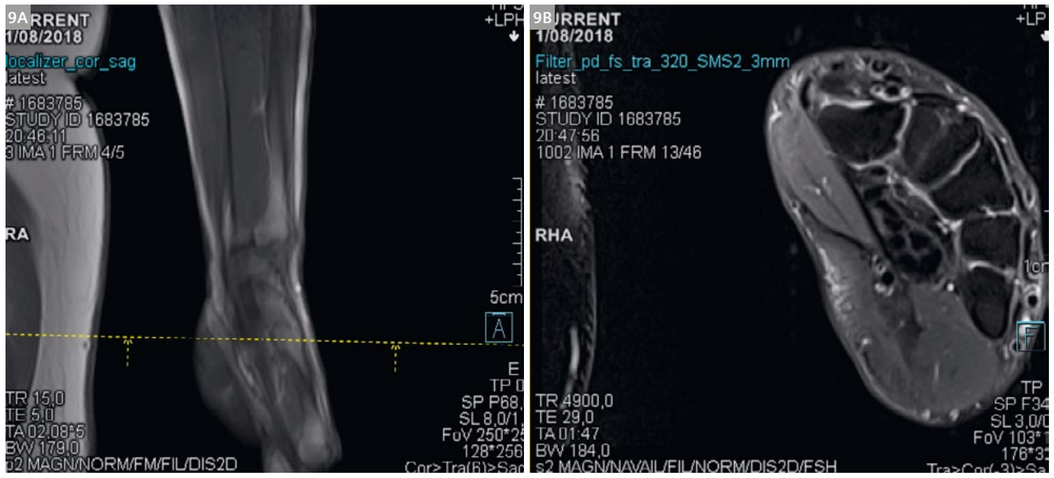

9 The days of the superman position are over. Since we have had a MAGNETOM Sola, all wrist exams are done with the wrist comfortably resting next to the body, and the dedicated wrist coil is more often replaced by the comfortable Ultra Flex Small 18-channel coil.

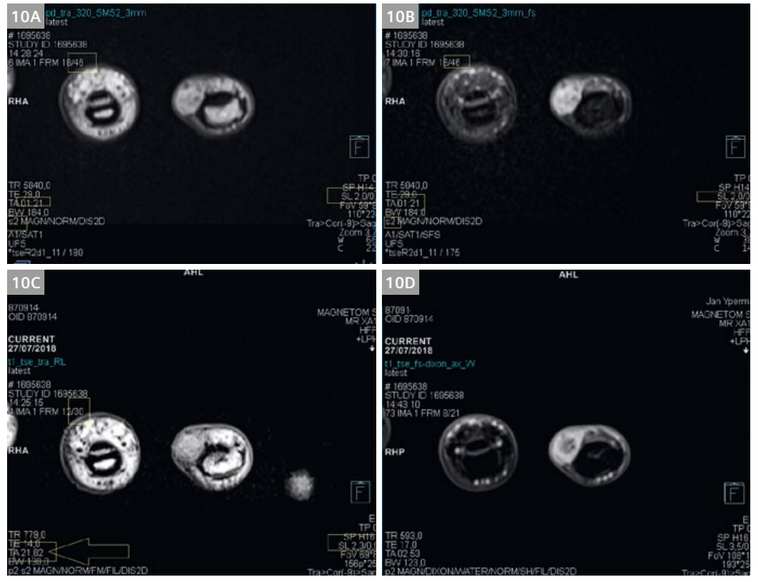

10 A 30-year-old female patient presented with bluish discoloration and swelling of the radial side of the ring finger, pain, and acceleration in swelling for several weeks. T1 and Proton Density iso – slightly hyperintense, PD fatstat hyperintense, peripheral fast-enhancing sharply demarcated subcutaneous mass with hypointense spots and hypoenhancing center. SMS makes it possible to have all these high resolution thin slices in an amazingly short acquisition time (notice 22 seconds for 30 slices T1 TSE 2.3 mm see 10C). Surgically confirmed partially thrombosed hemangioma). The T1 after contrast was done using Dixon fatsat since this challenging environment contains more air than tissue. Again, all images are ac-quired with the Ultra Flex Small coil.

Just as in wrist imaging, elbow imaging is no longer done using the knee coil in superman position, but conveniently off center with the elbow lying comfortably next to the body. Superman no longer holds a position in our department, he just got fired.

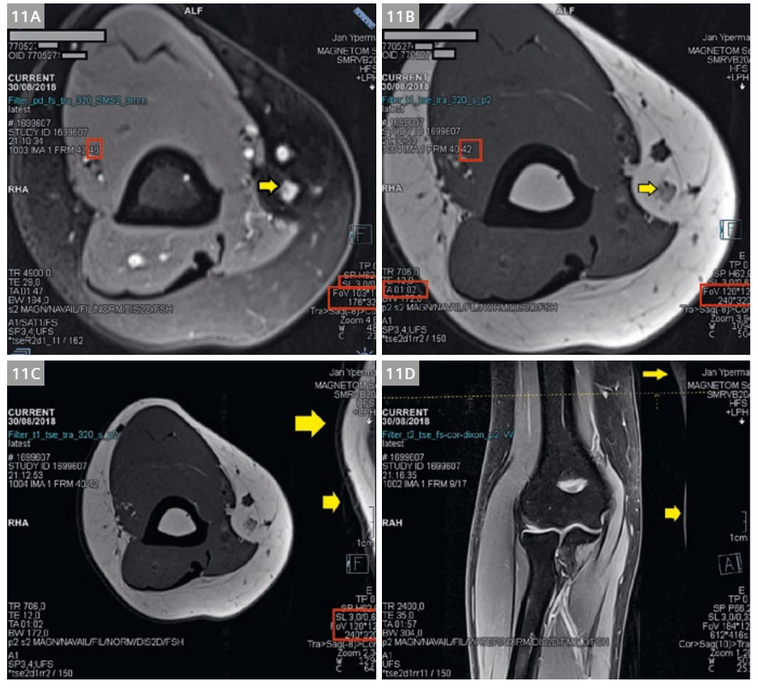

11 Elbow exam with the arm resting comfortably to the right of the abdomen (right flank indicated by large yellow arrows). SMS imaging T1 and PD fatsat with thin slices 3 mm, high in-plane resolution (0.5 mm) and 42 T1 TSE slices in one minute and two seconds. Notice the high image quality allowing you to zoom in and pick up details like the hilum of a small lymph node (arrows in 11A, B).

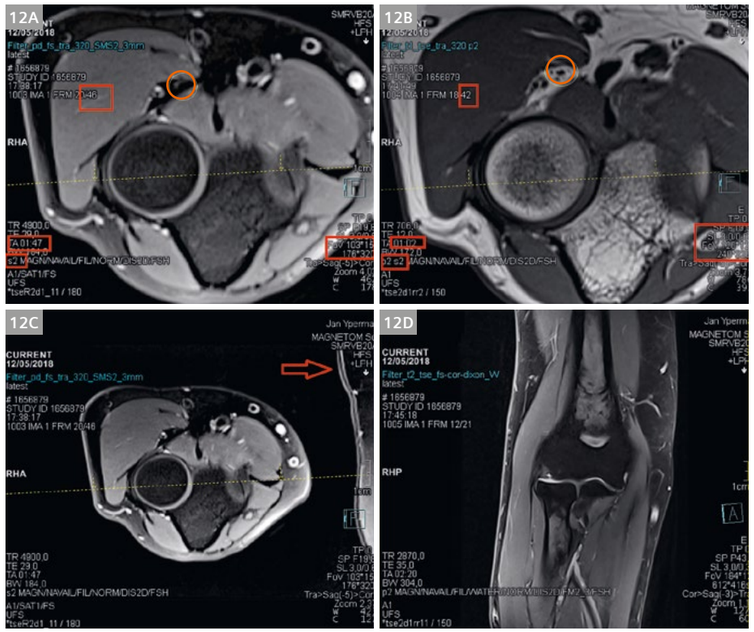

12 Our first elbow exam with the Ultra Flex Small coil; off center, arm resting comfortably to the right of the abdomen (right flank indicated by large red arrow). SMS imaging T1 and PD fatsat with thin slices 3 mm, high in-plane resolution (0.5 mm); acquisition of 42! T1 TSE slices in one minute and two seconds. Zoomed images in the upper row show detail such as annular ligament surrounding radial head or, for example, the course of the radial nerve (circle).

Learn more about Simultaneous Multi-Slice!

For more insights into this exciting new technology, designed for unprecedented speed in imaging to shorten patient's table time visit us at

www.siemens-healthineers.us/magnetom-world
> Hot Topics > Simultaneous Multi-Slice

Here many scientists and clinicians worldwide share their insights, experiences and perspectives on this innovative new technology.

The new 18-channel Knee Coil is easy to handle, lightweight, and particularly comfortable for our patients. In the first four months of our experience with 1.5T MAGNETOM Sola to date, we have not yet had a single patient who did not fit in the knee coil. As shown in Figure 13, the patient is laying comfortably with her feet first leaving sufficient room in the knee coil and sufficient room for the other leg.

GOKnee3D, with the appealing concept of high resolution scanning at short examination times using SPACE 3D with CAIPIRINHA-based 4-fold acceleration, was introduced as early as 2017 by Jan Fritz, M.D., of Johns Hopkins University School of Medicine [1]. The GOKnee T2 FS comes out of the 'Siemens sequences box' at 0.8 mm isotropic. We enhanced that resolution to 0.6 isotropic proton density, which still provided us with more than enough signal. The new knee coil has improved patient comfort significantly, allowing patients to lie still. Based on prior experience, meniscal and cartilage tear detection and characterization are highly facilitated by real 3D high resolution, while bone marrow edema is equally well depicted when compared to standard knee imaging.

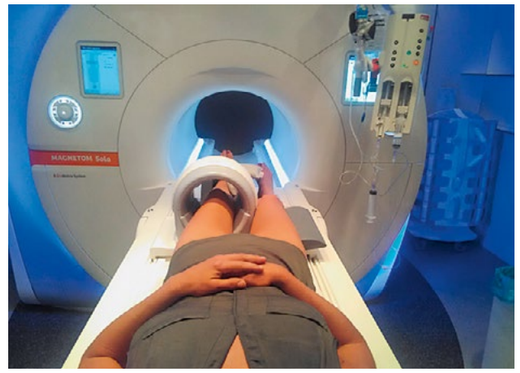

13 Sufficient room in the 18-channel Knee Coil with 1.5T MAGNETOM Sola.

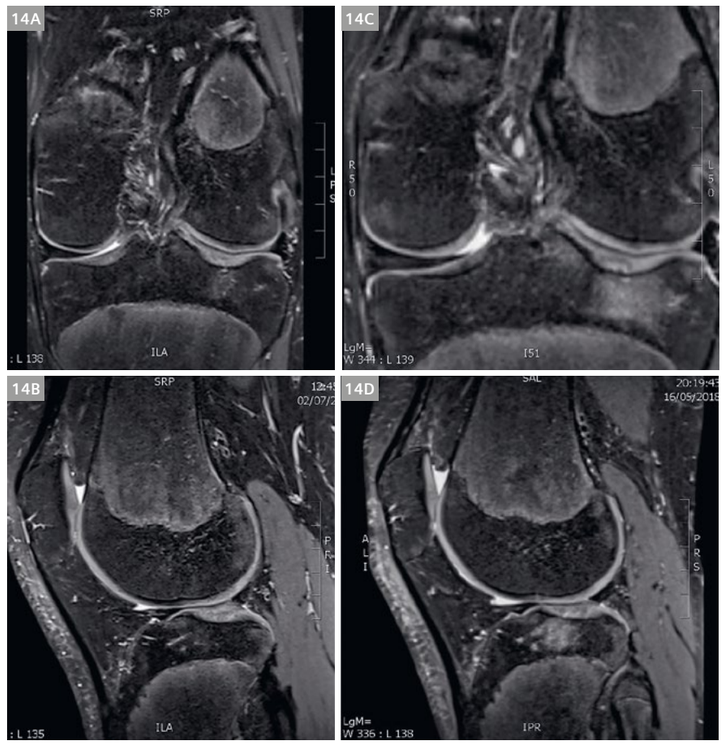

14 In May 2016, the GOKnee sequence **(14C, D)** demonstrates subchondral stress fracture and chondral fracture with adjacent bone marrow edema. Marked healing on the follow-up exam in February 2017 **(14A, B)**. Increasing resolution from 0.8 **(14C, D)** to 0.6 isotropic **(14A, B)** sharpens the image a great deal; still there is sufficient signal even at this higher resolution. The acquisition time for this higher resolution of 0.6 isotropic has increased to 6 min. Adding 38 x 3 mm slices, sagittal SMS T1 TSE takes another 40 seconds and an axial GE another 38 seconds, which altogether with the localizer adds up to a table time of less than 10 minutes.

GOKnee3D Protocols
Fast high-res 3D knee exams in 10 min. Download .exar1 files for 1.5 and 3T at
www.siemens.com/magnetom-world
> Clinical Corner > Protocols

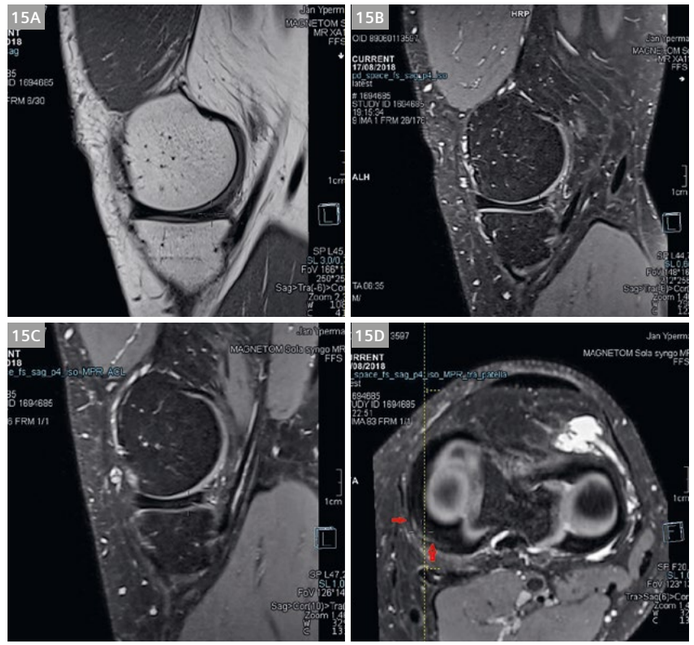

15 The axial reconstructions in the meniscal plane **(15D)** make it particularly easy to pick up small tears that were previously unrecognized, as is the case in this peripheral tear in the posterior horn medial meniscus (arrow) with hyperintense signal extending to the cartilage both on the native sagittal slice **(15B)** and 1 mm thick reconstruction **(15C)**. GOKnee3D is excellent at depicting small details.

Though not all knee pathology is subtle.

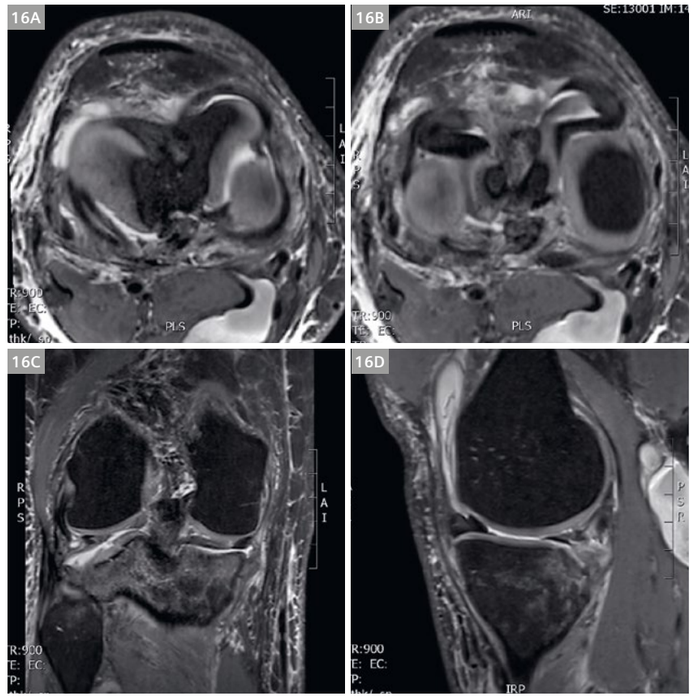

16 This patient endured a severe crash during a horse carriage race. GOKnee3D 0.6 isotropic reveals bilateral bucket handle meniscal tears, tibial plateau fracture, and torn cruciate ligaments. This resulted in hemarthrosis, ruptured capsule, and a Baker cyst. Bone marrow edema is easily depicted. Having a comfortable coil and comfortable position even in painful conditions is of real value and key to high image quality.

Seeing these consistent GOKnee3D results on MAGNETOM Sola makes it tempting to expand this concept further to the shoulder, ankle, wrist, hip, and elbow. This is how GOKnee performs on the elbow (same patient as in Figure 12).

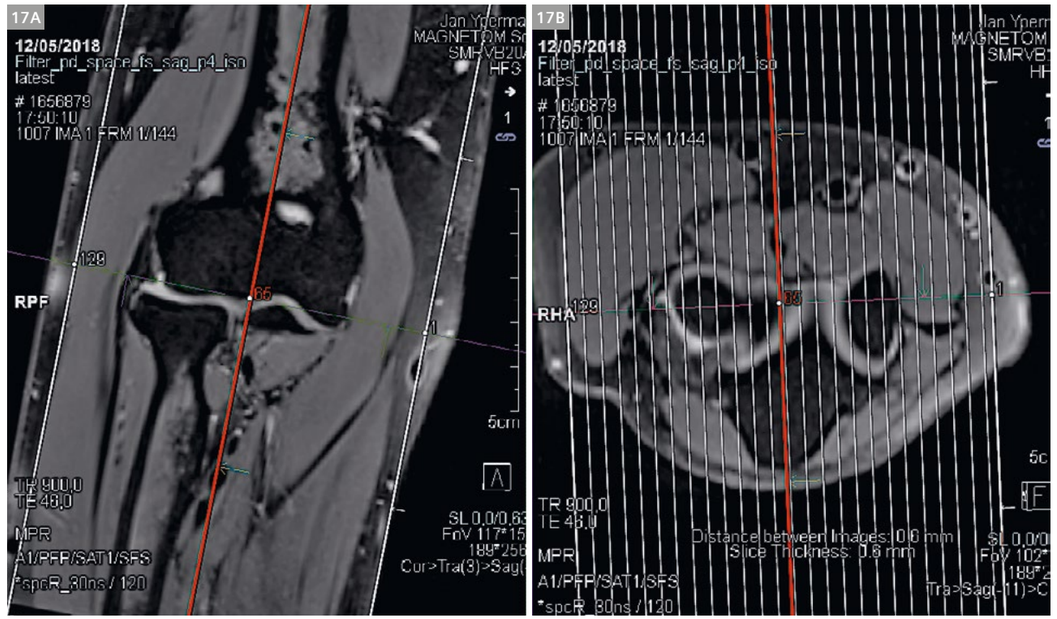

17 Screenshot of our very first 'GOElbow'. 0.6 isotropic acquisition enables high resolution reconstructions at will.

Since that first 'GOElbow' (Figures 12 and 17), all of our elbow exams enjoy the high resolution that Space3D_caipi4 technique offers, in addition to the SMS axial acquisitions (except in the presence of metallic hardware[1], that is). Other joints were quick to follow. Here is an example of cartilage lesions in hip imaging using 'GOHip'.

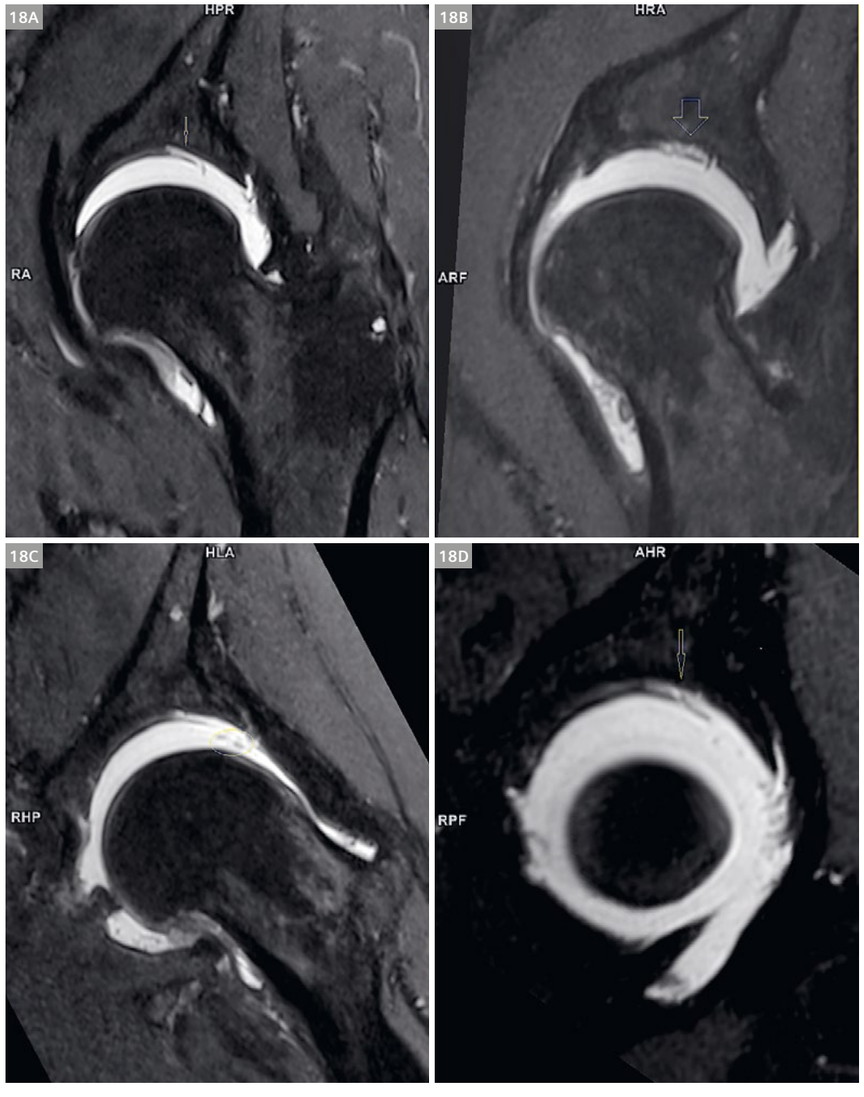

18 MR arthrogram hip exam (using skin traction), the Space3D_caipi4 sequence further enhanced up to 0.5 isotropic (5 min 41 acquisition time) with native slices **(18A)** and MPR reconstructions depicts cartilage delamination, denudation, and rice bodies in exquisite detail. To be consistent, we call this exam: 'GOHip'.

[1]*The MRI restrictions (if any) of the metal implant must be considered prior to patient undergoing MRI exam. MR imaging of patients with metallic implants brings specific risks. However, certain implants are approved by the governing regulatory bodies to be MR conditionally safe. For such implants, the previously mentioned warning may not be applicable. Please contact the implant manufacturer for the specific conditional information. The conditions for MR safety are the responsibility of the implant manufacturer, not of Siemens.*

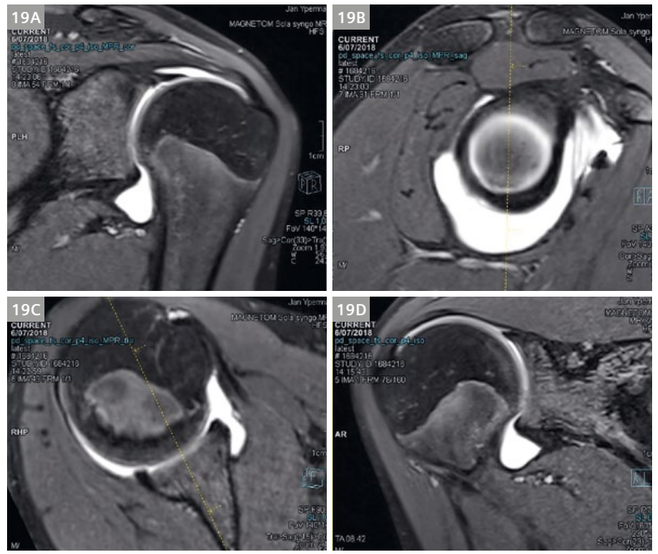

19 Normal MR arthrogram using Space3D_caipi4 technique, a.k.a., 'GOShoulder'. Coronal acquisition 0.5 mm isotropic resolution **(19D)** and three orthogonal thin slice MPR reconstructions. Exquisite cartilage delineation is shown.

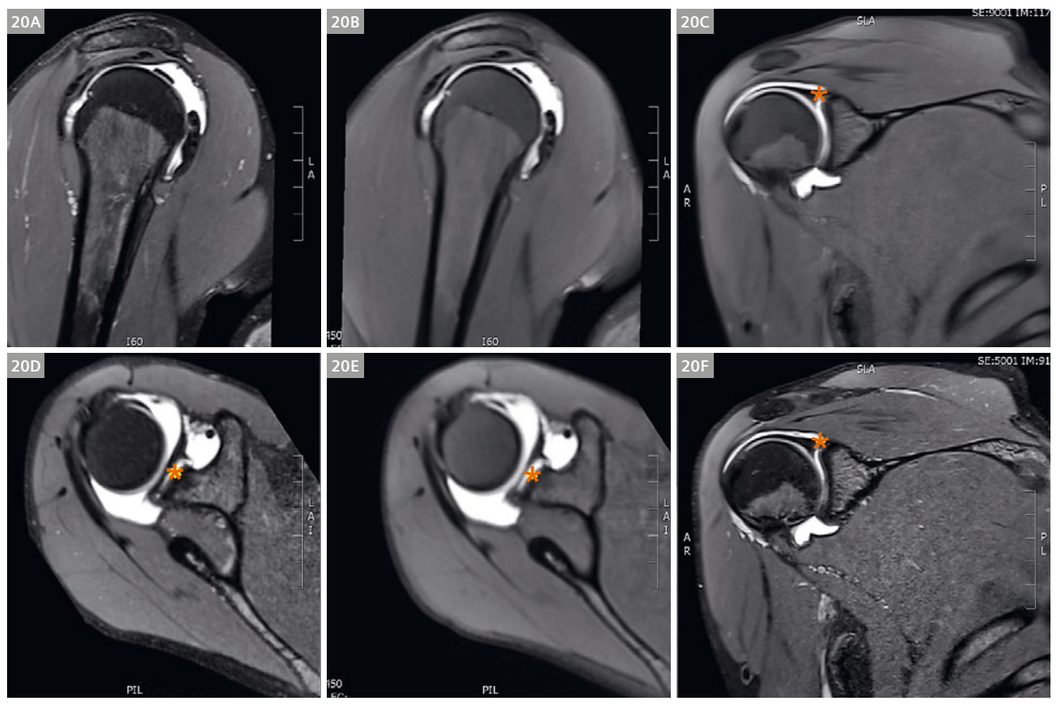

20 Changing a few parameters in the Space3D_caipi4 results in a nice T1 CAIPIRINHA 4 SPACE acquisition, ideal for an arthrogram. This young basketball player had unexplained shoulder pain during and after the game. Slap II lesion (*) easily demonstrated in two 'GOShoulder' acquisitions after arthrogram: T1 fatsat and PD fatsat Space3D_caipi4 each with 0.5 mm isotropic resolution. Coronal acquisition **(20C, F)** with axial **(20A, D)** and sagittal MPR reconstructions **(20A, D** and **20B, E)**.

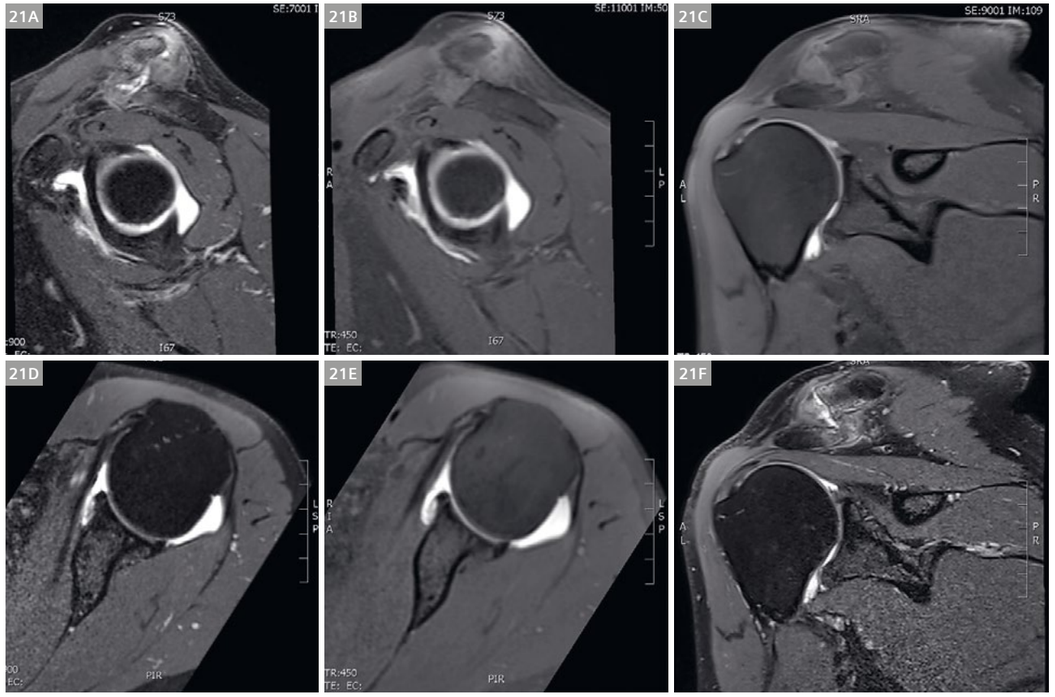

21 Luxated AC joint degree III to determine if there was a concomitant labral lesion. Coronal acquisition after arthrogram with axial and sagittal reconstructions performed. The scan was quick, easy, and robust even in this patient in pain.

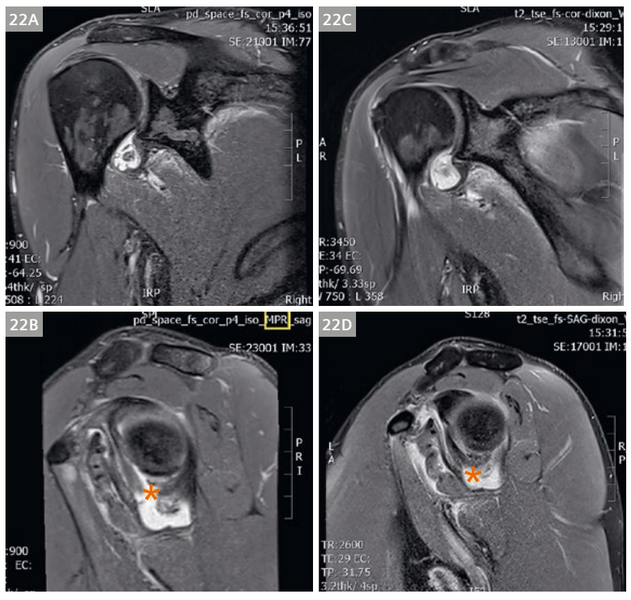

22 Patient who fell while cycling and landed on outstretched hand. No arthrogram was performed since the exam was within a week of trauma. 'GOShoulder' PD Space3D_caipi_ fatsat coronal acquisition 0.4 mm isotropic and sagittal 1 mm MPR **(22A, B)** and coronal and sagittal 3 mm Dixon fatsat PD **(22C, D)**.

Thin slices of 'GOShoulder' demonstrate more accurately the bony avulsion (orange star) of the anterior pillar inferior glenohumeral ligament. Even with these thin slices, there is still sufficient signal as compared to the classic 3 mm slices.

In conclusion, for larger joints GO is go-ing well with the "GO" meaning go-od. Things are going similarly well for smaller joints such as the ankle and wrist.

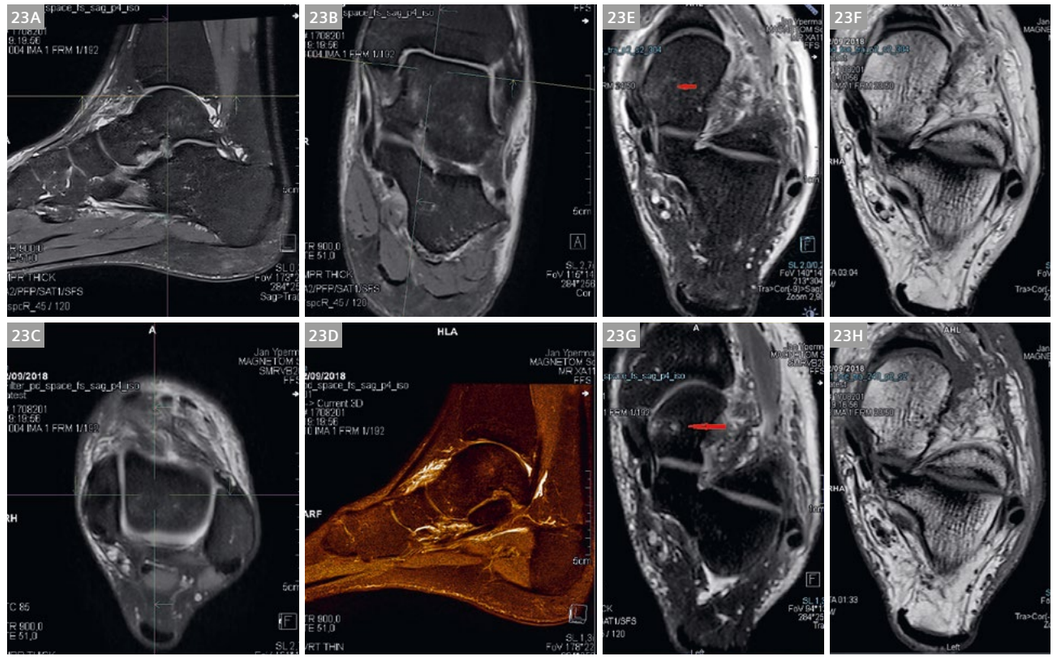

23 A basketball player presented with an ankle sprain. 3D isotropic imaging 0.5 mm. Overview in 3D left screenshot **(23A–D)**. Right Screenshot **(23E–H)** shows axial MPR reconstruction **(23G)** together with 2D ax SMS PD FS **(23E)** and ax SMS PD **(23F)** and SMS T1 TSE **(23H)**. MPR axial reconstruction 'GOAnkle' demonstrates bone edema (red arrow) actually even better than the 2D intermediate weighted FS. 'GOAnkle'!

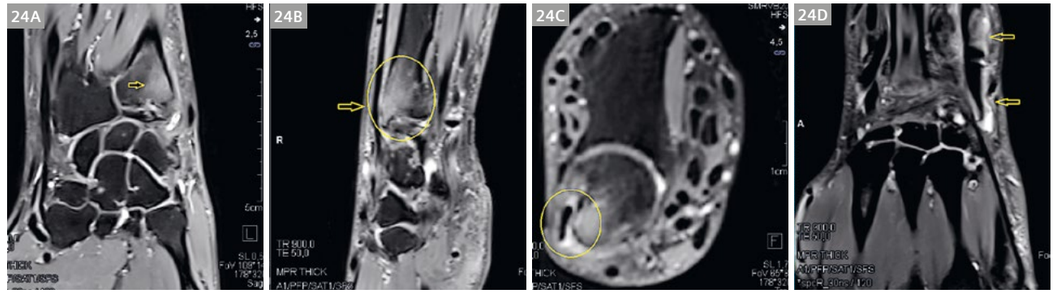

24 'GOWrist' with 0.5 mm 3D isotropic acquisition (5 minutes acquisition time) and MPR reconstructions in 3 directions with bone edema (yellow circle and arrow, 24A and B) distal ulna and styloid process and friction tenosynovitis (yellow circle and arrow, 24C and D) extensor carpi ulnaris tendon. Scan provides exquisite detail in sagittal and coronal planes with this 0.5 isotropic resolution. Even the axial MPR is diagnostic.

In conclusion: MAGNETOM Sola, SMS TSE, and 3D SPACE CAIPIRINHA 4 make a formidable team. The MAGNETOM Sola platform does indeed play an important role in the background with stable homogeneity of the magnetic field, stable RF pulses, and abundant gradient power to run rather than walk through *k*-space and, finally, high density coils to start with. Indeed, the success of 'GO-PickYourJoint' as well as the success of SMS TSE is highly dependent on the signal we get from the 18-channel Knee Coil, UltraFlex Small and Large, and even Body 30.

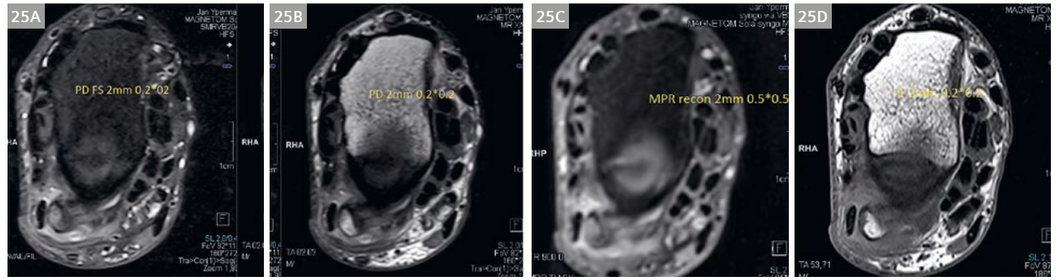

25 When comparing the axial MPR reconstruction 2 mm thickness and 0.5 inplane resolution, to the high resolution PD and T1 images, there is a clear difference in the inplane resolution, still the tenosynovitis and the bone edema are easy to interpret but thin slice high resolution axial images using SMS is clearly the winner here. Check acquisition time T1 **(25D)**: 54 seconds for 30 slices 2 mm "thick" 0.2 inplane resolution.

To prove the force of MAGNETOM Sola you need only take a look at the hips. The first hip exams caught my eye immediately. The signal is there in the cartilage.

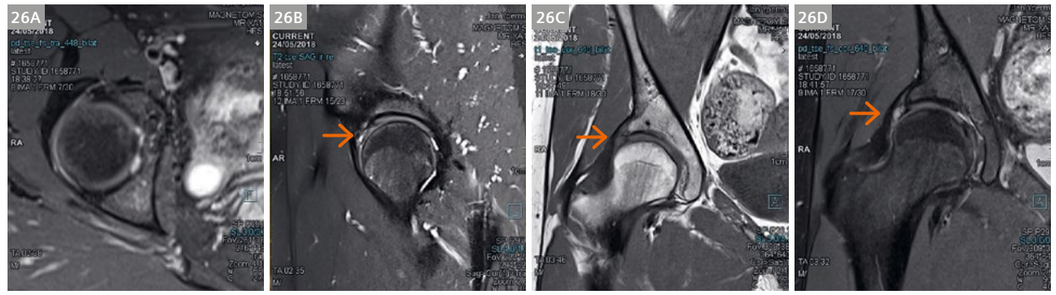

26

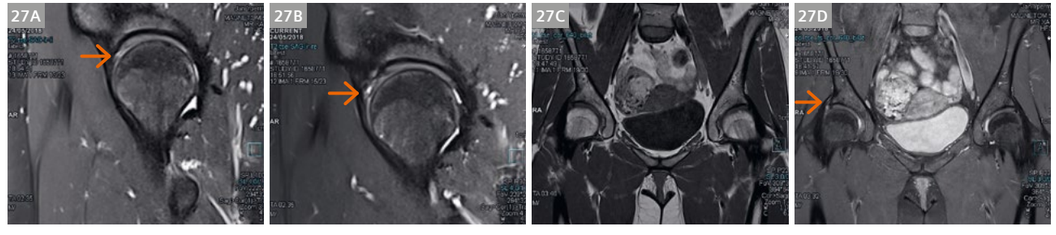

27 Same patient as in Figure 26. Coronal intermediate-weighted fatsat and T1 TSE 3 mm slices and 4 mm sagittal SPAIR fatsat revealing labral tear and cyst on right side and cartilage tears left side.

Contact

Johan Dehem, M.D.
Jan Yperman Ziekenhuis
Briekestraat 12
8900 Ypres
Belgium
Phone: +32 57 35 74 00
johan.dehem@yperman.net

Reference

1 Kalia V, Fritz B, Johnson R, Gilson WD, Raithel E, Fritz J. CAIPIRINHA accelerated SPACE enables 10-min isotropic 3D TSE MRI of the ankle for optimized visualization of curved and oblique ligaments and tendons. Eur Radiol. 2017 Sep;27(9):3652-3661.

MR Imaging of Joint Replacements

Reto Sutter, M.D.[1]; Mathias Nittka, Ph.D.[2]

[1] Balgrist University Hospital, University of Zurich, Zurich, Switzerland
[2] Siemens Healthineers, Erlangen, Germany

Introduction

The last 10 years have seen large technological advances in MR imaging of metal implants[1], and these are coming at the right time, as the number of patients with joint replacements has increased substantially over the last decade. Patients often arrive in the imaging suite with metal implants that can produce distortion artifacts that are detrimental to image quality. Thankfully, these image distortions can be reduced or even eliminated with the use of new MR imaging techniques.

In general, MR imaging relies on a highly constant magnetic field inside the bore. Even slight perturbations, such as those occurring at interfaces between human tissue and surrounding air may cause significant artifacts. The physical property behind this effect is called 'magnetic susceptibility' and unfortunately, the magnetic susceptibility of metal is much higher than that of tissue. Resulting distortions of the magnetic field can reach out far beyond the metal surface and affect the diagnostic quality of the surrounding anatomical structures.

This does not mean, however, that a patient with a metal implant cannot be helped diagnostically with MRI; it means that we must dig deeper into the MR toolkit to produce the best possible diagnostic MRI (Fig. 1).

Determining the type of artifact

The course of action is, in part, dictated by the type and extent of artifact. In some cases, the signal piles up to produce a very bright signal on the MR image. In other instances, signal is lost and only a large, dark area can be seen. There is also signal displacement, where a voxel is shifted from one place to a different location. The signal may be shifted within the imaged slice along the frequency encoding direction (but not along the phase encoding direction!), the so called in-plane distortion. It may be also dislocated with respect to the selected slice position, i.e. the displayed signal originates from a different spatial position than the expected image plane, what is called through-plane distortion [2]. Commonly applied spectral fat suppression techniques are also extremely susceptible to resonance frequency variations. Combating the issues created by insufficient fat suppression is critical to the diagnostic process.

[1] *The MRI restrictions (if any) of the metal implant must be considered prior to patient undergoing MRI exam. MR imaging of patients with metallic implants brings specific risks. However, certain implants are approved by the governing regulatory bodies to be MR conditionally safe. For such implants, the previously mentioned warning may not be applicable. Please contact the implant manufacturer for the specific conditional information. The conditions for MR safety are the responsibility of the implant manufacturer, not of Siemens.*

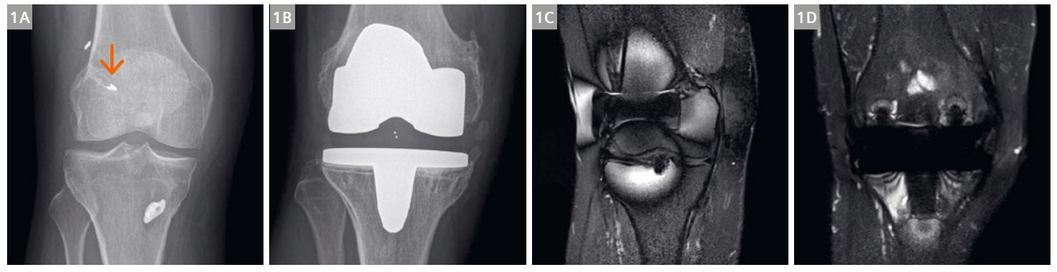

Drill fragment (Stainless steel) | Total knee arthroplasty (Titanium) | Metal artifacts may extend far beyond the actual metal object | Massive metal implant imaged with a STIR SEMAC sequence

1 **How do metal artifacts arise?**
The degree of artifact around the implant[1] is not only induced by its size, but also by the metal composition. **(1A, C)** Objects made of stainless steel, even when very small in size, induce a substantially augmented local magnetic field. Therefore, a conventional coronal STIR sequence without metal artifact optimization exhibits extensive artifacts induced by a broken off drill fragment (arrow) in a patient with anterior cruciate ligament (ACL) reconstruction. **(1B, D)** Titanium implants in general induce less distortions, however, in particular large structures require dedicated metal artifact reduction techniques to enable a diagnostic image quality. *Image reproduced with permission from [1], © Georg Thieme Verlag KG.*

Reducing metal artifacts

A simple, yet effective technique to reduce metal artifacts is to increase the bandwidth of the sequence. The bandwidth describes a property of the imaging sequence, linking the applied magnetic field gradients to the frequency spectrum required for encoding the image. In short, a high bandwidth applied to both signal excitation and signal reception turns the sequence less sensitive to distortions of the static magnetic field.
A recent study from Johns Hopkins Hospital [3] analyzing the effect of increased receiver bandwidth on imaging of ankle arthroplasty confirmed that this renders substantially improved images (Fig. 2). High bandwidth does come with some disadvantages: An increased readout dth decreases the signal to noise ratio (SNR). Furthermore, the specific absorption rate (SAR) is higher when using a high excitation bandwidth. As a consequence, high bandwidth protocols tend to exhibit longer scan times. To a certain degree, this may be compensated by longer echo train length when applying turbo spin echo sequences. However, it should be noted that long echo trains may cause an additional degradation of image quality around implants [3]. Other basic steps to improve MRI diagnostic quality are to:

1. Use thin sections, a small voxel size, and small field of view (FOV);
2. Perform the exam at a field strength of 1.5T rather than 3T, as the severity of the artifacts is in most cases directly proportional to the field strength;
3. Use turbo spin echo sequences rather than gradient or 3D sequences; and,
4. Set the frequency encoding gradient parallel to the long axis of the prosthesis/implant.

These and other techniques are an integral part of *syngo* WARP, providing a comprehensive set of sequence optimizations for metal implant imaging.

The problem with fat saturation

Fat saturated sequences are some of the most important sequences in any musculoskeletal MR imaging protocol, with the ability to visualize e.g. the anatomical distribution of fluid collections, bone marrow edema, and soft tissue edema. However, the presence of large or multiple metal artifacts often impedes fat saturation techniques and may result in a non-diagnostic image. Standard spectral fat saturation is based on different resonance frequencies of water and fat; when metal is present, the fat peak shifts to a different frequency and keeps the RF pulse from suppressing the signal from fat tissue. However, there is a technique that allows us to tackle this issue: short-tau inversion recovery (STIR).

Capitalizing on the different relaxation times of water and fat, first a 180-degree pulse inverts the longitudinal magnetization. Fat has a much shorter T1 relaxation time than water, so when during signal relaxation the fat is at a magnetization of zero, the excitation pulse only affects the water molecules and not the fat molecules, and this technique results in a more stable fat saturation in the presence of metal. Even better results are achieved by combining STIR with high bandwidth, but this still would not be sufficient for clinical use [4].

The *syngo* WARP STIR sequence employs a dedicated bandwidth matching for each RF pulse within the sequence, which is critical for robust STIR contrast around metal implants while still covering a large anatomical field of view (Fig. 3). Further improvements can be achieved by adding the View-Angle Tilting technique (VAT), another feature of the *syngo* WARP toolkit. VAT applies an additional compensation gradient which effectively cancels the in-plane displacement (Fig. 4). This technique allows to visualize periprosthetic tissues with only little residual artifacts, and with reasonable acquisition times.

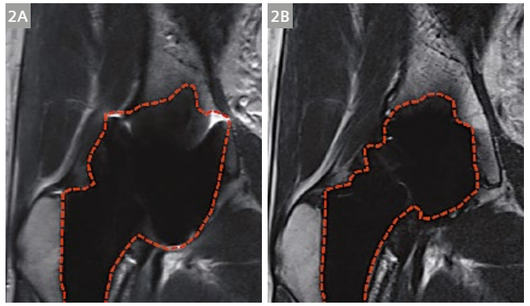

80 Hz/Pixel 390 Hz/Pixel

2 **Increasing the receiver bandwidth**
A simple but very effective step for reducing metal artifacts is increasing the receiver bandwidth, as shown in a 76-year-old patient with total hip arthroplasty. **(2A)** Coronal T2-weighted turbo-spin echo sequence with a standard receiver bandwidth of 80 Hz/Pixel shows large artifacts around the acetabular component. **(2B)** When the same sequence is repeated with an increased receiver bandwidth of 390 Hz/Pixel the artifacts around the acetabular component are substantially smaller.

Dealing with severe metal artifacts

For some implants it may be not sufficient to apply sequences with high bandwidth as described above. Typically structures composed of stainless steel or hardened surfaces frequently containing CoCr alloys are very difficult to handle.

In these cases an excessive distortion of the slice profile is the dominating factor, requiring a more powerful tool, which is able to correct for signal dislocated in through-plane direction.

A break-through in this field was achieved with the invention of the SEMAC (slice encoding for metal artifact correction) method [5] that has meanwhile been applied successfully in clinical imaging for several years [2]. The SEMAC technique employs the through-plane distortion correction to significantly reduce what can be called the "Potato Chip Effect". When you visualize the warped artifacts that occur because of through-plane distortion, the imaged plane looks like a potato chip, with distortions affecting several adjacent image planes. Image reconstruction using SEMAC substantially mitigates these distortions, allowing the radiologist to appreciate areas of osteolysis and other conditions that are obscured when imaging is performed without through-plane distortion correction (Fig. 5).

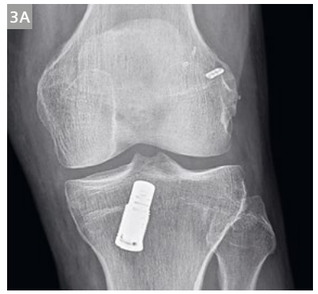

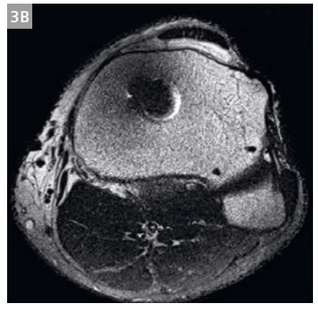

Spectral fat saturation

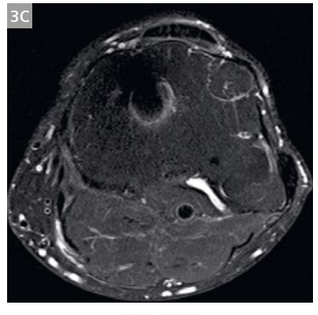

STIR WARP

3 **Two types of fat saturation**
Anterior cruciate ligament (ACL) reconstruction in a 69-year-old patient. **(3A)** Radiograph of the left knee showing large Ligamys screw in the tibial head. **(3B)** Axial intermediate-weighted turbo-spin echo sequence with spectral fat saturation and increased bandwidth shows complete fail of the spectral fat saturation at the level of the tibial head. **(3C)** Axial STIR WARP sequence with optimized inversion pulse shows stable and homogeneous fat saturation of the whole image.

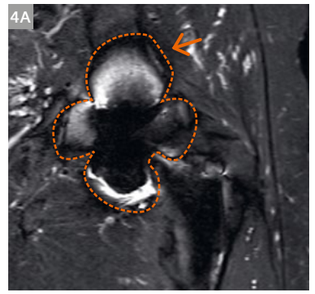

Standard STIR hiBW

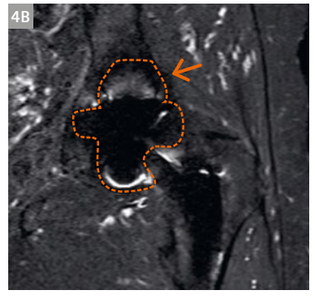

STIR WARP

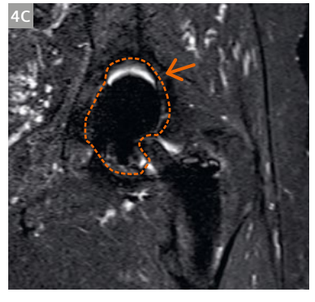

STIR WARP + VAT

4 **STIR WARP and View-angle Tilting (VAT)**
Different methods for metal artifact reduction in a 66-year-old patient with total hip arthroplasty (THA). **(4A)** The standard coronal STIR sequence with increased receiver bandwidth (hiBW) often allows for a basic diagnostic image quality, but suffers from many areals with failed fat saturation (arrow). **(4B)** STIR WARP with an optimized inversion pulse is much more stable for reduction of metal artifacts, with a smaller area of insufficient fat saturation. **(4C)** An additional compensation gradient shifts the view-angle during the readout, and this view-angle displacement cancels the in-plane displacement, resulting in an even better reduction of metal artifacts.

New horizons: Compressed Sensing SEMAC²

SEMAC depends on numerous slice encoding steps to gain the most benefit, requiring considerable additional scan time and thus poses some challenges, both to the time scheduling of a busy practice and also with respect to patient comfort.

In recent years a new technique emerged, known as Compressed Sensing (CS). It has opened new perspectives to accelerate the MR acquisition process in various fields and can now also be applied to SEMAC (Figs. 10, 11). The CS-SEMAC[2] technique is facilitated by the inherent sparsity of the acquired SEMAC data, since the actual distortions make up for just a small fraction of the acquired signal. Compressed Sensing SEMAC applies 8-fold undersampling of *k*-space in combination with an iterative reconstruction algorithm. As a result, images with very comparable diagnostic quality can be created from e.g. a six minute CS-SEMAC scan that would otherwise take approximately twelve minutes even with parallel imaging acceleration.

The number of recommended slice encoding steps for CS-SEMAC according to a recent study was 19 for STIR and T1-weighted images, and 11 slice encoding steps for T2-weighted images [6]. A study on knee implants by Fritz et al. [7] found that CS-SEMAC allows the acquisition of accelerated MR imaging with acquisition times of less than 5 minutes.

[2]The product is still under development and not commercially available yet. It is not for sale in the US. Its future availability cannot be ensured.

The plan in action

A sample protocol for hip prosthesis
At Balgrist University Hospital a protocol with a mix of techniques is in use for scanning hip implants: The first two sequences cover the whole prosthesis. A coronal STIR CS-SEMAC sequence gives the best visibility of the bone-metal-interface with an acquisition time of approximately six minutes. Additionally, a transverse STIR WARP sequence is acquired, allowing the coverage of a large field of view in less than 4 minutes. The second part of the protocol is focused on the joint and the periarticular muscles with turbo-spin echo sequences that feature a high receiver bandwidth, allowing to visualize soft tissue pathology with sequences that only require acquisition times of 2–3 minutes.

What is the clinical impact?
In patients with residual pain after total arthroplasty, soft-tissue related complications are the most common problem, followed by aseptic loosening and infection. Soft-tissue related complications include e.g., damaged or detached external rotator tendons and scarred abductor tendons with associated muscle atrophy and fatty muscle degeneration (Fig. 6).

One place where MRI can be of significant help is in differentiating between osteolysis and diffuse osteopenia next to the implant: While in conventional radiographs and computed tomography (CT) this can be difficult or even impossible, MR imaging allows the accurate differentiation between these two entities (Fig. 7). In patients with suspected infection the extent of the infected areas can be determined using STIR WARP or CS-SEMAC (Fig. 8). Naturally, aspiration is still required to determine the pathogen. Other complications can also be visualized such as the hypointense masses seen in metal-on-metal hip implants called pseudotumors (Fig. 9).

5 Unicompartmental knee arthroplasty
This 58-year-old male with unicompartmental knee arthroplasty underwent MRI to evaluate those parts of the knee joint that were not replaced. **(5A)** Radiograph of the left knee shows prosthesis components in the medial compartment. **(5B)** In the standard coronal STIR sequence optimized with high receiver bandwidth (hiBW) both the collateral ligament and the intercondylar notch are obscured (arrows). **(5C)** STIR SEMAC (slice encoding for metal artifact correction) and its reduction of through-plane metal artifacts improves the visualization of the collateral ligament and the intercondylar notch.

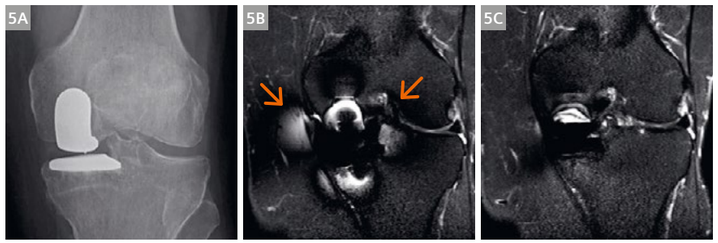

STIR hiBW STIR SEMAC

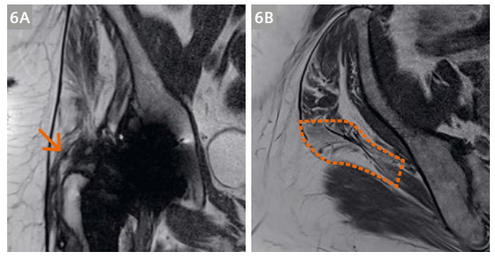

6 Abductor insufficiency
61-year-old female patient with pain and unsteady gait after total hip arthroplasty (THA), and positive Trendelenburg sign at clinical examination. **(6A, B)** At MR imaging improved with high receiver bandwidth a rupture of the gluteus medius tendon (arrow) and fatty degeneration of the respective part of the gluteus medius muscle (outlined areas) are depicted on a coronal T2-weighted and axial T1-weighted sequence.

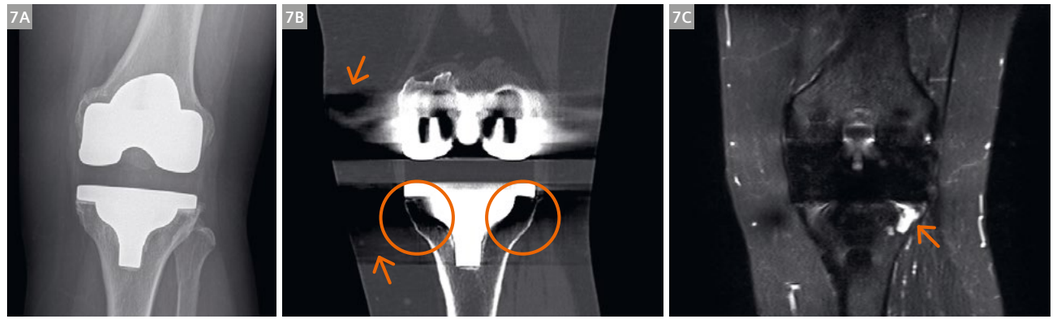

7 Osteolysis vs. Osteopenia
Painful total knee arthroplasty (TKA) in a 57-year-old female patient. **(7A)** Radiograph of the left knee is unremarkable. **(7B)** At computed tomography (CT) suspected areas of osteolysis are visible next to the tibial component (circles), however this region is partially masked by beam hardening artifacts (arrows). **(7C)** At MR imaging an osteolysis (arrow) is detected on a coronal STIR SEMAC sequence only on one side of the tibial component, but not on the other side.

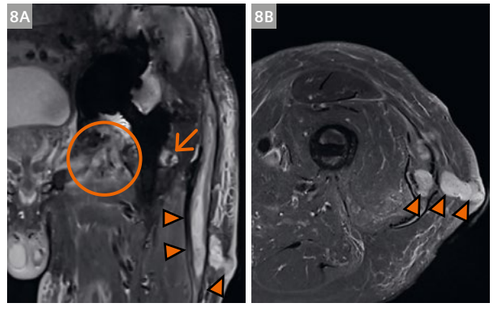

8 Infection
70-year-old patient with infected total hip arthroplasty. **(8A)** Coronal CS-SEMAC STIR sequence shows extensive soft tissue edema adjacent to the left hip joint, e.g. in the adductor region (circle), periprosthetic osteolysis (arrow) and soft tissue abscesses (arrowheads) with a cutaneous fistula. **(8B)** Soft tissue abscesses (arrowheads) and cutaneous fistula depicted on axial STIR WARP image at the level of the femoral shaft.

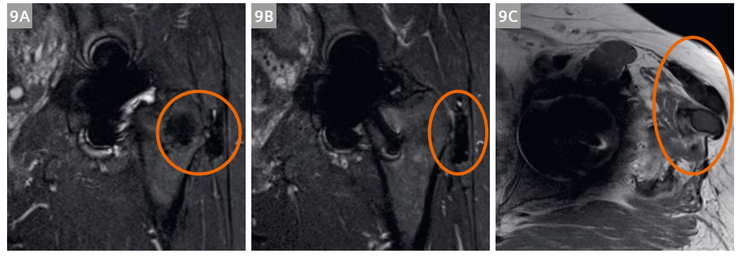

9 Metal-on-metal hip
42-year-old female patient with pseudotumors after short-stem metal-on-metal prosthesis. **(9A, B)** Coronal STIR SEMAC sequence shows intraosseous hypointense mass (circle) that is connected to a paratrochanteric soft tissue mass (circle) with similar morphology. **(9C)** The pseudotumors show finger-like extensions (circles) into the soft tissues that are visible on the axial T1-weighted turbo-spin echo sequence with high receiver bandwidth.

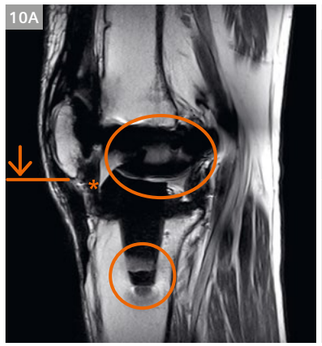

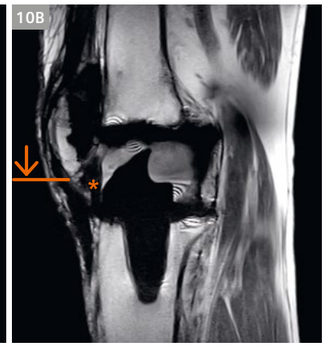

SEMAC CS-SEMAC

10 **Compressed sensing SEMAC of total knee arthroplasty**
Patella baja (low lying patella) due to arthrofibrosis in a 61-year-old patient with total knee arthroplasty (TKA). **(10A)** Sagittal intermediate-weighted image of the left knee with SEMAC [11 slice encoding steps, acquisition time 4:50 min] shows low lying patella (line and arrow) due to arthrofibrosis (asterisk), but residual through-plane artifacts at the level of the joint and the tip of the tibial peg (circles). **(10B)** Sagittal intermediate-weighted compressed sensing (CS) SEMAC image [15 slice encoding steps, acquisition time 4:22 min] is free of through plane artifacts and even faster than the standard SEMAC sequence.

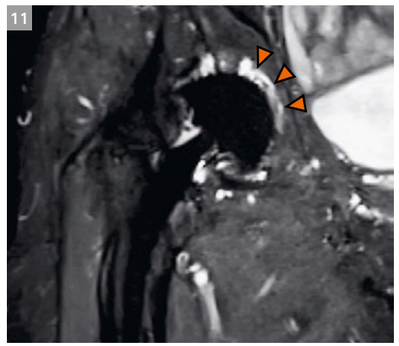

11 **Compressed sensing SEMAC of total hip arthroplasty**
Periprosthetic osteolysis (arrowheads) in a 66-year-old patient with painful total hip arthroplasty of the right hip. The compressed sensing (CS) SEMAC STIR sequence was acquired with 19 slice encoding steps, allowing for complete removal of through-plane artifacts and stable fat saturation with an acquisition time of 6:19 min.

Conclusion

Imaging joint replacements can be successfully done in clinical MRI if distortion from metal artifacts are reduced. In our experience, the quality of the MR images can be significantly improved using the following steps:

1. Increase the receiver bandwidth of the sequences. This simple and effective technique delivers improved diagnostic quality right away.
2. Use STIR instead of spectral fat saturation to gain a good overview of the pathology.
3. Acquire and utilize the advanced techniques such as *syngo* WARP and CS-SEMAC.

These reliable techniques will render a much clearer and, therefore, much more diagnostically powerful MR image. Not only does this make the MR suite a more valuable resource for the diagnosing physicians, but it also gives the patients the chance of better outcomes.

Contact

Reto Sutter, M.D.
Deputy Head of Radiology
University Hospital Balgrist
Forchstrasse 340
8008 Zürich
Switzerland
Tel.: +41 44 386 33 13
reto.sutter@balgrist.ch

References

1 Sutter R, Dietrich T. Reduction of metal artefacts in musculoskeletal imaging. Radiologie up2date 2016; 16(02): 127-144.
2 Sutter R, Ulbrich EJ, Jellus V, Nittka M, Pfirrmann CW. Reduction of metal artifacts in patients with total hip arthroplasty with slice-encoding metal artifact correction and view-angle tilting MR imaging. Radiology. 2012;265(1):204-14.
3 Kumar NM, de Cesar Netto C, Schon LC, Fritz J. Metal Artifact Reduction Magnetic Resonance Imaging Around Arthroplasty Implants: The Negative Effect of Long Echo Trains on the Implant-Related Artifact. Invest Radiol. 2017;52(5):310-316.
4 Ulbrich EJ, Sutter R, Aguiar RF, Nittka M, Pfirrmann CW. STIR sequence with increased receiver bandwidth of the inversion pulse for reduction of metallic artifacts. AJR Am J Roentgenol. 2012;199(6):W735-42.
5 Lu W, Pauly KB, Gold GE, Pauly JM, Hargreaves BA. SEMAC: Slice Encoding for Metal Artifact Correction in MRI. Magn Reson Med. 2009;62(1):66-76.
6 Jungmann PM, Bensler S, Zingg P, Fritz B, Pfirrmann CW, Sutter R. Improved Visualization of Juxtaprosthetic Tissue Using Metal Artifact Reduction Magnetic Resonance Imaging: Experimental and Clinical Optimization of Compressed Sensing SEMAC. Invest Radiol 2018; epub before print. http://doi.org/10.1097/RLI.0000000000000504
7 Fritz J, Ahlawat S, Demehri S, Thawait GK, Raithel E, Gilson WD, Nittka M. Compressed Sensing SEMAC: 8-fold Accelerated High Resolution Metal Artifact Reduction MRI of Cobalt-Chromium Knee Arthroplasty Implants. Invest Radiol. 2016;51(10):666-76.

Further reading

Jungmann PM, Agten CA, Pfirrmann CW, Sutter R. Advances in MRI Around Metal. JMRI.2017;46(4):972-991.

MR Spectroscopy in Neuroimaging – A Practical Guide to Integrate a Complex Technology into a Clinical Workflow

Marco Essig, M.D., Ph.D., FRCPC[1]; Craig Snell[1]; Lawrence Ryner, Ph.D.[1,2]

[1]Department of Radiology, Health Sciences Center Winnipeg, Canada
[2]Department of Physics and Astronomy, University of Manitoba, Winnipeg, Canada

Introduction

After the introduction of NMR spectroscopy in chemistry laboratories in the 1950s, it took decades for MR spectroscopy to eventually be used in a clinical neuroimaging environment. Even as late as 1996, Mauricio Castillo noted that magnetic resonance spectroscopy (MRS)had received little attention from the clinical radiology community. Indeed, most MR spectroscopic studies were initially performed by a small and dedicated group of individuals, mostly basic scientists, partly because MR spectroscopy did not produce "pictures" but resulted in "graphs" called "spectra", and also because of long acquisition times. Much has been done over the years to make the acquisition and processing of spectroscopy data easy, faster, and user friendly, but, still, the full integration of MR spectroscopy seems a challenge for many clinical Radiology departments.

In this article, we describe how MR spectroscopy and MR spectroscopic imaging can be integrated into the clinical workflow of a busy, high-volume MRI department using the example of brain tumor imaging.

MRS for brain tumor imaging

The goals and requirements for brain tumor imaging are making a diagnosis and/or a differential diagnosis, while accurately grading and delineating lesions for tumor description and risk assessment. Imaging is also involved in the decision-making process for treatment such as precise planning of surgical or radiotherapeutic interventions both of which require an optimal lesion detection and delineation. Following therapy, neuroimaging techniques have been shown to be very important for monitoring of disease and to identify and monitor possible therapy related side effects.

In recent years, functional neuroimaging techniques were implemented to optimize tumor characterization, with an emphasis on improved specificity to separate benign from malignant features. Specific characterization facilitates planning of the most appropriate treatment. Furthermore, functional neuroimaging of central nervous system (CNS) neoplasms can be expanded to the monitoring of ongoing therapy and for early detection of therapeutic side effects. The predictive assessment of therapy response and the monitoring of ongoing therapy to guide therapeutic intervention are major challenges in the current treatment of CNS neoplasms.

Proton magnetic resonance spectroscopy is one of the most important functional imaging techniques and provides detailed tumor information beyond the morphologic characteristics observed in standard images. Single Voxel Spectroscopy (SVS) is used to assess a single voxel covering the brain lesion or for larger lesions just a selection of the lesion. Chemical Shift Imaging (CSI), also known as MR spectroscopic imaging (MRSI), is used to assess multiple voxels within and surrounding the tumor. Both methods have become valuable clinical tools, especially in the diagnostic work-up of tumors and the differentiation of normal from pathological conditions.

^{1}H protons are used most commonly in clinical practice because of the abundance of ^{1}H protons in body tissue and the consequently high signal-to-noise ratio, although it is possible to acquire signal from phosphorous-31, carbon-13 and other nuclei. The spectroscopic characterization of brain abnormalities relies mostly on the calculations of ratios between the major proton metabolites including N-acetylaspartate (NAA – a neuronal marker), choline-containing compounds (Cho – a marker of membrane turnover), and creatine-phosphocreatine (Cr – important in the tissue cell energy cycle), and on the presence of lactate (Lac – a marker of anaerobic glycolysis), and lipids [1-6]. Brain tumors typically have a loss of NAA and an increase of the Cho content (Fig. 1).

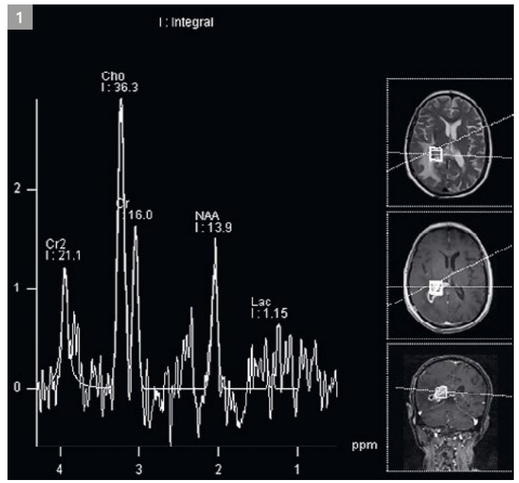

1 Brain tumor spectrum showing increased Cho and reduced NAA.

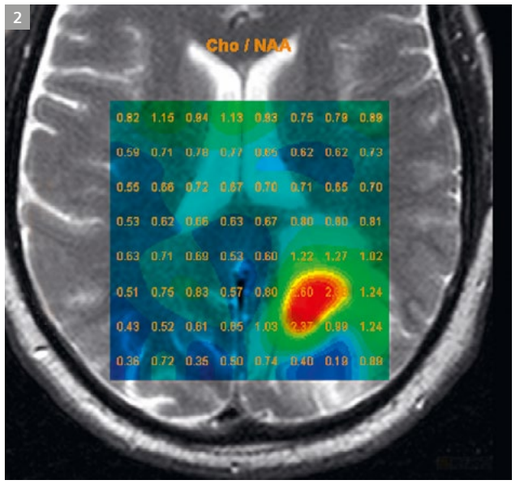

2 CSI example showing the spatial distribution of the Cho/NAA ratio.

MR spectroscopy has been used to differentiate non-tumor lesions, like harmatomas from gliomas [7-8]. In several studies, it has been reported that harmatomas did not differ significantly from the normal brain or physiological changes, while gliomas had lower NAA/Cr, Cr/Cho, and NAA/Cho ratios. In patients with seizures it is important to identify tumor changes from scar as this has a major impact on the further management of patients. In a study by Vuori et al. [6], patients experi-encing seizures who also had a cortical brain lesion on MR images were studied with proton MR spectroscopy. A metabolite ratio analysis was performed, and the metabolite signals in the lesion core were compared with those in the contralateral centrum semiovale and in the corresponding brain sites of control subjects to separately obtain the changes in NAA, Cho, and Cr. In their study, ten patients had a low-grade glioma (three, oligodendrogliomas; three, oligoastrocytomas; three, astrocytomas; and one, pilocytic astrocytoma), and eight had FCDM (five, focal cortical dysplasias and three, dysembryoplastic neuroepithelial tumors). They found that loss of NAA and increase of Cho were more pronounced in low-grade gliomas than in subjects with cortical developmental malformations. MR spectroscopy was also able to differentiate between subtypes of gliomas.

In a study by Law et al. [9], MR spectroscopy and MR perfusion enabled identification at a high sensitivity and a high positive predictive value for tumor grading when compared with conventional contrast enhanced MR imaging. It is well known that there are a certain percentage of high-grade tumors that do not present with a blood-brain-barrier disruption or vice versa. For the planning of biopsy and for the treatment decision and management, it is essential to identify the highest tumor grade in those often very morphologically homogeneous appearing tumors. The authors were also able to provide thresholds for the metabolite ratios for the diagnosis of a high-grade tumor. A review of the literature, taking into account differences in MR spectroscopic technique such as the choice of echo time (TE) and method for determination of metabolite ratios, demonstrated that the mean maximal values obtained for Cho/Cr and Cho/NAA and mean minimum values for NAA/Cr ratios in their study (1,7) were comparable to previously published data in differentiating between low- and high-grade gliomas.

As in many functional techniques, one of the challenges is the use of standardized data acquisition and post-processing techniques. For data acquisition, the same echo time (TE) should be used, and data from the contralateral unaffected brain tissue should be acquired. Studies comparing long and short TE acquisition found that a short TE provided a slightly better tumor classification [10-11]. In a study by Majos et al., long TE acquisitions were only beneficial in studies of meningiomas [12].

The development in modern scanner technology further allows for the simultaneous measurement of spectroscopic data from more than just a single voxel. This technique is called chemical shift imaging (CSI) or magnetic resonance spectroscopic imaging (MRSI) and enables the acquisition of multiple small voxels in two or even three dimensions, providing better information about the spatial heterogeneity of a lesion (Fig. 2). The voxel information can be used to calculate metabolite ratios, which can then be color-coded and superimposed on the anatomic images to better visualize hot spots within a tumor.

Follow-up assessment of cerebral tumors is a promising field for MR spectroscopy. Increases in size and contrast enhancement are typical findings in tumor progression but also reflect therapeutic-induced changes and/or postoperative changes. The ratio of choline to normal creatine level is usually significantly elevated in those areas consistent with tumor compared to those containing predominantly treatment effect. In fact, treatment effect is generally indicated by a marked depression of all the intracellular metabolite peaks from choline, creatine, and N-acetyl compounds.

MR spectroscopy alone may not be helpful in instances where patients have mixed histologic findings comprised of necrosis and tumor. Because of this heterogeneity and as a result of low spatial resolution, MRS findings of choline and NAA resonances below the normal range may indicate variable histologic findings ranging from radiation necrosis, gliosis, and macrophage infiltration to mixed tissues that contain some regions of tumor. The careful choice of voxel placement and interpretation of results in concordance with other imaging and clinical findings are critical in distinguishing between tumor and treatment-related changes. Furthermore, validation studies using image-guided tissue biopsy need to be performed to correlate imaging with histologic findings.

How to – MR Spectroscopy

Getting started

Before discussing the details of processing MR spectroscopy data using *syngo*.via, it is important to ensure that the acquisition of the spectroscopy data is optimized. This section provides some tips to assist in acquiring the single voxel and chemical shift imaging data.

As mentioned in the previous section, when setting up the CSI sequence selecting a lower TE (i.e., 30 ms) will yield better spectral quality in terms of tumor classification. Typically, the CSI sequence should be placed after the initial imaging sequences. This allows for the acquisition of imaging data in each plane so that the spectroscopy excitation voxel can be accurately placed on the contrast-enhancing or most suspicious tumor components. There are several important scanning parameters to keep in mind (Fig. 3):

1. Table position, found in the menu under System/ Miscellaneous/Position Mode, should be "REF mode". If ISO or FIXED mode is used, the isocenter will move and *syngo*.via will not be able to triangulate where the voxel was placed on the images with different ISO centers.
2. When the voxel is placed, click on the scroll header and select nearest, confirm placement on all three planes, and confirm that the voxel is not encroaching on any extraneous tissues.

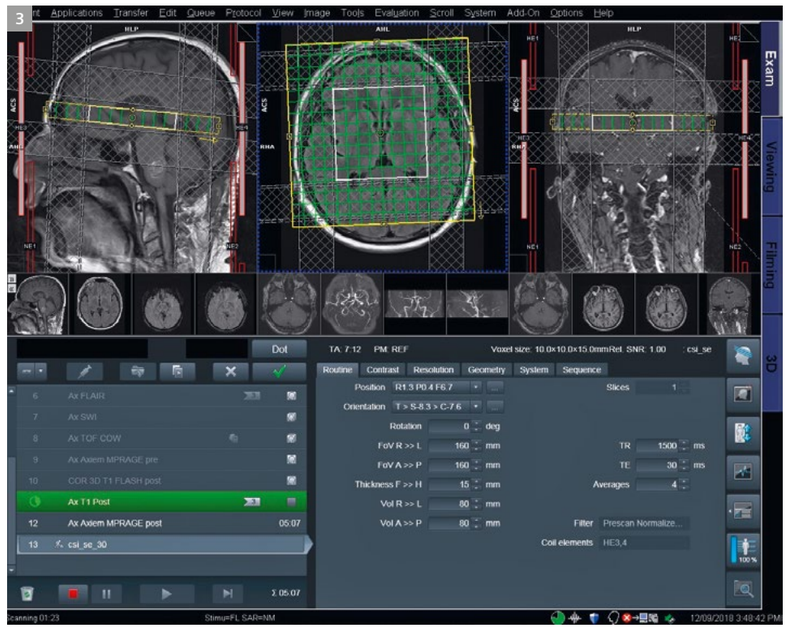

3 Setting up the CSI acquisition.

1. 2D Distortion Correction must be turned off when acquiring an imaging localizer for spectroscopy. If this is left on, the voxel location may be affected by the amount of distortion correction applied to the images. Note that distortion correction can be retroactively reversed so that images can still be used for voxel positioning.

Placing a voxel, whether for single voxel or CSI, will follow similar principles: Avoid including any lipid signal within the excitation voxel as this will cause a large lipid peak to dominate the spectrum; stay away from the skull as the bone marrow will also result in an overwhelming lipid peak; and try to stay from the sinuses where it might be difficult to optimize the magnetic field homogeneity, i.e., the shim. The voxel in Single Voxel Spectroscopy (SVS) is usually small enough (20 x 20 x 20 mm^3) that it can be accurately placed to avoid such extraneous tissues. Take care that the SVS voxel size is not set too small as this will result in very noisy spectra. CSI will require placement of several saturation bands to prevent contamination from tissues outside of the volume-of-interest (VOI). Saturation bands in all three planes are extremely helpful in eliminating these signals. Take care that the CSI voxel size does not get too small, as this will result in noisy metabolite images.

MR spectroscopy is extremely sensitive to **any** metal that might cause magnetic field inhomogeneities. Items such as metal dentures, belt buckles, shoes, metal clothing snaps, removable body piercings, etc., should be removed from the patient prior to the scan (standard MRI practice). In addition, the closer the voxel is to isocenter, the better the shim will be, as measured with the Full Width Half Maximum (FWHM). The FWHM indicates how broad or narrow the peaks in the spectrum will be. Typically for SVS the FWHM should be under 12 Hz and for 2D multi-voxel under 15 Hz, although these values are for 1.5T and can vary significantly depending on VOI location and size.

Locating data on *syngo*.via

Once logged into *syngo*.via, the data should be located. There are two ways to do this; send the dataset directly from the modality to the *syngo*.via server or query/retrieve the data from PACS on *syngo*.via. Configuration of a PACS node by the local service engineer will be required when sending from the modality (AE title, IP address, and port number will need to be provided).

Query/Retrieve PACS

Searching for cases on PACS is done in the DICOM retrieve header in the bottom third of the home screen. Identify the Source selection which is the local PACS server the data is stored on. The search filters header is where the patient demographics will be put in. Click the search button and observe all cases on PACS meeting the search criteria. Find the desired patient exam and select the retrieve icon (Fig. 4).

Browser search

Now that the data has been downloaded on to the server, search for it in the patient browser. In the top half of the patient browser, type the name in and search for the data (Fig. 5). Search the database manually if the search function is not working.

Now that the dataset has been located, open it with the MR Spectro Analysis program by right-clicking on the patient in the browser, select OPEN WITH, and scroll down to find “MR SPECTRO”. Selecting the star icon beside “MR Spectro” will identify this workflow as a favorite and make it easily accessible for subsequent analyses.

Selecting the protocol

After selecting the MR Spectro workflow, wait for the data to load, process, and display on the screen. This might take ten seconds or so. When MR SPECTRO opens,

4 Query/Retrieve window

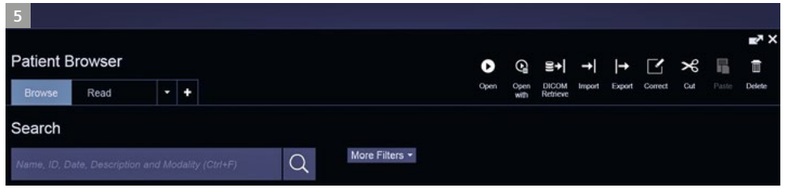

5 Browser search

multiple windows appear showing the spectral grid overlay on the anatomical image, the spectrum for the selected voxel, the orthogonal image planes with the spectral grid overlay, and the color metabolite map. The complete list of data series can be viewed by clicking the small arrow located to the side. The series that are highlighted in blue in the Data Groups window are the ones that have been automatically selected by the program (Fig. 6). Different series can be dragged and dropped into any window as long as the requirements mentioned in “Getting started” were followed. Every window will have tools in each corner to alter that specific window if needed. Note that the default screen window configuration will be different depending on the monitor resolution and size.

6 Data Groups

Furthermore, there are many different configurations that can be used for viewing. Simply click the “4 windows” icon located just to the right of MR Spectro Analysis label (Fig. 7) and select the desired template.

The next step is only required if you wish to add metabolites to the analysis. You should only have to do this once – *syngo*.via will remember the workflow protocol. To select the metabolites that are to be analyzed, click the Spectro browser icon (Fig. 8) found at the bottom of the MR Spectro Analysis window.

The following example shows how to add the lactate metabolite to the analysis. Highlight csi_se_30 (Fig. 9) and select edit. A new window will appear. Select “Prior Knowledge” and click the + icon (Fig. 10). Another window will appear – this is where all the metabolites are listed. Scroll down, highlight lac_se_30, and click the select icon (Fig. 11). This loads the lactate metabolite acquired with a spin echo sequence at an echo time of 30 ms into the analysis. Save the protocol with a new name. Select “Save as” and save the new protocol as “csi_se_30_lac”.

The last step is to select the new protocol. Right click on the series in the MR Spectro window and click on “Select Protocol”. Choose the new protocol that was just created (Fig. 12). The program will automatically reprocess the data and queue it at the bottom of the Spectro workflow.

Defining the result table

The next step is to modify the Result Table to select the desired metabolites and metabolite. Select myo-inositol (mIns), NAA, Cho, Cr1, Cr2, and Lac. Creatine is often used as a baseline in spectral analysis since its concentration stays fairly constant. The choline to NAA ratio (Cho/NAA) is another common ratio used in assessing brain tumor spectra, since the choline peak is often elevated and the NAA peak is often reduced. In the spectrum window, click on the ruler in the top right corner. This will be where the result table is defined (see Fig. 13). In the pop-up window, there are useful examples of how to enter the desired equations. Using creatine as the base, defined values will display when adding the Integrals.

7 Configuration icon

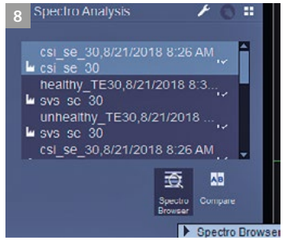

8 Spectro browser icon

9 Editing the csi_se_30 protocol

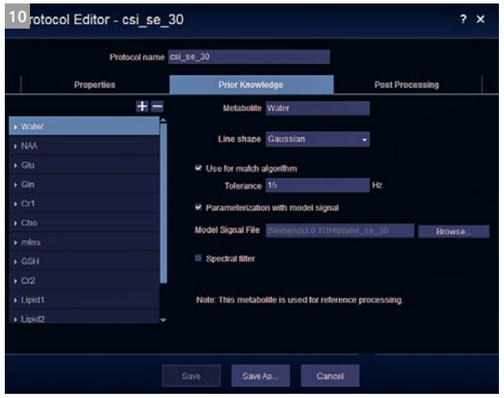

10 Entering prior knowledge

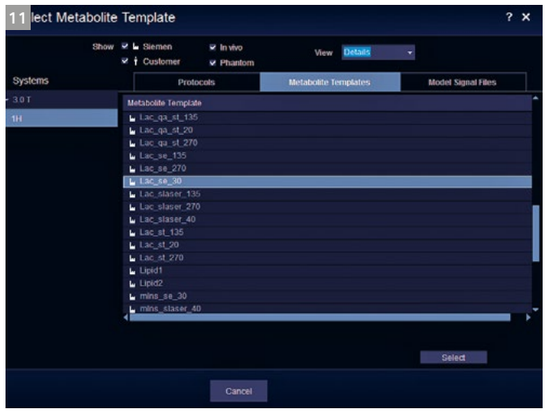

11 Selecting the lac_se_30 protocol

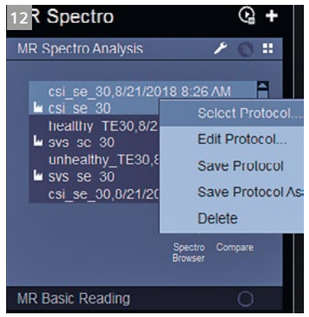

12 Selecting the analysis protocol

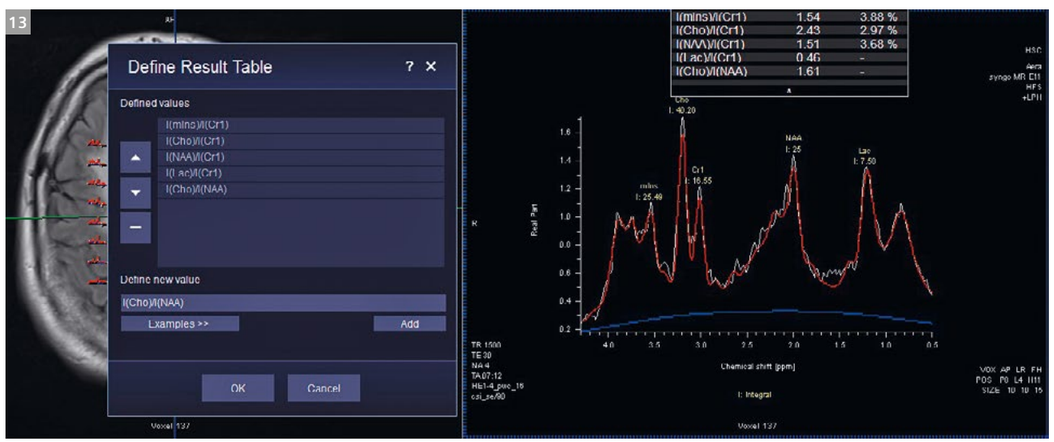

13 Defining the result table

The first column in the table is the label of the metabolite ratio. The second column is the actual value of that ratio. The third column is the percent variation which is a measure of how good the spectral fit was. A rule-of-thumb is that metabolite ratios with percent variations greater than 20% should not be considered accurate. The lower this number is, the better the fit.

The result table can be manipulated in many ways; adding and subtracting different combinations of ratios will yield results tailored to specific differential diagnoses. After the result table is properly defined, click "OK" and *syngo*.via will remember these values for all subsequent analyses when the protocol is saved.

Defining metabolite maps

Metabolite images or maps are another way of visualizing the spatial variation of metabolites across the brain, and for seeing "hot spots" for certain metabolites and ratios. The "Define Metabolite Image" window (Fig. 14) is used to define which maps to display, using equations similar to the way the result table was defined. Metabolite map windows are typically on the right-hand side of the monitor. First, drag and drop the image-underlay series into the window from the Data Groups (Fig. 6). Note that the available series are displayed as "Data groups" by default, but can be viewed as "Thumbnails", or "Study/Series" by selecting the dropdown. Any image series can be chosen (usually axial T1 post gad) as long as the series was scanned under the specifications mentioned in getting started, i.e., same isocenter, no 2D distortion correction, etc. Once the series is loaded in the window, select the ruler (define metabolite image) in the upper right-hand corner and define any type of color map that is required (Fig. 15) Whether they are single metabolite maps, or ratios, use the same method as was used for defining the result table.

If gaps are seen in the metabolite image, it might be because a spectrum has been automatically identified as a "Low quality voxel". This means that the spectral fitting was unreliable in this voxel and it shouldn't be used in the diagnosis. It is also possible to manually identify voxels as "Low quality", should this be necessary. For example, if the metabolite map for lactate shows a very bright spot, click on that voxel and examine the spectrum. If a very high lipid signal is observed, then mark that voxel as "Low quality" so that it doesn't mislead the radiologist.

Exporting results to PACS

Now that the Result Table has been generated and the metabolite images have been defined, the results can be sent to PACS for reporting and archiving purposes. Under Tools (bottom third of screen), click the arrow below the "layout snapshot" icon. There are three options. Snapshot

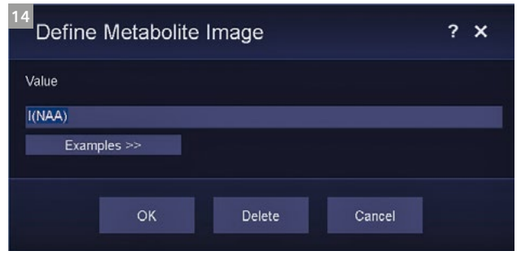

14 Defining the metabolite image

will take a screen shot of every window that is highlighted blue. Layout Snapshot will take a screen shot of all 4, or 6 windows, depending on the window configuration. "Snapshot to finding" will add the selected windows into the chosen findings folder that is identified by a checkmark. A new findings folder is created for each new snap-shot; therefore once the initial snapshot is done, use the "Snapshot to finding" icon. These preceding snapshots to findings will be archived into the findings folder that were selected. Each findings folder should be exported to PACS in a different series. Review all snapshots made in the findings navigator by double clicking on the small picture icon. When all the snapshots are done, right click on the findings and select export to PACS (Fig. 16). For CSI, ensure that the full voxel position is included in the snapshot, as in Fig. 17 and 18.

Healthy vs. unhealthy analysis

It can be useful to select two spectra from the full CSI dataset, one corresponding to the spectrum with the most abnormal spectral ratios (labeled "Unhealthy") and another from contralateral normal appearing brain tissue (labeled "Healthy"). Once the *syngo*.via spectroscopy analysis is configured with all the tables and all the maps defined, select the two representative "Healthy" and "Unhealthy" voxels (Figs. 17, 18) and collect a snapshot of each for export to PACS for interpretation by the radiologist.

Strengths/limitations

Overall, the *syngo*.via MR spectroscopy analysis software is extremely user-friendly and easy for technologists, radiologists, and other clinical staff to use.

- The modern graphic user interface makes full use of multiple windows, context-sensitive mouse-clicks, and a well thought out workflow.
- A key benefit is that the software package is ready-to-use, right from the start, and does not require the acquisition of any additional scans on various spectroscopy phantoms.

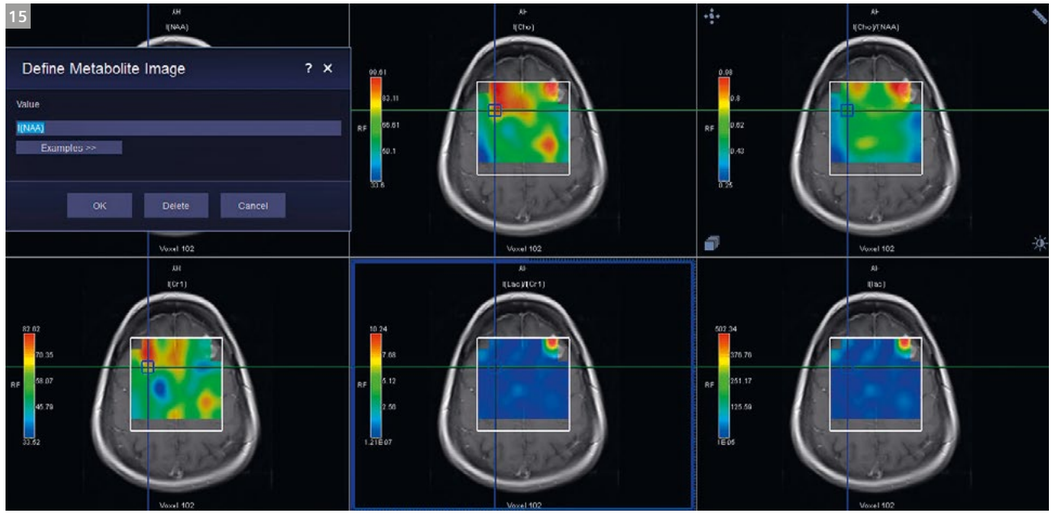

15 Examples of metabolite maps

16 Exporting to PACS

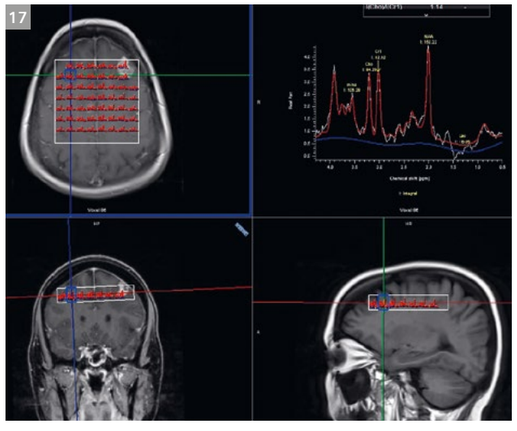

17 Selecting the voxel for the "Healthy spectrum"

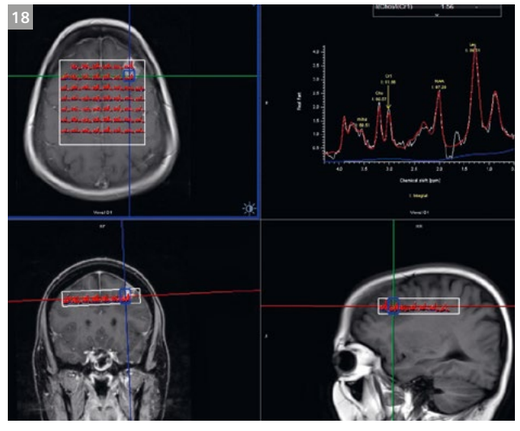

18 Selecting the voxel for the "Unhealthy spectrum" corresponding to the brain tumor spectrum with the "worst" spectral ratios

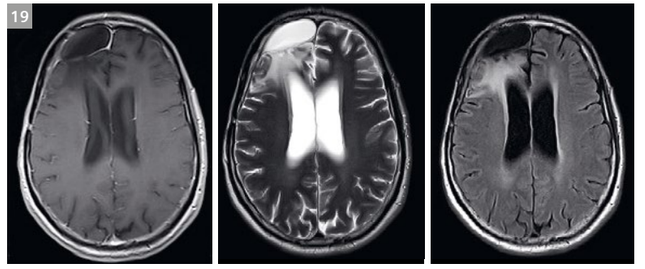

19 T1, T2, and FLAIR images of a patient following radiation therapy of a high-grade oligodendroglioma

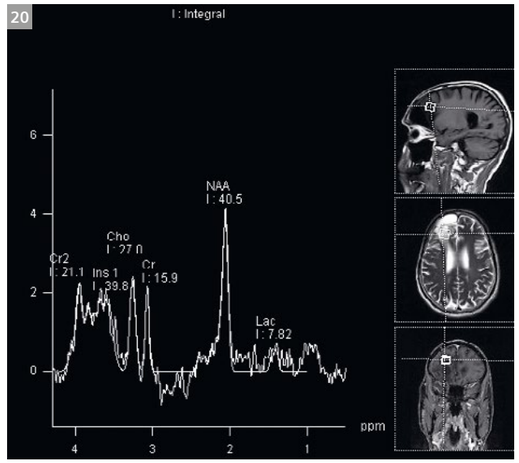

20 Single voxel spectrum from the suspicious area showing relatively normal Cho to NAA ratio

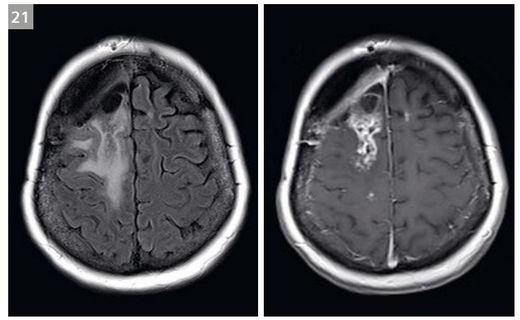

21 Second patient with a glioblastoma multiforme showing FLAIR and T1-weighted image

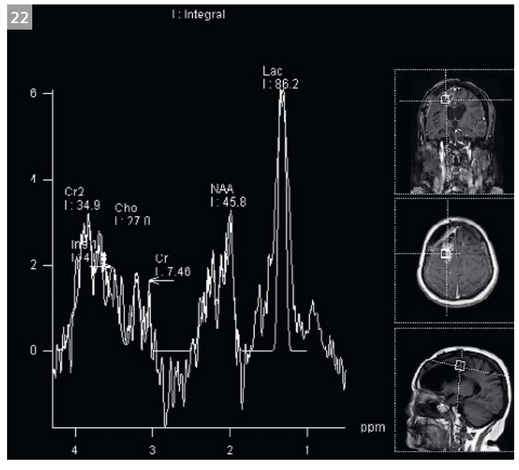

22 Single voxel spectrum from the suspicious area showing relatively normal Cho to NAA ratio, with some changes in the lactate/lipid region

- The spectral fitting routine has been fully updated from previous versions and now utilizes robust time-domain fitting which is less dependent on perfect phasing as is required for spectral domain fits.
- Inclusion of a goodness of fit measure in the Results Table helps in determining which spectral fits are reliable (e.g., rule of thumb is a variation of less than 20%).
- Automatic marking of spectra with low quality fits helps the user determine which fits are reliable and which aren't.

Any software package comes with limitations that are often fixed in subsequent releases, based on customer feedback.

- The lack of an ability to sum multiple spectra from a user-selected region of interest in the CSI grid makes it hard to fully assess larger tumors extending over multiple voxels.
- Other advanced CSI software packages come with the ability to shift the CSI grid in order to position voxels more precisely over suspicious regions in the image; this ability is lacking in this software package.

It should also be noted that there is an Advanced Mode that can be configured in the Workflow Step Configuration which provides some additional functionality to the software. Users wishing to have this enabled should consult Siemens service.

Patient cases

Two patient cases are presented to demonstrate the utility of MR spectroscopy in helping to differentiate treatment-related changes from progressing tumor as observed in standard MR imaging.

In this first patient case, the standard T1- and T2-weighted imaging (Fig. 19) appeared to demonstrate an increase in tumor size after radiation therapy of the high-grade oligodendroglioma.

Single voxel spectroscopy from the suspicious region indicated (Fig. 20) showed a relatively normal ratio of Cho to NAA signal without the signature elevation of the Cho to NAA ratio found in brain tumor tissue, thus indicating that the changes are not likely related to tumor progression but rather related to treatment effects..

A second patient case with glioblastoma multiforme shows a suspicious area posterior to the resected region following chemotherapy and radiation therapy (Fig. 21).

Single voxel spectroscopy from a voxel located in the middle of the suspicious region is shown in Figure 22. With no increase in the Cho to NAA ratio and some changes in the lactate/lipid region at 1.3 ppm, these changes in the MR imaging are most likely treatment-related changes and not a progressing tumor.

Conclusion

The *syngo*.via MR spectroscopy analysis software is a powerful, easy-to-use tool that streamlines and simplifies the use of MRS and MRSI as a routine functional imaging method in a high-volume MRI department. Using a standardized acquisition and analysis workflow, as outlined in this article, enables the use of this complex technology in a quick, easy-to-implement process on a day-to-day routine basis that provides key information to the radiologist. This functional information can be used for better workup and differential diagnosis of brain tumors, for treatment planning, and for differentiation between tumor progression and pseudo effects following treatment.

Acknowledgements

The authors thank Jerry Moran, Siemens Canada Research Collaborations Manager, and Uwe Boettcher, Siemens Healthineers Germany, for their assistance in setting up and providing instructions on the use of the *syngo*.via spectroscopy package.

References

1 Alger JR, Frank JA, Bizzi A, et al. Metabolism of human gliomas: assessment with H-1 MR spectroscopy and F-18 fluorodeoxyglucose PET. Radiology 1990; 177:633-641.
2 Negendank WG, Sauter R, Brown TR, et al. Proton magnetic resonance spectroscopy in patients with glial tumors: a multicenter study. J Neurosurg 1996; 84:449-458.
3 Meyerand ME, Pipes JM, Mamourian A, Tosteson TD, Dunn JF. Classification of biopsy-confirmed brain tumors using single-voxel MR spectroscopy. AJNR Am J Neuroradiol 1999; 20:117-123.
4 Dowling C, Bollen AW, Noworolski SM, et al. Preoperative proton MR spectroscopic imaging of brain tumors: correlation with histopathologic analysis of resection specimens. AJNR Am J Neuroradiol 2001; 22:604-612.
5 Demaerel P, Johannik K, van Hecke P, et al. Localized 1H NMR spectroscopy in fifty cases of newly diagnosed intracranial tumors. J Comput Assist Tomogr 1991; 15:67-76.
6 Vuori K, Kankaanranta L, Hakkinen AM et al. Low-grade gliomas and focal cortical developmental malformations: differentiation with proton MR spectroscopy. Radiology 2004 Mar; 230(3):703-8.
7 Wilson M, Cummins CL, Macpherson L, et al. Magnetic resonance spectroscopy metabolite profiles predict survival in paediatric brain tumours. Eur J Cancer 2013; 13:457-464
8 Norfray JF, Darling C, Byrd S, et al. Short TE proton MRS and neurofibromatosis type 1 intracranial lesions. J Comput Assist Tomogr 1999; 23:994-1003
9 Law M. MR spectroscopy of brain tumors. Top Magn Reson Imaging 2004 Oct; 15(5):291-313.
10 Delorme S, Weber MA. Applications of MRS in the evaluation of focal malignant brain lesions. Cancer Imaging 2006 Jun 22; 6:95-9.
11 Galanaud D, Nicoli F, Chinot O, Confort-Gouny S, Figarella-Branger D, Roche P, Fuentes S, Le Fur Y, Ranjeva JP, Cozzone PJ. Noninvasive diagnostic assessment of brain tumors using combined in vivo MR imaging and spectroscopy. Magn Reson Med 2006 Jun; 55(6):1236-45.
12 Majos C, Julia-Sape M, Alonso J, Serrallonga M, Aguilera C, Acebes JJ, Arus C, Gili J. Brain tumor classification by proton MR spectroscopy: comparison of diagnostic accuracy at short and long TE. AJNR Am J Neuroradiol 2004 Nov-Dec; 25(10):1696-704.

Contact

Lawrence Ryner, Ph.D.
University of Manitoba
Dept. of Radiology,
Medical Physics
ON-3 Cancer Care Manitoba
820 Sherbrook Street
Winnipeg, Manitoba, MB R3T 2N2
Canada
Tel.: +1 204-787-1400
lryner@cancercare.mb.ca

Marco Essig, M.D., Ph.D., FRCPC
Professor and Chair,
Department of Radiology
Medical Director of Diagnostic Imaging, WRHA
GA-216, General Centre – HSC
820 Sherbrook Street
Winnipeg, Manitoba, MB R3T 2N2
Canada
Tel.: +1 204-787-1335
messig@exchange.hsc.mb.ca


Lawrence Ryner


Marco Essig


Craig Snell

The Various Definitions of TR

Gary R. McNeal, MS (BME)
Cardiovascular MR R&D Team, Siemens Healthineers, Chicago, IL, USA

Introduction

In the practice of Cardiac MRI, various definitions of the parameter TR (Time of Repetition) have evolved as gated pulse sequence have become increasingly complex. Understandably this causes significant confusion among most users. In some cases, the original concept of TR seems to be lost. This article describes the various definitions of TR.

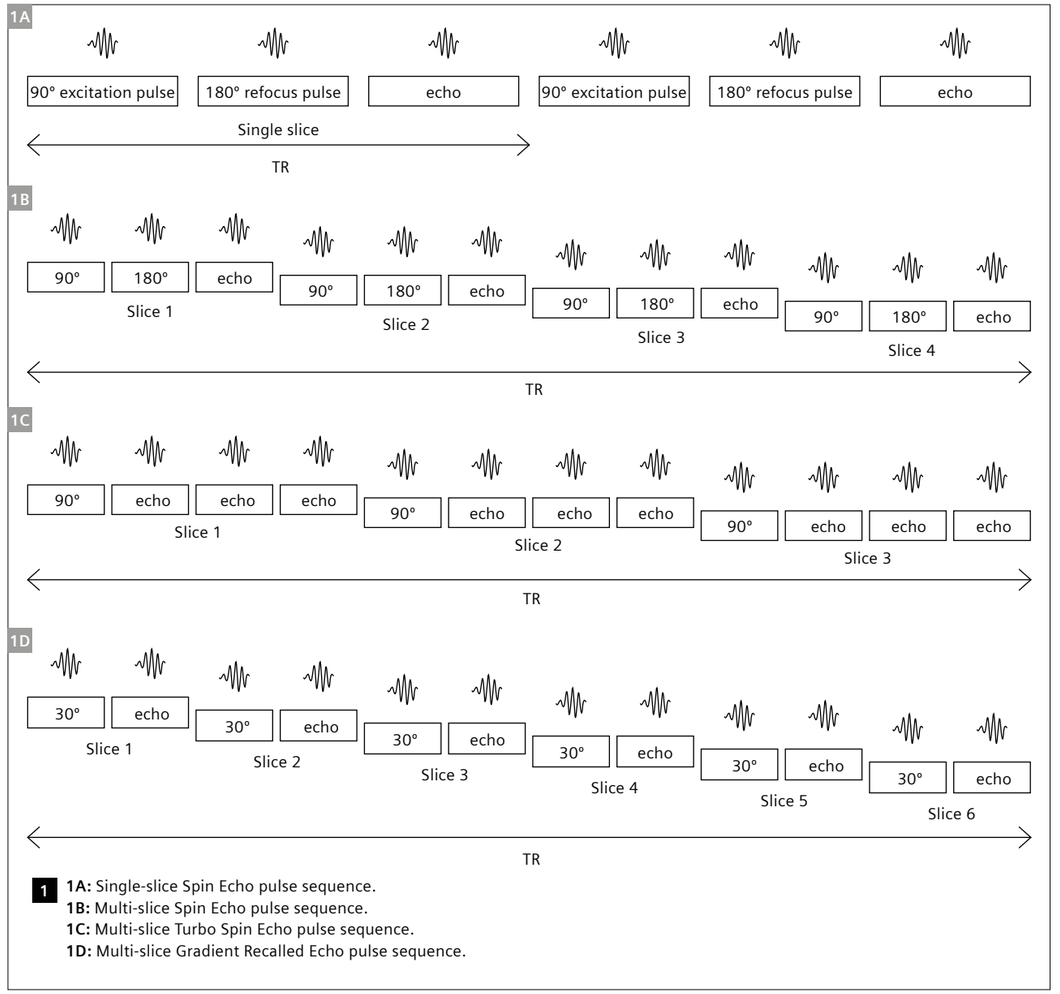

1 **1A:** Single-slice Spin Echo pulse sequence.
1B: Multi-slice Spin Echo pulse sequence.
1C: Multi-slice Turbo Spin Echo pulse sequence.
1D: Multi-slice Gradient Recalled Echo pulse sequence.

Definition 1

The conventional definition of TR is the repetition time between successive excitation pulses for the same slice. This is demonstrated by a single-slice Spin Echo (SE) pulse sequence in which each slice consists of a 90° excitation pulse, a refocusing pulse, and an echo (Fig. 1A).

This conventional definition of TR also applies to a multi-slice SE pulse sequence in which as many slices as possible are interleaved within the selected TR (Fig. 1B). For T1 weighting we typically select a relatively short TR (< 1000 ms),or for T2 weighting a relatively long TR (> 2000 ms).

This conventional definition of TR also applies to a multi-slice Turbo Spin Echo (TSE) pulse sequence in which each slice consists of a single excitation pulse with multiple refocusing pulses and multiple echoes (Fig. 1C). Since there are more echoes per slice, a TSE sequence requires fewer repetitions than a SE sequence with the same TR, but accordingly fewer slices may be acquired within the selected TR.

This conventional definition of TR also applies to a multi-slice Gradient Recalled Echo (GRE) pulse sequence which contains no refocusing pulses at all (Fig. 1D). Each slice consists of a single excitation pulse and a series of gradient reversals to form an echo. TR is defined as the time between successive excitation pulses for the same slice in a GRE sequence, just like in SE and TSE sequences.

Definition 2

When a pulse sequence is cardiac triggered, the definition of TR can become a bit more complicated. Often the TR displayed in the user interface does not reflect the conventional definition of TR, but instead is used to define some other aspect of sequence timing relative to the cardiac cycle. In the discussion that follows, the TR displayed to the user will be denoted $TR_{protocol}$, while the effective TR, defined conventionally as the time between successive excitation pulses, will be indicated as $TR_{effective}$.

When cardiac triggering is used in a multi-slice spin-echo sequence, the $TR_{effective}$, according to the conventional definition, is the repetition time between successive heartbeats. This is demonstrated by a cardiac triggered multi-slice SE pulse sequence (Figure 2A), but may apply as well to multi-slice TSE and GRE pulse sequences. Each slice is excited only once per heartbeat, so $TR_{effective}$ equals the R-R interval. As the heart-rate increases, the $TR_{effective}$ decreases because the R-R interval decreases. Since each slice is acquired at a different phase of the cardiac cycle, this technique is often called a multi-slice multi-phase cardiac triggered pulse sequence. On the other hand, $TR_{protocol}$ for such a sequence is defined as the time actually used to acquire all the slices within the cardiac cycle.

A common method to increase the $TR_{effective}$ is to trigger the pulse sequence on every second or third heartbeat (Fig. 2B), in which case $TR_{effective}$ is twice or three times the R-R interval. This strategy is often used to control the image contrast for T2-weighted or IR-weighted pulse sequences.

Definition 3

Cardiac triggered cine pulse sequences create a movie effect of the beating heart or flowing blood by acquiring a series of images at different phases throughout the cardiac cycle. Various types of cine techniques include TrueFISP, Flash, Phase Contrast, and Grid-Tagging pulse sequences. The $TR_{protocol}$ definition for a cine sequence is the repetition time between consecutive cardiac phases, also known as the Temporal Resolution of the sequence. This definition of TR is demonstrated by a simple cardiac triggered cine pulse sequence (Fig. 3A), in which only one echo is acquired per cardiac phase (non-segmented). In this non-segmented acquisition, the $TR_{protocol}$ represents both the repetition time between successive cardiac phases (Temporal Resolution) and the repetition time between successive excitation pulses ($TR_{effective}$).

Often, however, multiple echoes are acquired per cardiac phase to reduce the required number of repetitions (Fig. 3B), a scheme called "segmented" data collection. In a segmented cine pulse sequence the $TR_{protocol}$ represents the repetition time between the center echo of successive cardiac phases (Temporal Resolution) but no longer represents the repetition time between successive excitation pulses ($TR_{effective}$). The Temporal Resolution in Figure 3B is five times longer than in Figure 3A, although the echo spacing ($TR_{effective}$) is the same in both.

If the center echo is re-sampled between successive segments, and echoes are shared from the prior and next segments, the Temporal Resolution can be improved by reducing the center-spacing between successive phases (Fig. 3C). In an "echo-shared segmented" cine pulse sequence, $TR_{protocol}$ represents the repetition time between the center echo of successive cardiac phases (Temporal Resolution), and is always less than the comparable $TR_{protocol}$ without echo-sharing. In this example of an echo-shared segmented cine pulse sequence, the total number of echoes acquired per repetition is six (5 + 1), however the $TR_{protocol}$ (Temporal Resolution) after echo-sharing is only three echoes (6 : 2).

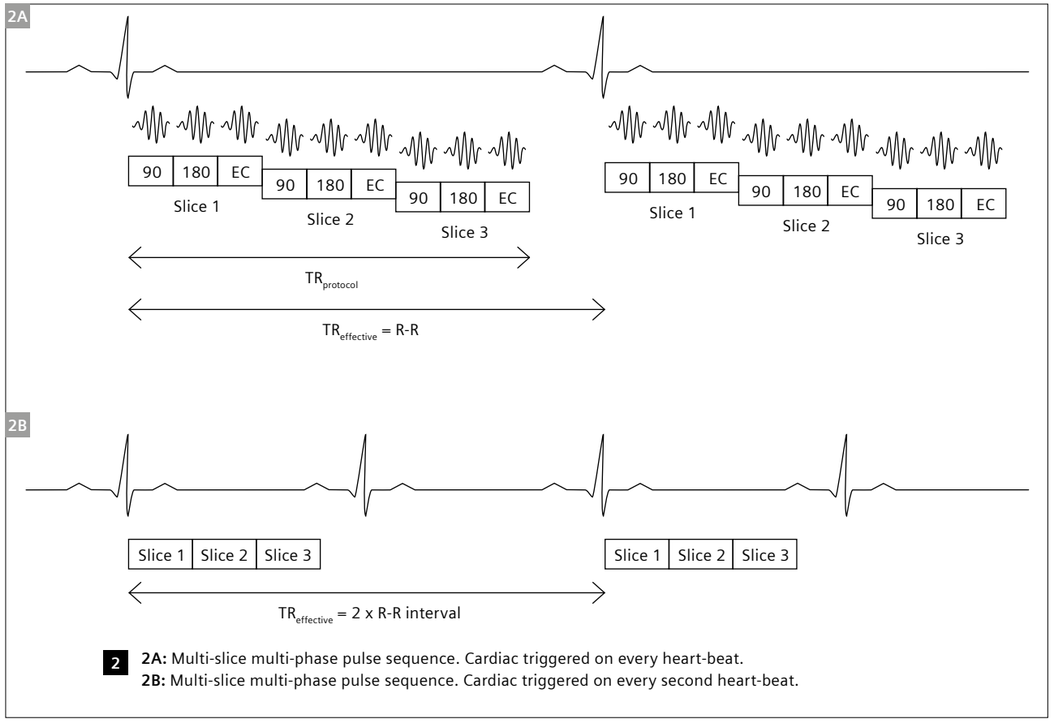

2 **2A:** Multi-slice multi-phase pulse sequence. Cardiac triggered on every heart-beat.
2B: Multi-slice multi-phase pulse sequence. Cardiac triggered on every second heart-beat.

Figures 3D and 3E demonstrate an example of an echo-shared segmented GRE cine pulse sequence.
In this example the total number of echoes acquired per repetition is twenty four (23 + 1), however the effective temporal resolution with echo-sharing is only twelve echoes (24 : 2) with a spacing of 43.32 ms between the centers of successive phases.

- The total number of cardiac phases is 17.
- The number of echoes per phase is 23.
- The temporal resolution per phase is 43.32 ms.

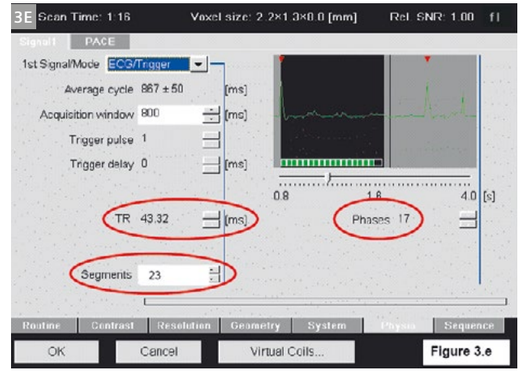

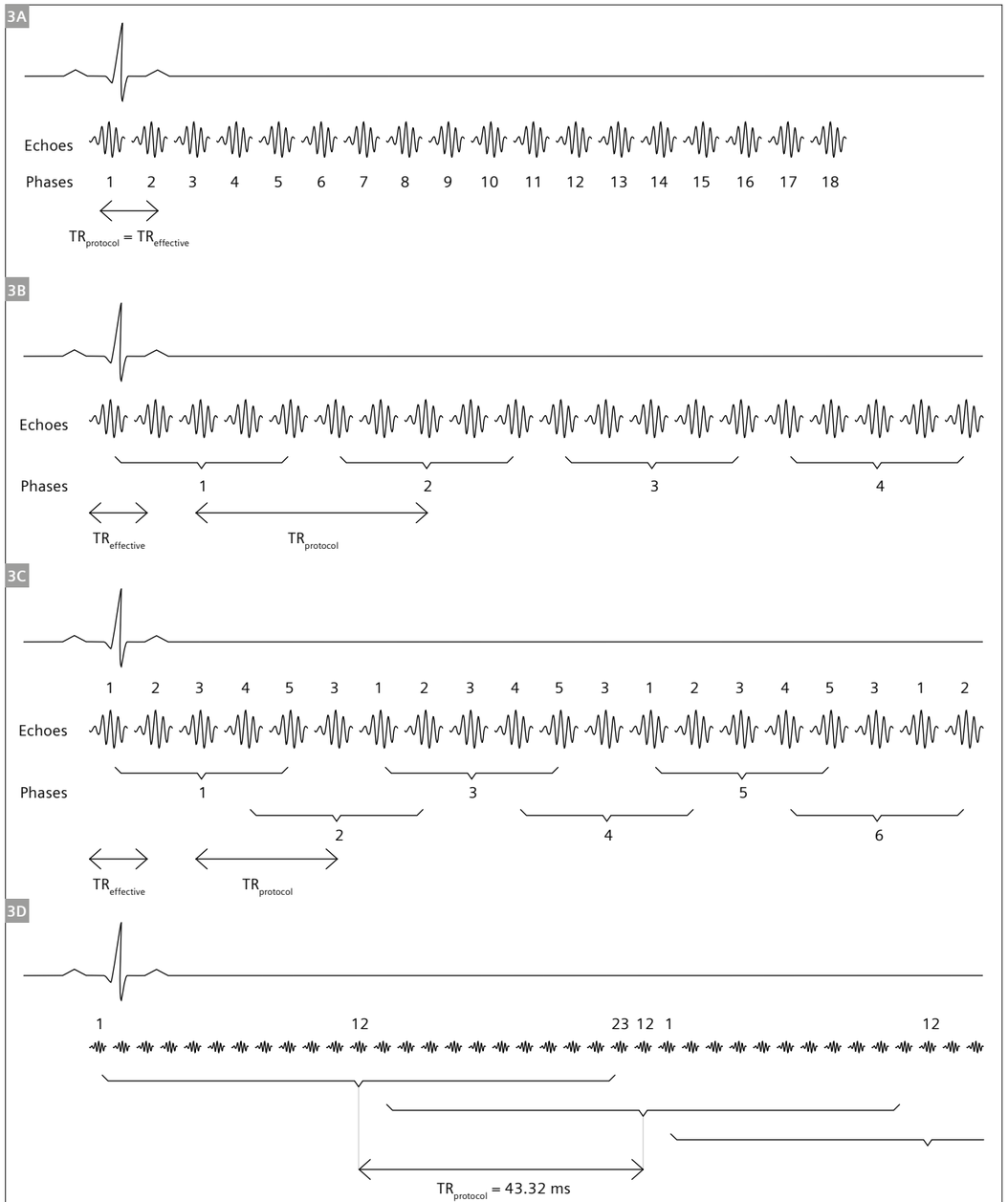

3 **3A:** Cardiac triggered cine pulse sequence. Non-segmented data collection.
3B: Cardiac triggered cine pulse sequence. Segmented data collection.
3C: Cardiac triggered cine pulse sequence. Echo-shared segmented data collection.
3D: Echo-shared segmented GRE sine pulse sequence.

Definition 4

Some cardiac triggered pulse sequences produce a single static image rather than cine images of the heart, and have yet a different definition of $TR_{protocol}$ (Figs. 4A, B). The $TR_{protocol}$ represents the minimum time needed to collect the train of echoes for a single diastolic-triggered segment. You should always set the $TR_{protocol}$ to its minimum possible value in this situation. You can still think of the minimum $TR_{protocol}$ as the Temporal Resolution of the sequence, but there is only one image produced rather than a cine series. This applies to any non-cine cardiac triggered pulse sequence containing no Inversion Recovery (IR) or Saturation Recovery (SR) preparation pulses. Examples of cardiac triggered pulse sequences using this definition of TR include TrueFISP 2D localizers and Flash 2D angiography techniques.

As demonstrated in the *syngo* Physio Taskcard for a segmented TrueFISP 2D localizer pulse sequence (Fig. 4B):

- The total number of echoes in the segment is 41.
- The temporal resolution of the segment is 152.3 ms (green bar).
- The trigger delay prior to the segment is 647 ms (grey bar).

In the previous example of a TrueFISP 2D localizer pulse sequence (Fig. 4B) only 41 echoes were collected per heartbeat, so several heartbeats were required to completely create the image. Such a scheme is known as "segmented" data collection. However, the same pulse sequence could be slightly modified to operate as a "single-shot" data collection in which all the echoes needed to create the image are collected in one long segment within a single heartbeat (Fig. 4C). The temporal resolution is still defined as the minimum time to collect all the echoes (minimum $TR_{protocol}$), but it is much greater than in the previous example because many more echoes are collected in the segment.

As demonstrated in the *syngo* Physio Taskcard for a single-shot TrueFISP 2D localizer pulse sequence (Fig. 4C):

- There is only 1 segment which contains of all the required echoes.
- The temporal resolution of the segment is 343.5 ms (green bar).
- The trigger delay prior to the segment is 456 ms (grey bar).

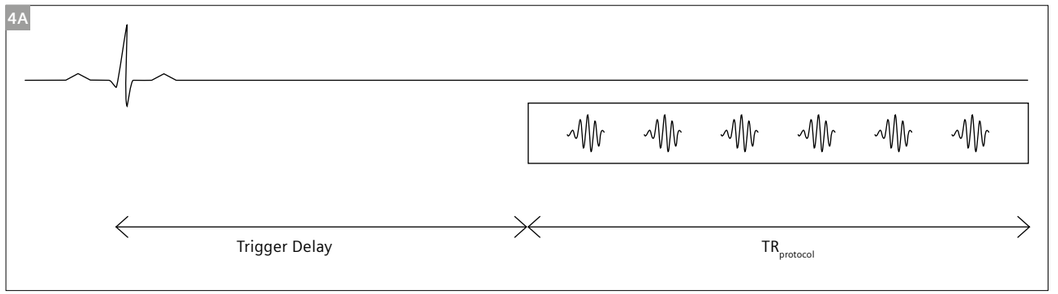

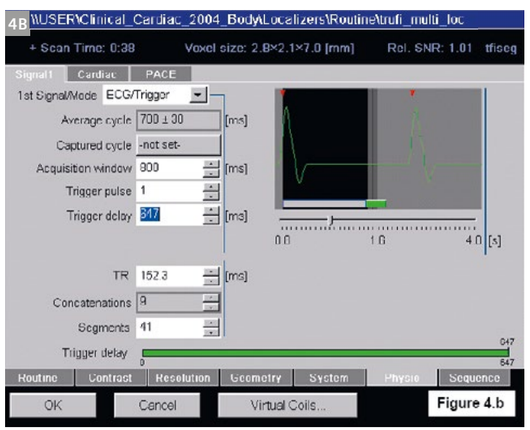

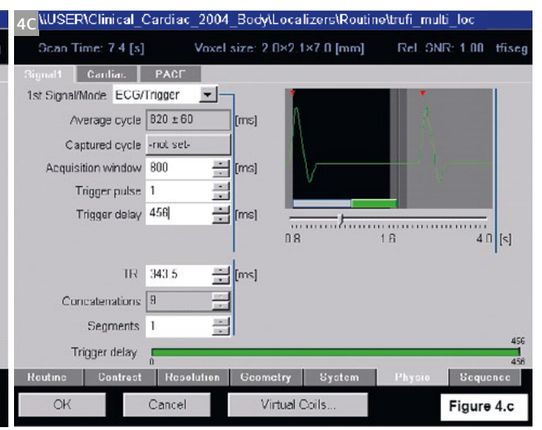

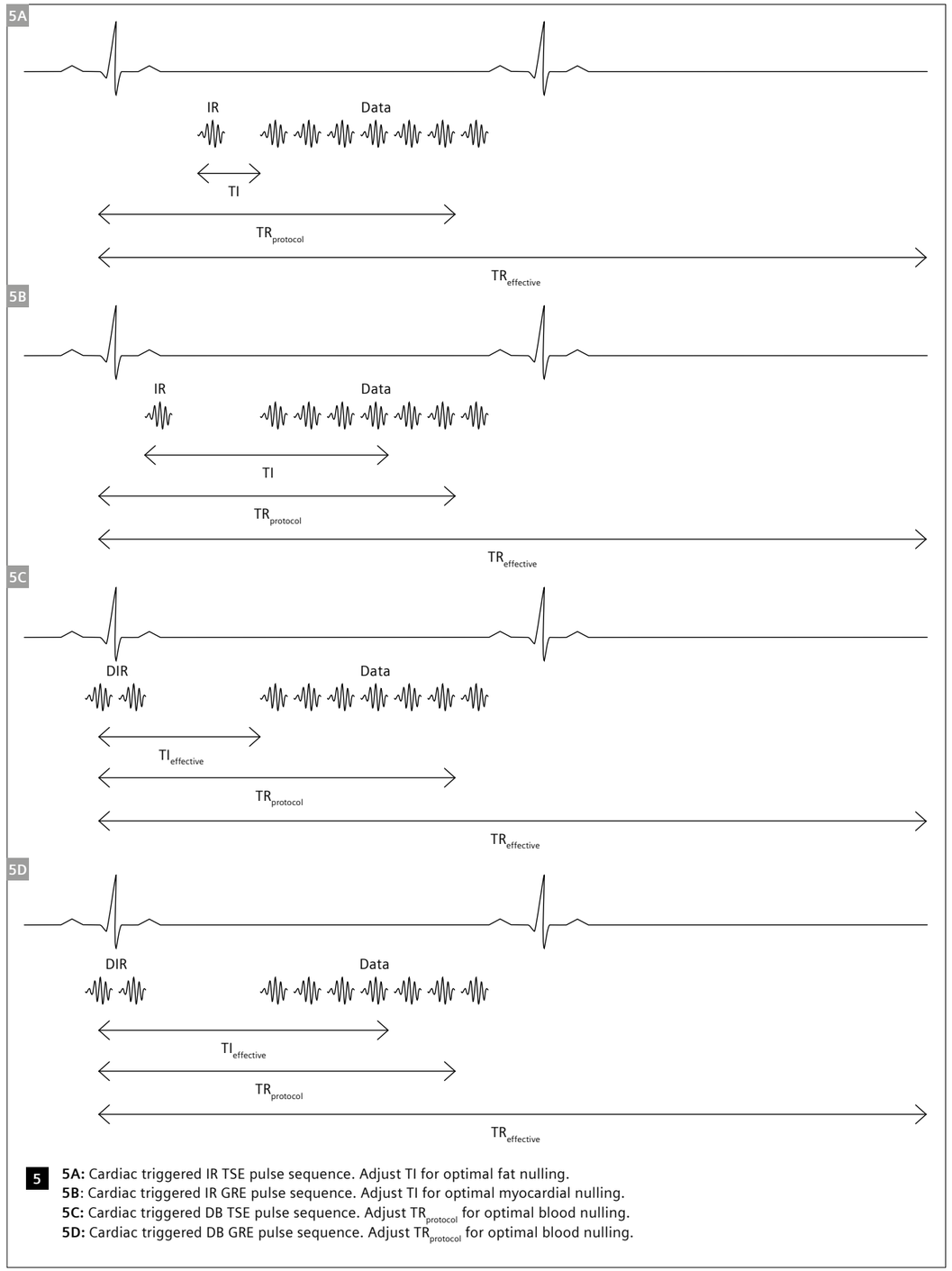

5 **5A:** Cardiac triggered IR TSE pulse sequence. Adjust TI for optimal fat nulling.
5B: Cardiac triggered IR GRE pulse sequence. Adjust TI for optimal myocardial nulling.
5C: Cardiac triggered DB TSE pulse sequence. Adjust $TR_{protocol}$ for optimal blood nulling.
5D: Cardiac triggered DB GRE pulse sequence. Adjust $TR_{protocol}$ for optimal blood nulling.

MAGNETOM Flash Special USA Edition · 02/2020 How-I-do-it

Definition 5

Yet another definition of TR applies to a cardiac triggered pulse sequence containing an Inversion Recovery (IR) preparation pulse (Figs. 5A, B). The $TR_{protocol}$ is defined as the time between the QRS trigger and the end of the data segment, and is used to adjust the timing of the data segment within the cardiac cycle. In an IR TSE pulse sequence the TI is defined as the time between the IR preparation pulse and the beginning of the data segment (Fig. 5A), and is typically adjusted for optimal fat nulling. In an IR GRE pulse sequence the TI is defined as the time between the IR preparation pulse and the center of the data segment (Fig. 5B), and is typically adjusted for optimal myocardial nulling. In these sequences the data segment is typically acquired every other heartbeat, so the $TR_{effective}$ is twice the R-R interval.

In order to null the signal from flowing blood, we can apply a Double Inversion Recovery (DIR) preparation pulse at the QRS trigger and wait several hundred milliseconds to acquire the data segment in the late diastolic portion of the cardiac cycle (Fig. 5C). The DIR pulse, also known as a Dark Blood (DB) pulse, is available for Turbo Spin Echo, TrueFISP, and TurboFlash pulse sequences. The TR in the protocol ($TR_{protocol}$) is defined as the time between the DB pulse and the end of the data segment. Since there is no TI available in a DB protocol, the $TR_{protocol}$ is used to adjust the location of the data segment for optimal blood nulling. Figure 5C demonstrates a cardiac triggered DB TSE pulse sequence in which the effective inversion delay time for blood nulling ($TI_{effective}$) is measured from the DB pulse to the beginning of the data segment. Figure 5D demonstrates a cardiac triggered DB GRE pulse sequence in which $TI_{effective}$ is measured from the DB pulse to the center of the data

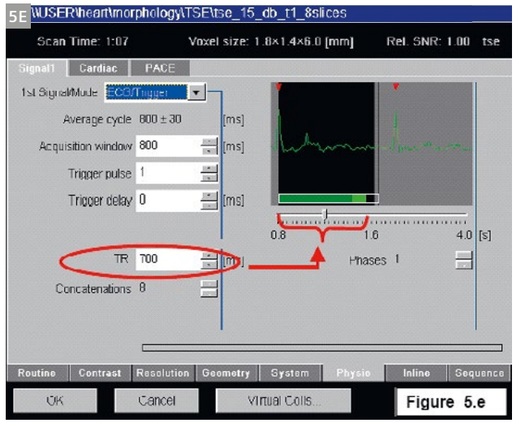

Figure 5.e

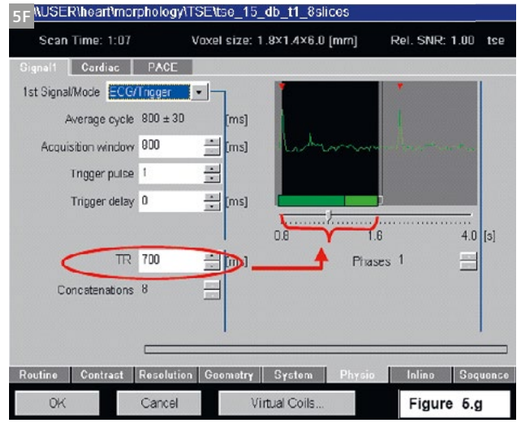

Figure 5.g

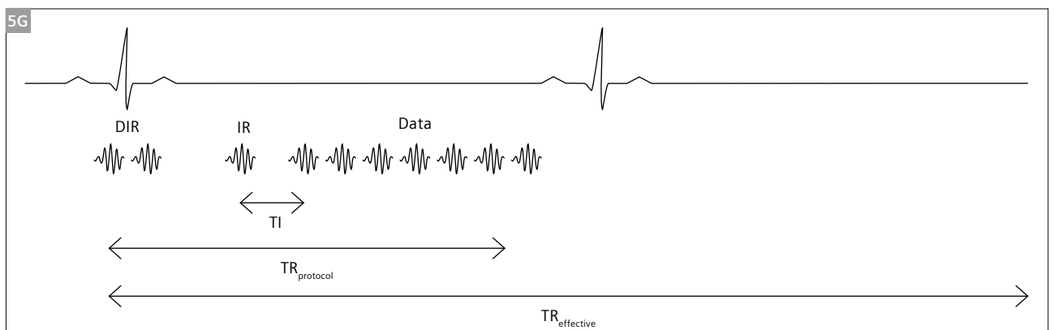

5 **5G:** Cardiac triggered DB STIR pulse sequence. Adjust $TR_{protocol}$ for optimal blood nulling. Adjust TI for optimal fat nulling.

segment. In these sequences the data segment is typically acquired every other heartbeat, so the $TR_{effective}$ is twice the R-R interval.

In the example of the *syngo* Physio Taskcard for a DB TSE pulse sequence (Fig. 5E) the TR of 700 ms includes the DB pulse (at the ECG trigger), the inherent inversion delay time (dark-green bar), and the data segment (light-green bar). Trigger delay must be zero because the inversion delay is included within TR.

If we add a third IR preparation pulse to a double IR TSE pulse sequence, we have a Dark Blood STIR pulse sequence (Fig. 5G). $TR_{protocol}$ is adjusted for optimal blood nulling and $TI_{protocol}$ is adjusted for optimal fat nulling. In these sequences the data segment is typically acquired every other heartbeat, so the $TR_{effective}$ is twice the R-R interval.

Figure 5F is an example of the *syngo* Physio Taskcard for a DB STIR pulse sequence. The dark-green bar within the TR includes the Double IR pulse and the inversion delay time for blood nulling. The light-green bar within the TR includes the single IR pulse and the inversion delay time for fat nulling, plus the data segment. Trigger delay must be zero because the inversion delay is included within the TR.

Another example is a FatSat IR Flash 3D pulse sequence for coronary angiography, without a Navigator pulse (Fig. 5H) or with a Navigator pulse (Fig. 5I). The TI is measured from the IR pulse to the beginning of the data segment (centric ordering) and is adjusted for optimal myocardial nulling. The FatSat pulse immediately precedes the data segment. The navigator pulse immediately precedes the FatSat pulse. There is no double IR pulse for blood nulling.

Definition 6

Yet another definition for TR is used in the IR- or SR-prepared GRE (TurboFlash or TrueFISP) pulse sequences (Fig. 6A). These sequences can be used for T1-weighted single-shot imaging that requires multiple slices acquired within a single heartbeat with high temporal resolution. $TR_{protocol}$ consists of the minimum time duration needed for the SR preparation pulse, plus the delay period thereafter, plus the data segment. $TR_{protocol}$ can be thought of as the "time per slice." TI is measured from the IR- or SR-preparation pulse to the center of the data segment, and is adjusted for optimal myocardial signal.

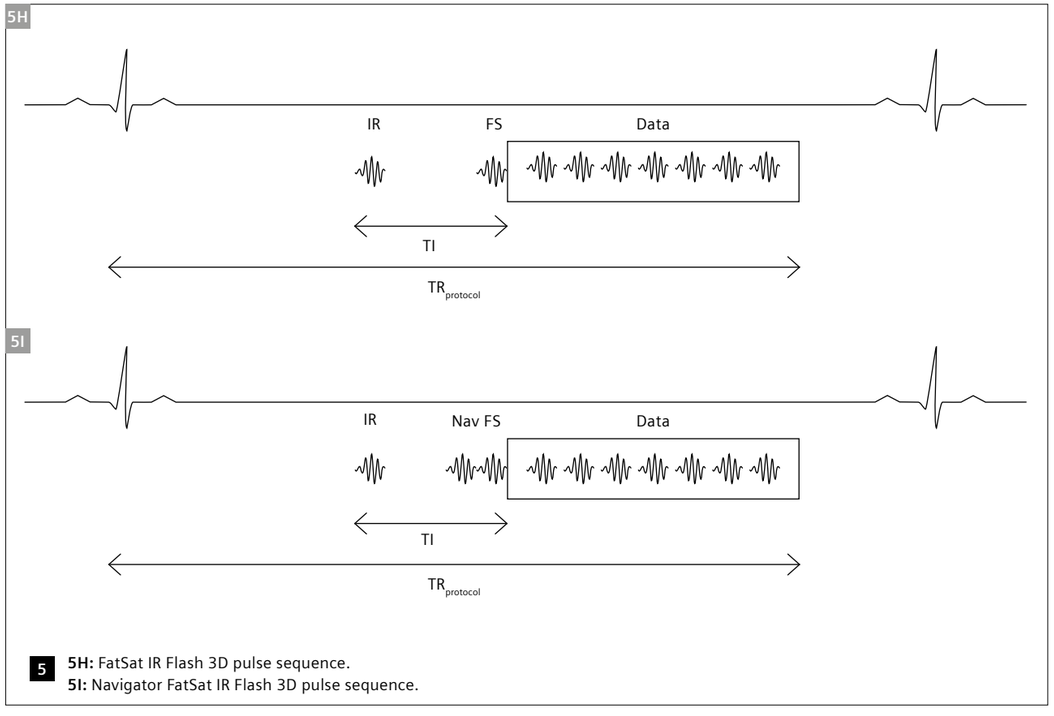

5 **5H:** FatSat IR Flash 3D pulse sequence.
5I: Navigator FatSat IR Flash 3D pulse sequence.

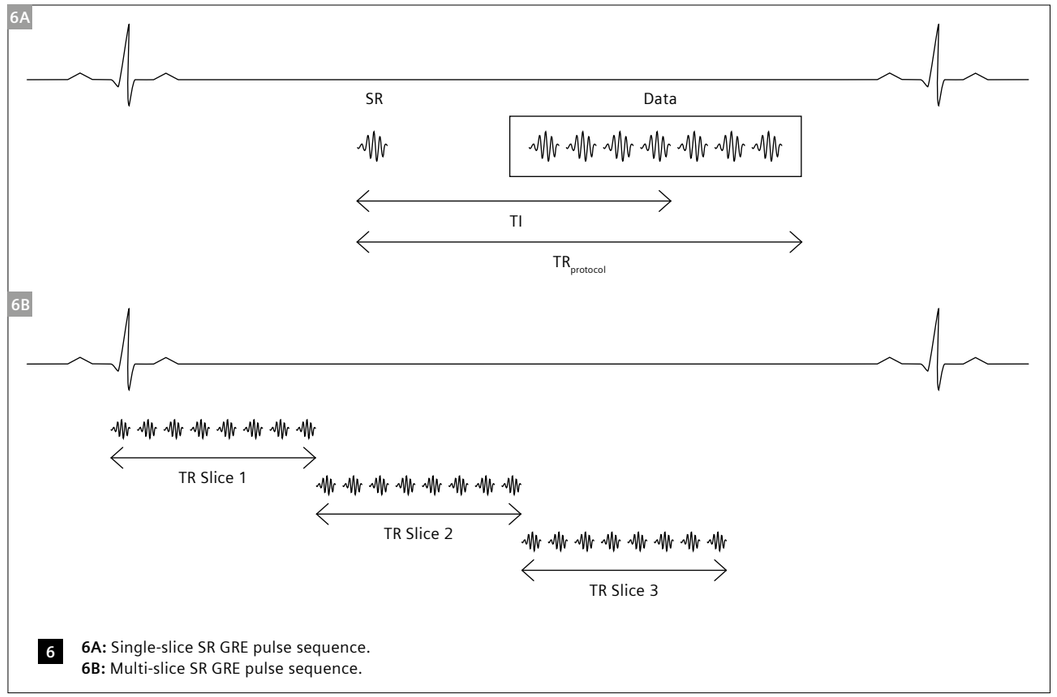

6 **6A:** Single-slice SR GRE pulse sequence.
6B: Multi-slice SR GRE pulse sequence.

SR Data

In an SR GRE pulse sequence the data segment is a "single-shot" of all required echoes for the entire slice. Typically, 3 to 5 slices can be acquired within each heartbeat (Figs. 6B, C).

While the physical definition of TR will always mean only one thing, the time between successive excitation pulses, a number of variations have resulted from the necessity of controlling a pulse sequence within the cardiac cycle. Hopefully, this brief explanation with diagrams will make it a little easier for everyone to understand.

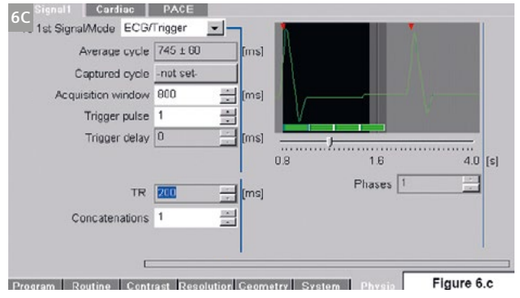

Figure 6.c

Contact

Gary McNeal, MS (BME)
Advanced Application Specialist,
Cardiovascular MR Imaging
Siemens Healthineers
737 N. Michigan Ave, Ste 1600
Chicago, IL, 60611
USA
gary.mcneal@siemens-healthineers.com

Why Siemens Healthineers?

At Siemens Healthineers, our purpose is to enable healthcare providers to increase value by empowering them on their journey toward expanding precision medicine, transforming care delivery, and improving patient experience, all enabled by digitalizing healthcare.

An estimated 5 million patients globally benefit every day from our innovative technologies and services in the areas of diagnostic and therapeutic imaging, laboratory diagnostics, and molecular medicine, as well as digital health and enterprise services.

We're a leading medical technology company with over 120 years of experience and 18,500 patents globally. With about 50,000 dedicated colleagues in over 70 countries, we'll continue to innovate and shape the future of healthcare.

Siemens Healthineers Headquarters
Siemens Healthcare GmbH
Henkestr. 127
91052 Erlangen, Germany
Phone: +49 9131 84·0
siemens-healthineers.com

USA
Siemens Medical Solutions USA. Inc.
Healthcare
40 Liberty Boulevard
Malvern.. PA 193S5-9998, USA
Phone:+1-888-826-9702
siemens-h.ealthineers.us

Published by Siemens Medical Solutions USA, Inc. · Order No. MR-18-NAM-320 · Printed in USA · 02.2020 · ®Siemens Medical Solutions USA, Inc., 202